Role of Cytoskeletal Alignment, Independent of Fluid Shear Stress, in Endothelial Cell Functions

Keri Beth Vartanian
B.S., University of Arizona, 2003

Presented to the Division of Biomedical Engineering within
The Department of Science & Engineering
and the Oregon Health & Science University
School of Medicine
in partial fulfillment
in the requirements for a degree of
Doctor of Philosophy
in
Biomedical Engineering

May 2009

Department of Science & Engineering
School of Medicine
Oregon Health & Science University

CERTIFICATE OF APPROVAL

This is certify that the Ph.D. dissertation

Keri Beth Vartanian

has been approved

Dr. Monica Hinds
Thesis Advisor, Assistant Professor

Dr. Stephen Hanson
Professor

Dr. Owen McCarty
Assistant Professor

Dr. Tania Vu
Assistant Professor

Dr. Kent Thornburg
Professor

I would like to dedicate this to my family, my most ardent supporters: my parents, Ken and Karen; my sisters, Kristina and Kim; my brother-in-laws, Vic and Josh; my fiancé, Richard; and the newest addition to the family, my nephew Sebastian.

Acknowledgements

The graduate school experience is often dictated by the quality of your advisor. That being said, I would like to first and foremost thank my advisor, Dr. Monica Hinds. I simply cannot list all that Dr. Hinds has done to help me during this process and in my career. So, I will thank Dr. Hinds here for those attributes that make her such a great advisor. Thank you for always taking the time to listen to my ideas, thank you for the many discussions and insight on this project, thank you for always being understanding and patient, thank you for sending me to several conferences to present my research, thank you for pushing me to apply for grants and to write papers, and thank you for your endless encouragement and support over the past five years.

I would like to thank Dr. Stephen Hanson, Dr. Owen McCarty, and Dr. Tania Vu for participating on my advisory committee. I would like to thank all of them for taking the time out of their busy schedules to meet with me, discuss my project, read and edit my writing, and, most importantly, for providing a different perspective on my research. I would like to also thank Dr. Kent Thornburg for agreeing to serve on my committee for my defense and taking the time to meet with me and learn about my project.

Dr. Sean Kirkpatrick wrote the MATLAB code used in this research to quantify cytoskeletal alignment. When Dr. Kirkpatrick heard about the research I was doing he thought his MATLAB program would be of use so he generously contributed it to my project. I would like to thank Dr. Kirkpatrick for not only allowing me to use his MATLAB program, but for also taking the time to help me tailor it to my research needs and for explaining the image analysis concepts to me.

I would like to thank Dr. Ken Chrobak, Andy Golden, and Dr. Joe Tien at Boston University for assistance and guidance with the micropatterned silicon templates. I would like to thank David Levitz for technical help with quantification of fluorescent intensity using MATLAB. I would like to acknowledge and thank Tara White and Michelle Berny for help with the platelet and leukocyte studies. Also, to my lab mate and friend Brandon Markway, thanks for listening, discussing, and giving me someone to bounce ideas off of, even over Skype.

Last, but not least, I would like to thank my family and friends. Mom, Dad, Kris, Kim, Vic, Josh, Richard, Sebastian, Kirsten, and Kelly, thank you for your constant encouragement and support in all of my endeavors.

Table of Contents

List of Figures

List of Tables

List of Abbreviations

AcLDL	acetylated low-density lipoprotein
ADP	Adenosine diphosphate
ANOVA	analysis of variance
AP-1	activator protein 1
APC	activated protein C
ATP	Adenosine triphosphate
BAEC	bovine aortic endothelial cell
BCE	bovine capillary endothelial cell
bp	base pair
BSA	bovine serum albumin
dpi	dots per inch
DNA	deoxyribonucleic acid
cDNA	complementary deoxyribonucleic acid
Col I	collagen I
Col IV	collagen IV
DMSO	dimethyl sulfoxide
DPB	dense peripheral band
E-selectin	endothelial selectin
EC	endothelial cell
ECM	extracellular matrix
ELISA	enzyme-linked immunosorbent assay
eNOS	endothelial nitric oxide synthase
EPC	endothelial progenitor cell
ePTFE	expanded polytetraflouroethylene
ERK	extracellular signal-regulated kinase
FAs	focal adhesions
FITC	Fluorescein isothiocyanate
FN	fibronectin
FSS	fluid shear stress

FVIIa	activated factor VII
FXa	activated factor X
GAPDH	Glyceraldehyde 3-phosphate dehydrogenase
GDP	guanosine diphosphate
GTP	guanosine triphosphate
HBSS	Hanks balances salt solution
HCl	hydrochloric acid
HRP	horse radish peroxidase
HUVEC	human umbilical vein endothelial cell
ICAM	intracellular cell adhesion molecule
IF	immunofluorescence
IL-1β	interleukin 1 beta
IκB	inhibitor of kappa B
JNK	c-Jun amino terminal kinase
KLF2	kruppel-like factor 2
kDa	kilodalton
L-selectin	leukocyte selectin
LFA-1	leukocyte function associated antigen - 1
LPS	lipopolysaccharide
LN	laminin
MAPK	mitogen-activated kinases
MCP-1	monocyte chemoattractant protein 1
MLEC	mouse lymph node endothelial cell
MMP	matrix metalloproteinase
MP	micropattern
MPEC	micropattern elongated endothelial cell
MT	microtubule
MTOC	microtubule organizing center
NFκB	nuclear factor kappa B
NP	non-pattern
NO	nitric oxide
ox-LDL	oxidized low density lipoprotein
p-FAK	phosphorylated focal adhesion kinase
P-selectin	platelet selectin

PAI-1	plasminogen activator inhibitor 1
PAK	p21-activated kinase
PBS	phosphate buffered saline
PDF	probability density function
PDMS	polydimethylsiloxane
PFA	paraformaldehyde
PPP	platelet poor plasma
PRP	platelet rich plasma
qtPCR	quantitative polymerase chain reaction
RGD	arginine – glycine – aspartic acid
RNA	ribonucleic acid
mRNA	messenger ribonucleic acid
siRNA	short interference ribonucleic acid
SA	surface area
SD	standard deviation
SEM	standard error of the mean
SI	shape index
SMC	smooth muscle cell
SRF	serum response factor
TCP	tissue culture plastic
TF	tissue factor
TFPI	tissue factor pathway inhibitor
TGF-β	transforming growth factor beta
TIMP	tissue inhibitor matrix metalloproteinase
TM	Thrombomodulin
TNF-α	tumor necrosis factor alpha
uPA	urokinase plasminogen activator
VCAM	vascular cell adhesion molecule
VEGF	vascular endothelial growth factor
VEGFR2	vascular endothelial growth factor receptor 2
VECAD	vascular endothelial cadherin
VLA-4	very late antigen – 4
vWF	von Willebrand factor

Abstract

Role of Cytoskeletal Alignment, Independent of Fluid Shear Stress, in Endothelial Cell Functions

Keri Vartanian, B.S.

Doctor of Philosophy
Division of Biomedical Engineering
The Department of Science and Engineering
and the Oregon Health & Science University
School of Medicine

May, 2009
Thesis Advisor: Monica Hinds, Ph.D.

The cardiovascular disease atherosclerosis is directly linked to the functions of the endothelium, the monolayer of endothelial cells (ECs) that line the lumen of all blood vessels. EC functions are affected by fluid shear stress (FSS), the tangential force exerted by flowing blood. In vivo FSS is determined by vascular geometry with relatively straight vessels producing high, unidirectional FSS and vessel branch points and curvatures producing low, oscillatory FSS. While these distinct FSS conditions differentially regulate EC functions, they also dramatically affect EC shape and cytoskeletal structure. High and unidirectional FSS induces EC elongation and cytoskeletal alignment, while concurrently promoting EC functions that are athero-protective. In contrast, low and oscillatory FSS induces cobblestone-shaped ECs with randomly oriented cytoskeletal features, while simultaneously promoting EC functions that create an athero-prone vascular environment. Whether these distinct EC shapes and cytoskeletal structures influence EC functions, independent of FSS, is largely unknown. ***The overall hypothesis of this study is that cell shape and cytoskeletal structure regulate EC functions through mechanisms that are independent of FSS.*** Due to advances in surface engineering in the field of micropatterning, EC shape can be controlled independent of external forces by creating spatially localized surface cues. In this research, lanes of protein were micropatterned on glass surfaces to induce EC elongated shape in the absence of FSS. In Aim 1, micropattern-elongated EC (MPEC) shape and cytoskeletal structure were fully characterized and determined to be comparable to FSS-elongated ECs. Thus, inducing EC elongation on micropatterned lanes provides a platform for studying the functional consequences of EC shape, independent of FSS. Using this model, the following important markers of EC functions related to atherosclerosis were evaluated to determine the influence of EC shape and cytoskeletal alignment: extracellular matrix deposition (Aim 2), inflammatory function (Aim 3), and thrombotic potential (Aim 4). The results indicate that EC-elongated shape and cytoskeletal alignment participate in promoting selected EC functions that are protective against atherosclerosis, independent of FSS. Since EC shape is governed by the cytoskeleton, this data suggests that the cytoskeleton plays an active role in the regulation of EC functions that promote cardiovascular health.

CHAPTER I

Introduction

The overall focus of this research is the study of atherosclerosis, a cardiovascular disease characterized by the buildup of fatty deposits in the blood vessel wall. Fatty buildups, commonly referred to as plaques, cause blood flow to become restricted and ultimately can cause a heart attack or stroke. Interestingly, these fatty deposits are primarily found in regions of vasculature that bifurcate and curve. Vascular geometry greatly affects blood flow. In straight vessels, blood flows in one direction and exerts a high, unidirectional fluid shear stress (FSS), the drag force exerted by blood tangent to the vessel wall. In contrast, blood flow in bifurcated/curved vessels is multidirectional and exerts low, oscillatory FSS. These differing blood flow profiles have a dramatic effect on the cells of blood vessels, in particular, on endothelial cells (ECs).

ECs form a continuous monolayer, known as the endothelium, which lines the lumen of all blood vessels and forms an interface between flowing blood and the vessel wall. The major function of the endothelium is the regulation of vascular homeostasis. ECs regulate vascular tone, permeability, the surrounding microenvironment, inflammation, and thrombogenicity. Under basal condition, ECs promote a semi-permeable, non-inflammatory, and non-thrombogenic surface. Alterations in EC functions are directly related to FSS and can be attributed to the focal development of atherosclerotic plaques in vascular curves and bifurcations.

The FSS-mediated EC response has been a source of intense interest for several decades. The dramatic effects of FSS on both EC shape and EC function have been well established. The high, unidirectional FSS of long, straight vessels induces

elongated EC shape, aligned cytoskeletal components parallel to the direction of flow, and athero-protective EC functions. The low, oscillatory FSS found in bifurcated and curved vessels induces cobblestone-like EC shape, randomly oriented cytoskeletal components, and promotes athero-prone EC functions. Thus, FSS-induced EC shape and function are inextricably linked, such that FSS-dependent EC shapes and functions happen concurrently both in vivo and in vitro. The direct influence of these drastically different EC shapes (elongated and cobblestone) and cytoskeletal organizations on EC functions has not been investigated independent of FSS. The objective of this study is to determine whether the shape of ECs affects their athero-protective or athero-prone functions, and whether these shape-dependent effects are independent of changes induced by FSS. ***The overall hypothesis of this study is that cell shape and cytoskeletal structure regulate EC functions through mechanisms that are independent of FSS*.** The control of EC shape, independent of FSS, is made possible by recent advances in surface engineering using micropatterning. Previous research using micropatterned surfaces showed that controlling the size and shape of the deposition area of adhesive proteins allowed for control of EC shape. These investigations also established that EC shape regulated cell proliferation, apoptosis, differentiation, and migration. Therefore, this research study employed micropatterns to induce EC shape and cytoskeletal structure that mimic in vivo conditions and determined whether EC shape contributes to the regulation of extracellular matrix (ECM), inflammation, and thrombogenicity, all of which are abnormal in the atherosclerotic environment.

Overall, the goal of this study was to achieve a basic science understanding of the role of EC shape. Resulting insights into the role of EC shape in atherosclerotic-prone cell functions may in turn lead to improved therapeutic strategies. For instance, the success of synthetic vascular grafts is improved by the presence of a fully functional EC layer on the innermost surface. Currently, this requires putting endothelial cells on the graft surface followed by further manipulation to promote cell function. If shape regulates cell functions, the design of the surfaces of vascular grafts could be modified to optimize EC shape and function.

CHAPTER II

Central Hypothesis and Specific Aims

2.1 Central Hypothesis

The central hypothesis of this study is that cell shape and cytoskeletal structure regulate EC functions through mechanisms that are independent of FSS. To address the central hypothesis, four specific aims were designed to characterize shape-dependent cytoskeletal structure, extracellular matrix (ECM) environment, inflammation, and thrombogenicity.

2.2. Specific Aims

2.2.1. Aim 1: To characterize EC cytoskeletal structure for ECs elongated by micropatterned lanes compared to fluid shear stress. The cytoskeleton is a dynamic structure regulating cell shape, spreading, and migration. Extensive evidence shows that actin and microtubules, two major components of the cytoskeleton, align and elongate in the direction of flow in athero-protective regions and become disorganized in athero-prone regions where ECs have cobblestone-like shape [6, 7]. This cytoskeletal reorganization has been investigated under FSS, but cytoskeletal alignment has not been established independent of this external force. ***The hypothesis for this aim is that ECs elongated on micropatterned lanes have comparable cytoskeletal structure compared to FSS-elongated ECs*.** The EC cytoskeleton, actin and

microtubules, were characterized under four conditions: (1) micropattern-elongated, (2) FSS-elongated, (3) micropattern-elongated plus FSS, and (4) Non-patterned cobblestone. Image analysis of immunofluorescence (IF) stained ECs were used to quantify actin and microtubule organization and polarization of the microtubule organizing center (MTOC). ECs elongated on micropatterned lanes were treated with known actin and microtubule inhibitors to isolate their individual roles in FSS-independent cytoskeletal reorganization.

2.2.2. Aim 2: To determine whether ECs deposit ECM in a shape-dependent manner. The production and regulation of ECM contributes to EC functions and the development of atherosclerosis. In athero-prone regions, the integrity of the ECM is compromised, weakening the vessel wall, and contributing to atherosclerotic plaque rupture. ***The hypothesis to be tested is that polygonal ECs will produce a pathological athero-prone ECM microenvironment compared to elongated ECs.*** The relationship between EC shape and the local environment was studied by measuring ECM production by micropattern-elongated and cobblestone-shaped ECs. IF and ELISA was used to determine EC production of the major ECM components: collagen IV, fibronectin, and laminin.

2.2.3. Aim 3: To determine the relationship between EC shape and the expression of immunogenic markers. ECs within athero-prone regions of the vasculature are dysfunctional, which ultimately promotes the development of atherosclerosis. One of the initiating events in atherosclerosis is an increase in EC-mediated inflammatory response. ***The hypothesis to be tested is that elongated ECs have decreased immunogenic function compared to cobblestone shaped ECs.*** Micropattern-elongated ECs, FSS-elongated ECs, and cobblestone ECs were evaluated. Quantitative Polymerase chain reaction (qtPCR) was used to determine the expression of the following inflammatory genes: monocyte chemoattractant protein-1 (MCP-1), E-selectin, vascular cell adhesion molecule-1 (VCAM), and intracellular cell adhesion molecule-1 (ICAM). To evaluate inflammatory function, EC leukocyte adhesiveness was determined by flowing U937 cells over the EC surface.

2.2.4. Aim 4: To determine the relationship between EC shape and thrombogenicity. ECs within athero-prone regions of the vasculature are dysfunctional and exhibit increased thrombogenic potential***. The hypothesis to be tested is that EC elongated shape is associated with decreased thrombogenic function compared to cobblestone ECs.*** Thrombogenic gene expression was characterized for micropattern-elongated ECs, FSS-elongated ECs, and cobblestone ECs using qtPCR. The expressions of the following genes were evaluated: tissue factor (TF), tissue factor pathway inhibitor (TFPI), thrombomodulin (TM), von Willebrand factor (vWF), and eNOS. EC thrombogencity was functionally evaluated by quantifying platelet adhesion to the EC surface.

Chapter III

Background

3.1. The Vessel Wall - Arteries

Arteries are blood vessels that carry blood from the heart to all of the body's organs and tissues. Arteries are made up of three major layers separated by elastic fibers referred to as the elastic lamina. The artery layers listed from outermost to innermost are the: (1) adventia, (2) media, and (3) intima (Fig. 3.1). The adventia consists mainly of collagens and elastic fibers, which form a strong covering surrounding the vessel [8]. The media is made up of concentrically organized smooth muscle cells (SMCs) and is responsible for vascular tone [8]. The intima, the focus of this research, is made up of a monolayer of ECs, known as the endothelium, and a subendothelial space (SES), consisting of an extracellular matrix basement membrane [8]. ECs act as the primary regulators of vascular homeostasis. As the interface between the vessel wall and flowing blood, ECs regulate thrombogenicity, vascular permeability, monocyte recruitment, and vasodilation/constriction [9, 10]. The development of cardiovascular disease has been strongly correlated to the loss of EC function [10, 11].

Figure 3.1

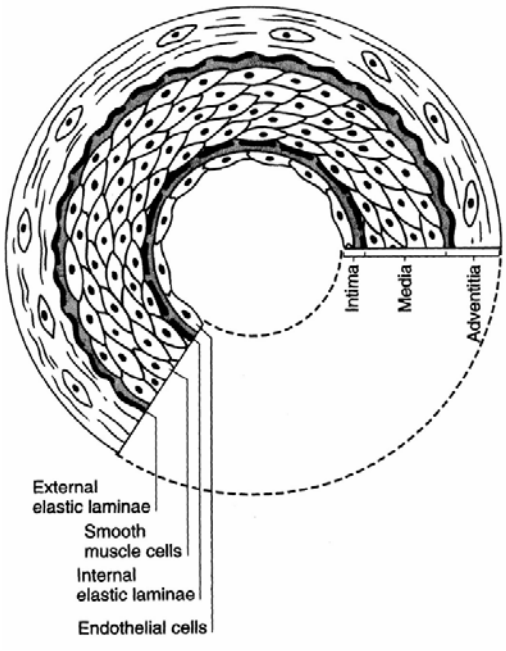

Figure 3.1. Cross-sectional schematic of an artery. The three major vessel layers listed from innermost to outer most are the: intima, media, and adventia. The associated extracellular matrix layers are also represented. The subendothelial space (SES) is found between the endothelial and internal elastic laminae. Image taken from Kusumoto, Cardiovascular Pathophysiology [1].

3.2. Cardiovascular Disease

Cardiovascular disease is the number one cause of death in the industrialized world [12]. Atherosclerosis, a cardiovascular disease affecting millions of people each year [12], is characterized by the hardening of arteries and build-up of fatty plaques within the arterial wall. Atherosclerotic fatty plaques develop in several stages over a long period of time. The first stage of atherosclerosis is characterized by two major EC-mediated events including: (1) monocyte recruitment (inflammation) and (2) increased vascular permeability (e.g. plasma protein and LDL uptake) [13]. In the second stage, monocytes that have transmigrated into the SES become activated and differentiate into macrophages [13]. At the same time LDL becomes oxidized (ox-LDL) [13]. In the SES, activated macrophages take up ox-LDL through the scavenger receptor and ultimately transform into cholestryl-ester-rich foam cells [13]. In the third stage, the fatty streak develops, which is comprised of foam cells, matrix molecules (collagen, elastin, proteoglycans), smooth muscle cells (SMCs), and a thin, abnormal endothelial layer [13].

As the atherosclerotic plaque transforms into a mature lesion, the lipid core can become necrotic, cholesterol crystals form in the extracellular matrix, and macrophage recruitment and connective tissue synthesis continues [13]. In the final stages, the mature lesion causes narrowing of the vessel lumen and a thickened intima. This atherosclerotic plaque restricts blood-flow and when ruptured can cause thrombosis which leads to heart attacks and strokes.[13, 14] The pathogenesis of atherosclerosis is highly localized to branched and bifurcated regions of the vasculature (Fig.3.2 A) [3, 15]. Two major features of these athero-prone regions of vasculature are: (1) disturbed blood flow with low fluid shear stress (FSS), and (2) dysfunctional ECs with cobblestone-like morphology (Fig. 3.2 B & C) [2, 5, 15, 16].

3.3. Hemodynamics

Vascular geometry dramatically affects the hemodynamics of blood flow. Blood flowing in relatively straight vessels has a non-reversing pulsatile flow profile [2]. In regions where the vasculature bifurcates or curves, the blood flow profile becomes disturbed with regions of flow reversals [2, 5, 15].

Flowing blood exerts three major forces on blood vessels (Fig. 3.3): (1) radial compressive, (2) circumferential tensile, and (3) fluid shear stress (FSS) [2]. The first two forces are felt by the entire thickness of the vessel wall and originate from differences between intramural and extramural pressure [2]. The third force, FSS, is the force tangent to the vessel wall and therefore is exclusively exerted on the endothelium [2]. In large arteries, where blood can be treated as a Newtonian fluid, FSS can be approximated as the fluid viscosity times the velocity gradient perpendicular to the direction of shear stress (Fig. 3.3 [2]). Blood circulating through relatively straight vessels, with non-reversing pulsatile flow, exerts high, unidirectional FSS on the endothelium with a mean FSS of 10-20 dynes/cm^2 [9, 17]. High, unidirectional FSS is considered athero-protective (details below). In contrast, blood circulating in bifurcated and curved vessels, with disturbed and reversing blood flow, induces low, oscillatory FSS with a mean of < 4 dynes/cm^2 [2, 15, 18-20]. Low, oscillatory FSS is considered athero-prone [5, 15]. These two FSS profiles differentially influence and regulate EC shape, cytoskeletal structure, and various EC functions.

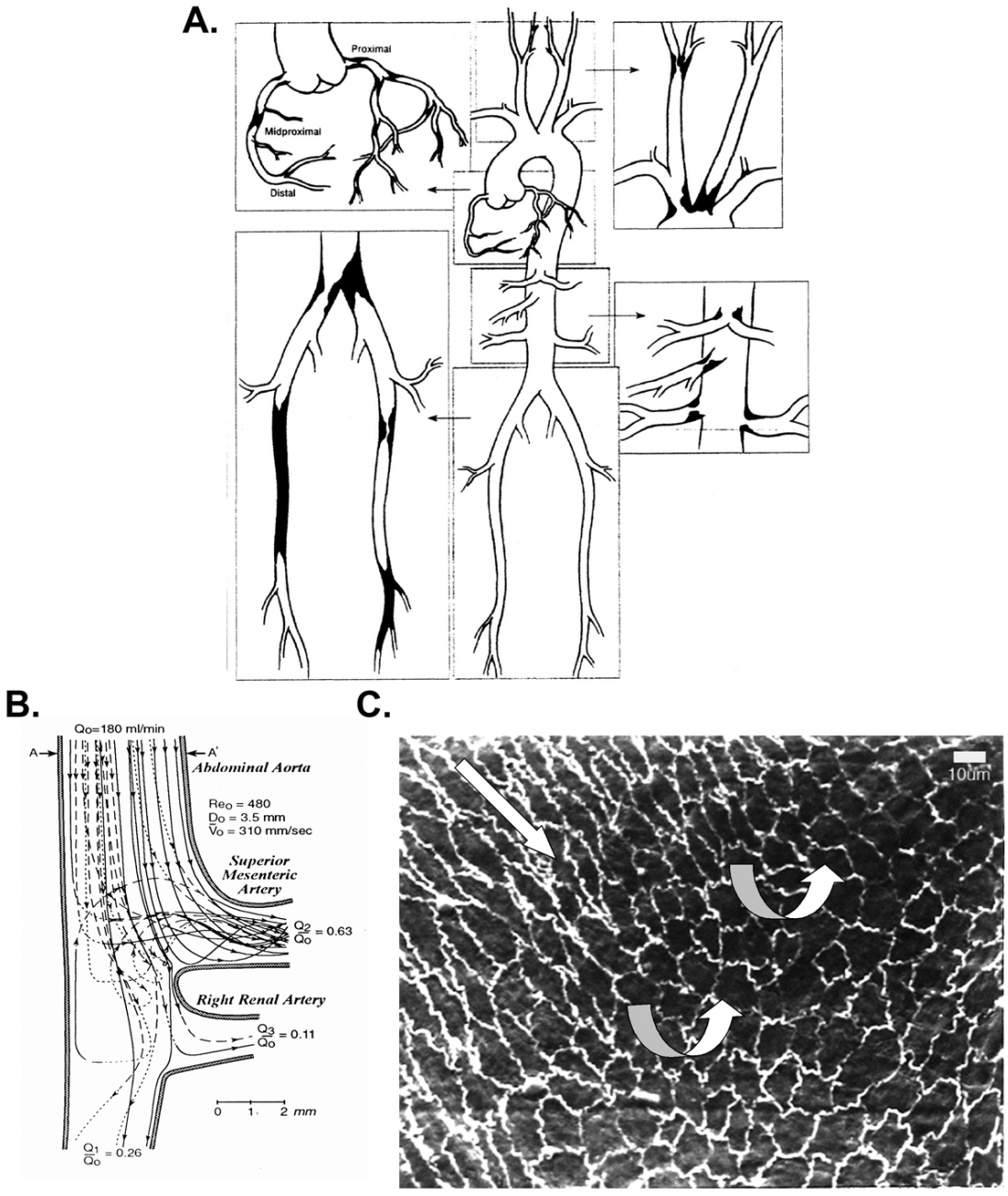

Figure 3.2. Diagrams and image representing atherosclerosis prone regions of the vasculature and the associate hemodynamics and EC shape. **A.** Vascular regions of the vasculature prone to the development of atherosclerotic plaques highlight in black. Taken from Debakey, et al., [3]. **B.** Schematic of disturbed blood flow profile in a branched vessel prone to atherosclerosis. Taken from Barakat, et al., [2]. **C.** Scanning Electron Microscopy image of a region of flow separation in a baboon aorta demonstrating the dramatic change in EC shape from elongated under unidirectional flow and cobblestone under multidirectional flow. Arrows represent direction of flow. Taken from Davies, et al., [5].

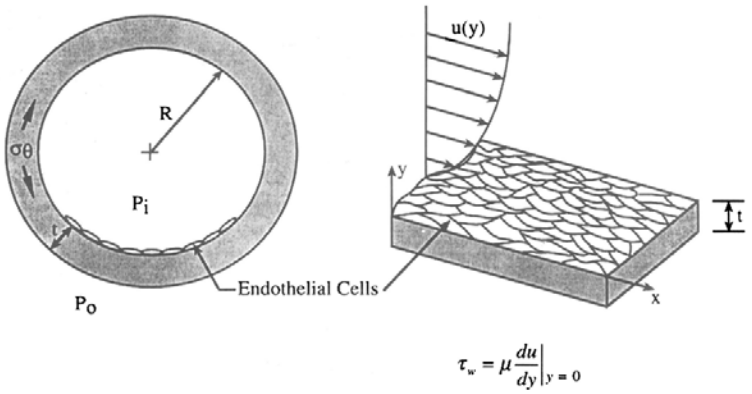

Figure 3.3. Representative illustration of the forces exerted on the vessel wall. Left : Radial compressive and circumferential tensile pressure. Right: Fluid shear stress due to tangent to the vessel wall and the equation used to calculate fluid shear stress in Newtonian fluids (viscosity μ multiplied by the gradient of the velocity perpendicular to the vessel wall). Taken from Barakat et al [2].

Influence of FSS on EC shape: FSS dramatically affects EC shape and cytoskeletal structure in vivo and in vitro. Non-reversing pulsatile flow with high, unidirectional FSS (athero-protective) induces EC elongation and cytoskeletal alignment parallel to the direction of flow [5, 21, 22]. Disturbed, multidirectional flow, which induces low, oscillatory FSS (athero-prone) correlates to cobblestone EC shapes with randomly oriented cytoskeletal structure [5, 21, 22]. Thus, EC elongated and cobblestone shapes are associated with athero-protective and athero-prone regions of the vasculature, respectively. Figure 3.2 C taken from Davies, et al., [5] demonstrates this dramatic change in EC morphology very clearly through a scanning electron micrograph (SEM) of the endothelial lining in a curved vascular region where the FSS changes from high and unidirectional to low and oscillatory. In the case of EC elongation, the sequence of cytoskeletal alignment and roles of individual cytoskeletal components will be discussed further in Chapter V. While cytoskeletal reorganization is thought to occur to accommodate FSS [22], it is not known if the resulting EC shapes and cytoskeletal structures have functional consequences in the absence of FSS.

Influence of FSS on EC Function: Extensive investigations both in vivo and in vitro have shown that FSS regulates EC function including vasoactive substance secretion, protein and gene expression, and cell metabolism [23, 24]. The functional responses to FSS are time dependent. Initial responses to FSS are the activation of mechanosensitive ion channels and the oscillations in intracellular calcium [25]. These

changes occur in a matter of seconds. Several minutes of FSS induces changes in signaling cascades including mitogen-activated kinases (MAPK) and activation of transcription factors including nuclear factor kappa B (NFκB) [25]. Importantly, it has been shown that FSS ultimately affects EC gene and protein expression directly related to atherosclerosis, and this expression is disparately regulated by high, unidirectional (athero-protective) and low, oscillatory (athero-prone) FSS (Table 3.1). For example, high FSS induces an athero-protective EC phenotype characterized by decreased expression of TF, increased eNOS, decreased VCAM expression, and decreased monocyte recruitment [19]. It has been suggested that cells can distinguish between athero-protective and athero-prone FSS through mechanosensory proteins at the cell surface that transmit the signal throughout the cell via the cytoskeleton to nucleus, focal adhesions, and cell-cell contacts [26, 27]. This cytoskeleton-mediated distribution of signaling throughout the cell is known as “decentralization theory” [27]. Therefore, it is feasible to consider EC shape and cytoskeletal structure as possible regulators of EC function. However, studies investigating the role of EC shape and cytoskeletal alignment as a variable independent of the effects of FSS are limited.

3.4. Surface Engineering and EC shape

Micropatterning, a developing technology used to engineer surfaces for cell adhesion, is used to control cell shape independent of external forces. A variety of methods have been developed in this field, including self assembled monolayers (SAMs), microfluidics, and microcontact printing. Each method utilizes polydimethylsiloxane (PDMS) to create a mold containing the topographical pattern of a silicon template (details described in Common Materials and Methods Section 4.3). The main differences between each method include surface preparation and protein transfer. SAMs require gold coated glass surfaces to preferentially attract the sulfur-containing end of functionalized alkanethiols. The PDMS is used to transfer a pattern of hydrophobic alkanethiols (e.g. methyl terminated hexadacanethiol [$HS(CH_2)_{15}CH_3$]) and the remaining area is back-filled the with hydrophilic alkanethiols (e.g. tri(ethylene-glycol) terminated alkanethiol [$HS(CH_2)_{11}(OCH_2CH_2)_3OH$]). Proteins selectively adhere to hydrophobic regions controlling cell adhesion and spreading. SAMs are complex; requiring extra steps to create gold-coated glass and access to highly purified alkanethiols to promote complete monolayer assembly. Microfluidic and microcontact have become the more widely used techniques for creating micropatterned surfaces due

to their straightforward approach and easy application. Both techniques are described in detail in the Common Materials and Methods Section 4.4. Briefly, microfluidic micropatterning utilizes micropatterned PDMS inverted and sealed onto a glass slide to create channels for incubation with substrate. Microcontact micropatterning adsorbs substrate directly to the micropatterned PDMS and the substrate is transferred to the glass by stamping. Both use blocking agents (e.g. bovine serum albumin, Pluronics) to passivate the remaining non-patterned areas. Micropatterned surfaces have been implemented to study specific cell-substrate and cell-cell interactions, as well as the consequences of controlled cell spreading and cell shape. Studies investigating shape-dependent cell function on micropatterned surfaces are reviewed below.

Cytoskeleton: Bovine capillary endothelial cells (BCEs) on both 10 μm and 30 μm wide micropatterned lanes elongated within 48-72 hours with aligned actin [28]. This actin alignment was also commonly observed in other investigations of EC elongation on micropatterned lanes [28-30], demonstrating a link between EC elongation and actin alignment that was independent of FSS. Alignment of the cell adhesion component vinculin, which is linked to actin, also was seen in bovine aortic ECs (BAECs) on grooved 3.5 μm wide micropatterned lanes with varying micron to nano-scale depths [30]. In a study investigating regulation of the cytoskeleton, HUVECs on micropatterned lanes were observed to have a thick dense peripheral band with few centralized actin fibers [31]. The lack of actin stress fibers ultimately lead to apoptosis [31, 32]. Transfecting the HUVECs with constitutively active Rho, a GTPase that regulates actin dynamics, increased actin fiber formation and phosphorylation of focal adhesion kinase (p-FAK) in HUVECs on the 15 μm wide lanes, which subsequently rescued the HUVECs from apoptosis [31]. Thus, using micropatterned surfaces to control EC shape also can dictate cytoskeletal structure, and therefore micropatterning can be utilized to determine cytoskeletal structural effects on cell functions.

General cell functions: Cell shape and surface area has also been shown to regulate apoptosis, proliferation, and differentiation [33]. Chen, et al., extensively studied these shape-dependent cell functions in bovine capillary ECs (BCEs) using micropatterned surfaces [28, 33, 34]. They found BCEs restricted to small, square areas of <500 μm^2 induced cell rounding and apoptosis [28, 33, 34], while increasing the square area to >1500 μm^2 promoted cell proliferation [28]. BCE proliferation rate increased with surface area (SA) and was optimal at >2200 μm^2 [28]. DNA synthesis was also directly correlated with the SA of BCE, but did not depend on ECM contact

area [35], suggesting that the SA of BCE regulated cell proliferation in a manner that was independent of the extent of interaction with the ECM. Interestingly, on micropatterned 10 μm fibronectin (FN) lanes, when the SA of BCE was limited to 1000 μm^2, the BCE became quiescent and underwent capillary differentiation [28]. On both micropatterned 10 μm and 30 μm wide FN lanes, BCEs became elongated and remodeled the underlying FN into a fibrillar structure within 6-24 hrs of adhesion [28]. BCEs on 30 μm lanes maintained this fibrillar FN structure, but BCEs on 10 μm lanes showed dramatic reorganization of FN into a large tendril within 48-72 hrs [28]. Taken together, this data indicates that EC shape has a critical role in the regulation of fundamental cell functions

Migration: BAECs on the 15 μm wide lanes demonstrated significantly accelerated migration rates in the direction of the lane compared to 30 μm lanes and control surfaces [36]. The BAECs on 15 μm and 30 μm wide micropatterned lanes had comparable SA and but significantly different shape indices, a measure of cell roundness, of ~ 0.3 and ~ 0.5, respectively [36]. Thus, the increased migration speed on 15 μm wide lanes is attributed to cell shape and not SA [36]. It should be noted that on micropatterned 15 μm collagen lanes the SI of BAECs (~0.3) is similar to the SI of BAEC under athero-protective laminar flow in-vivo and in-vitro [36]. Micropatterned lanes created with step increases in collagen substrate concentration revealed that BAECs migrated towards increased substrate concentration where they formed larger focal adhesions (FA) and had increased spreading area [37]. This cell migration towards more adherent cell surfaces is referred to as haptotaxis. A threshold of 6 dynes/cm^2 FSS applied opposing the direction of haptotaxis was required to overcome this preferred migration direction [37]. An in-depth evaluation of BAECs on 20 μm wide fibronectin lanes also found that the elongated BAECs primarily migrated parallel to the direction of the lane [38]. When 15 dynes/cm^2 FSS was applied either parallel or perpendicular to the direction of the BAEC on micropatterned lanes migration rate decreased and no preferential direction was established [38]. This migration due to the application of external forces is referred to as mechanotaxis. Interestingly, BAECs on nonpatterned surfaces exposed to the same FSS preferentially migrated in the direction of FSS [38]. Thus, BAEC shape dramatically affects the response to mechanical force and resulting mechanotaxis.

Gene Expression: Human umbilical vein ECs (HUVECs) on circular and spindle shaped micropatterns of varying diameter showed decreases in eNOS production

dependent on EC shape and pattern diameter [29]. HUVECs on spindle micropatterns had less eNOS than HUVECs on circular micropatterns, both compared to control nonpatterned HUVECs, and within each shape (circular or spindle) the eNOS levels declined with decreasing diameter [29]. HUVECs elongated on 20 μm wide micropattern lanes or rounded on 60 μm diameter micropatterned circles, showed increased mRNA levels of intracellular adhesion molecule-1 (ICAM) that were five and three times greater than non-patterned controls, respectively [39]. Mouse lymph node ECs (MLECs) on the same micropatterns described above (20 μm wide lanes and 60 μm diameter or circles) used to induced elongated and circular cell shape showed that elongated MLECs and circular MLECs had no significant difference and a 1.5 times increase in VCAM expression compared to control non-patterned cells, respectively [39]. Overall, this evidence suggests that EC elongation can influence regulation of specific genes involved in vascular health.

3.5. Research Purpose

The studies reviewed above are beginning to unlock the role of cell shape in the regulation of cell functions. Furthermore, several studies have shown that the stability of the cytoskeleton can orchestrate gene transcription and protein expression [40, 41]. In particular, the expression of the important molecules including NFκB, IL-1β, and TGF-β all have been linked to actin and microtubule dynamics [42, 43]. It is the hypothesis of this research that EC shape and cytoskeletal structure mediate EC regulation of atherosclerosis-related cell functions. To investigate this, EC shape was controlled using micropatterned surfaces, creating elongated ECs on collagen I lanes. The aims were designed to evaluate the role of EC shape on (1) cytoskeletal alignment, (2) ECM deposition, (3) inflammation, and (4) thrombogenicity. Resulting insights into vascular pathology provided by a fundamental understanding of the role of EC shape may lead to improved therapeutic strategies. For example, understanding how EC shape influences cell function will be important for designing more efficient approaches for creating endothelialized cardiovascular devices.

3.6. Vascular Grafts

In 2005, over 600,000 people in the United States alone required treatment for blocked or narrowed arteries due to atherosclerotic plaques [44]. Common treatments include replacing or bypassing the diseased vascular regions with a new vessel, usually

taken from the saphenous vein or mammary artery, or other mechanical interventional procedures for arterial revascularization or repair (e.g. angioplasty) [44]. In 30% of patients that require vascular bypass surgery there are not suitable autologous sources of vessels available [44]. The success of small caliber synthetic replacement vessels, e.g., expanded polytetraflouroethylene (ePTFE), is severely limited due to lack of compliance, graft thrombogenicity, and robust wound healing responses leading to intimal hyperplasia. A five year study of small caliber ePTFE reported a patency rate of 38% compared to 68% for autologous vessel grafts [45, 46]. It is widely agreed upon that ECs are required to improve synthetic graft patency [44].

Since realizing the need for a luminal endothelial covering 20 years ago, attempts to endothelialize graft surfaces have included single or two-stage seeding processes [44]. Single stage seeding of vascular grafts involves extracting the ECs and seeding them on the graft surface within a single operation [44, 45]. While this method showed promising results in animal models [47], increased patency rates have not been seen in human patients [48]. The advantages of this method are the short time frame in which the EC seeding takes place and lack of ex vivo manipulation which can lead to sterilization issues and can be costly [44, 45]. The disadvantages are the low EC numbers obtained from the endothelial extraction and insufficient EC adhesion time needed to resist FSS [44, 45]. Two-stage seeding uses an EC extraction step, ex vivo EC expansion using tissue culture, and ex vivo adhesion to the graft surface [44]. Several clinical trials using this method have shown improved patency rates compared to synthetic graft alone [49-53]. Advantages of this method are the large cell numbers obtained during cell culturing and the additional adhesion time [44]. The disadvantages are the time requirements (several weeks), the need for multiple operations, and the cost and sterilization issues associated with prolonged ex vivo manipulation [44]. Some researchers have taken this method a step further and applied FSS-preconditioning to ex vivo endothelialized synthetic grafts [54-57]. The FSS-preconditioning steps are used to (1) enhance EC retention due to EC remodeling under FSS and (2) promote healthy EC function. This additional pre-conditioning step did demonstrate increased EC retention and graft patency rates in animal models [54-57]. However, the two-step seeding process, with or without the addition FSS pre-conditioning step, has not become widely used due to the disadvantages listed above and because it is impractical for emergency situations.

Since the single-step seeding process is more desirable for vascular graft applications, improvements to the process are being developed. A variety of biochemical coatings have been applied to the graft surface to enhance EC retention and decrease thrombogenicity. These coatings include matrix molecules (e.g. collagen, fibronectin), peptide fragments (e.g. RGD), and anticoagulant conjugated proteins (e.g. albumin-heparin), to name a few [45]. While coating the graft surface begins to address EC adhesion, none of them work to promote the appropriate EC function (e.g. decreased monocyte recruitment). The results of this research could provide evidence for a promising alternative approach to creating functional ECs in a single-step seeding process using micropatterned surfaces. It has already been shown that BAECs on textured 95 μm wide and 32 μm deep micropatterned polymer surfaces exposed to 60 dynes/cm^2 FSS had increased cell retention compared to controls [58], However, investigations of micropatterned surfaces to create functional ECs are limited and do not address thrombogenic and athero-protective EC functions. This research uses micropatterned lanes to create elongated ECs to evaluate EC functions that are both important in the regulation of atherosclerosis, and crucial for promoting the success of vascular grafts including: (1) cytoskeletal alignment, (2) ECM deposition, (3) non-immunogenic surface, and (4) decreased thrombogenicity. If successful, micropatterning the surface of vascular constructs, including grafts and stents, could provide a new approach to increase the success of single-step EC seeding by increasing EC retention and regulating EC function.

3.7. Summary

In vivo, ECs assume an elongated shape that is athero-protective in relatively long, straight vessels where FSS is uni-directional. In contrast, ECs assume a cobblestone shape in athero-prone bifurcated and curved vessels, where FSS is low and oscillatory. There have been many investigations concerning the effect of the blood FSS on EC functions that may contribute to atherosclerosis, including ECM production and EC gene and protein expression. However, the influence of cell shape alone on atherogenic cell functions is unknown. Thus this research utilized micropatterning of surfaces to control cell shape, thereby allowing determination of whether EC shape regulates cytoskeletal alignment, ECM deposition, inflammation, and thrombogenicity.

Table 3.1 FSS-EC expression and function

EC Response	High, Unidirectional FSS	Low, Oscillatory FSS
Shape	•elongated/elliptical [16, 59]	•cobblestone [16, 59]
Cytoskeleton	•Aligned parallel to FSS [27, 59-61]	•Randomly oriented [27, 59-61]
Proliferation	•decreased [62, 63]	• increased [62, 63]
Apoptosis	•decreased [19, 63]	•increased [19, 63]
Vascular Permeability	•decreased [19, 64, 65]	•increased [19, 64, 65]
ECM		
Collagen IV	• thicker fibers formed vs. to static [66] • randomly oriented [66]	• thicker fibers formed vs. to static [67] • randomly oriented [67]
Fibronectin	• thicker fibers formed vs. to static, fibers align with flow [66] • 1.8x increase at 48 hrs vs. to static [66] • downregulated gene expression [62]	• thicker fibers formed vs. to static, randomly oriented fibers [67] • 2.96x increase at 48 hrs vs. to static • upregulated gene expression [62]
Laminin	• thicker fibers formed vs. to static, randomly oriented fibers [66] • 2.3x increase at 48 hrs vs. to static [66]	• thicker fibers formed vs. to static, randomly oriented fibers [67] • 5.67x increase at 48 hrs vs. to static [67]
Inflammation		
E-selectin	•no change in mRNA, decrease in protein translation (TNF- α stimulated) [68] •decreased gene expression [62]	•increase protein expression [69] •increased gene expression [62]
VCAM-1	•decreased protein expression after stimulation with TNF-α [68] •decreased gene and protein expression [19, 63, 70] • no change in expression [71]	•30x increase in expression vs. static [72] • induced mRNA expression vs. static [73] •increase gene and protein expression [62] •no change in protein expression [69]
ICAM-1	•increased gene expression [19, 71, 74, 75] •no effect on gene or protein expression [76]	•increase protein expression [69] •increase gene expression [62]
MCP-1	•initial increase at 4 hrs, followed by decreased expression [77] •decreased gene expression [62]	•sustained increase [19, 76, 78] •increased gene expression [62]
Coagulation		
TF	• transient increases in TF over 12 hrs [79] •no change in TF expression [80]	•increase in TF mRNA and protein [80]
TFPI	•increase in TFPI mRNA and protein [80] •increase in TFPI secretion [81, 82]	•no change in TFPI expression [80]
vWF	• 1.8x increase in mRNA at 26 hrs [83] •no effect on mRNA, increased secretion [84]	
TM	• early transient increases followed by significant downregulation [85] • 330% and 200% increase at 8 and 24 hrs, respectively [86]	•no change in TM expression [85]
eNOS	•upregulated eNOS and increased production of NO [76, 87-90]	•no change in eNOS or production of NO [76, 90] •decrease in eNOS gene and protein [88]

Chapter IV

Common Materials and Methods

4.1. Endothelial Cell Isolation and Maintenance

Mature EC Isolation: Carotid arteries were harvested from male baboons and placed in 1% antibiotic:PBS buffer. The carotid arteries were cleaned, rinsed, and digested with 600U/ml collagenase for 5 minutes followed by mechanical disruption [91]. EBM (Lonza) was dripped through the carotid artery to dislodge the ECs. The ECs were plated on 50 µg/ml collagen I (BD Biosciences) coated 6-well plates in EGM-2 (Lonza) supplemented with 8% fetal bovine serum (FBS, Hyclone).

EC maintenance: ECs were incubated at 37^{o}C and 5% CO_2 and maintained in the media in which they were isolated. At the first passage, ECs were trypsinized and expanded onto 50 µg/ml collagen I coated flasks and maintained in EGM-2 media with 8 % FBS. Media was exchanged every 2 days and ECs were maintained through passage 6. Low passage cells were frozen at 1x10^{6} cells per cryogenic tubes in EGM-2 supplemented with 40% FBS and 10% dimethylsulfoxide (DMSO) and frozen in freezing canisters (Nalgene^{TM}) containing isopropanol at -80^{o}C for 24 hours. The cell vials were transferred to a liquid nitrogen tank for long term storage.

4.2. Confirmation of EC phenotype

Immunofluorescent staining (described in section 4.8) was used to confirm the presence of important endothelial markers. Prior to fixation and staining, a live Dil-AcLDL uptake assay was performed. AcLDL (2.5 μg/ml) was added to the media for one hour, followed by 10 minute incubation with normal media and fixation. Monoclonal primary antibodies for VEGFR2 (1:10, clone 260.4, Sigma), VE-CAD (1:10, clone F-8, Santa Cruz Biotech.), CD-31 (1:50, clone JC/70A, Biocare Medical), TM (1:10, clone 1009, Dako), vWF (1:10, clone F8/86, Dako), and eNOS (1:10, clone 6C6, Zymed) were followed by secondary antibody Alexa Fluor 488. Staining of vWF included a permeabilization step (see Section 4.8). Staining was visualized and imaged at 40 X.

4.3. Silicon Template and PDMS Stamps

Micropatterns were designed using AutoSketch (Autodesk) and printed on photomylar masks at 20,000 dpi at CAD/Art Services Incorporated (Bandon, Oregon). Silicon templates for micropatterning were fabricated by Standford Microfluidics Foundary or were made at Boston University (BU) and gifted from Dr. Tania Vu (OHSU) or Dr. Joe Tien (BU). The template fabrication process requires a clean room (Class 10,000) and employs photolithography by means of light sensitive photoresist. Briefly, a thin layer of photoresist (positive or negative) is spun on the surface of a clean silicon wafer followed by a soft baking step. UV light is shown through the photomylar mask onto the photoresist-coated silicon wafer. After UV exposure, the wafer is placed in developer and the portion of photoresist exposed to UV light either dissolves (positive photoresist) and unexposed regions solidify or the portions exposed to UV light solidifies (negative photoresist) and unexposed regions dissolve. A final hard baking step solidifies the remaining photoresist on the silicon wafer creating a template with topographical features corresponding to the micropattern design on the photomylar mask. The template was fluorinated with 1H, 1H, 2H, 2H-Perfluorooctyltricholorsilane to create a hydrophobic surface, which aids in the detachment process when creating polydimethylsiloxane (PDMS) molds. PDMS was made by mixing at a 10:1 wt/wt ratio, the 184-elastomer base with the elastomer curing agent (Sylguard, Dow Corning). The PDMS mixture was poured onto the silicon templates, placed under a vacuum to remove

bubbles, and cured in an oven for 2 hours at 80^{o}C to polymerize. The polymerized PDMS was carefully peeled from the surface and stored at room temperature.

4.4. Surface Preparation

Two widely accepted micropatterning methods were used throughout these studies, (1) Microfluidic and (2) Microcontact. Both methods have been described by Folch and Toner [92]. For the microfluidic method (Fig. 4.1 A) , the PDMS was cut into approximately 1 cm^2 stamps and sealed onto a glass surface with the micropattern-side down forming channels. These microfluidic channels were surrounded on one end with 50 µg/ml collagen I. A vacuum was applied to the other end of the channels to pull the collagen I into the channels where it was incubated for 1 hour. After incubation, the surface and channels were rinsed with PBS, the stamp was removed, and the entire slide was treated with 5 mg/ml heat-denatured bovine serum albumin (BSA, Sigma) for 1 hour to passivate the non-collagen coated surfaces. The slides were rinsed several times with PBS in preparation for EC plating. For the microcontact printing method (Fig. 4.1 B), PDMS stamps were cut into approximately 1 cm^2 stamps and the micropattern-side was incubated with collagen I for 1 hour at room temperature. After incubation, the PDMS stamp was rinsed several times with PBS, dried, and placed micropattern-side down on a glass slide over night at 4^{o}C to transfer the collagen I micropattern to the glass surface. The PDMS was then carefully removed; the glass is rinsed and incubated with 5 mg/ml BSA for 1 hour. After rinsing, the slides were ready for cell plating (Fig. 4.1 C). Control non-patterned surfaces were created by incubating a droplet of collagen I on the glass for 1 hour followed by 1 hour of 5 mg/ml BSA.

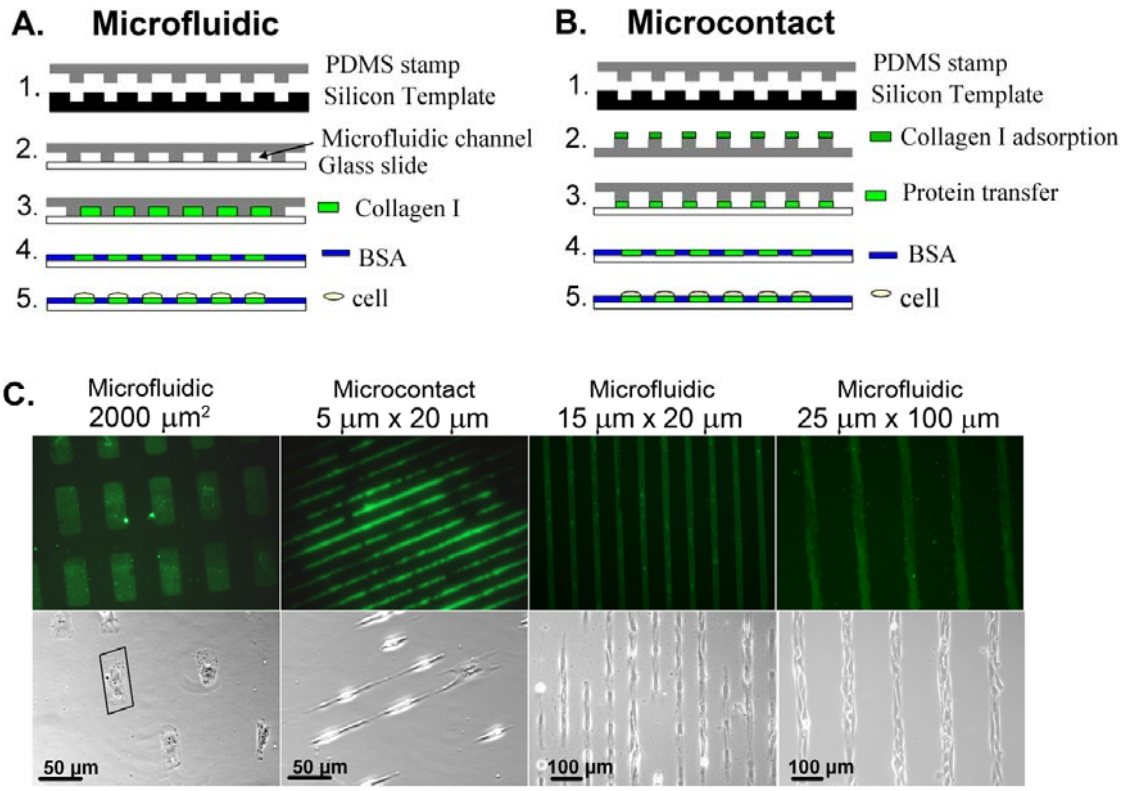

Figure 4.1 Micropatterning methods and representative images. **A.** Schematic of microfluidic micropatterning. **B.** Schematic of microcontact micropatterning. **C.** Images of micropatterned surfaces and cells employing both micropatterning methods.Top: Image of micropatterned FITC-collagen I with micropattern feature dimensions and method for application listed above. Bottom: Corresponding image of ECs on the micropatterned FITC-collagen I surface.

4.5. Endothelial Cell Plating

Isolated ECs were used until passage 6. Confluent ECs were trypsinized using recombinant trypsin (rTypLE, Invitrogen) to prevent proteolysis of cell adhesion molecules. ECs were plated on micropatterned and control non-patterned surfaces at $4x10^4$ cells/cm^2 in EGM-2 (Lonza). At 1 hour, non-adherent ECs were removed and media was replaced.

4.6. Flow Studies

Two parallel-plate flow chambers were used to apply FSS to ECs (Aims 1, 3, & 4). One chamber was created in our lab to accommodate rectangular slides (Aim 1) and the other was purchased from Glycotech for circular slides (Aims 3 & 4). The chamber designed by our lab consisted of two parallel plates with a 250 μm spacer above the glass slide. Metal plates with ten screws were used to secure and seal the chamber (Fig. 4.2 B). The Glycotech chamber also utilized parallel plates with a 254 μm spacer, but this chamber is sealed using a vacuum through a single port that equally distributes suction through several small holes around the perimeter of the chamber (Fig. 4.2.B). For both chambers, EGM-2 media was pulled through size 14 tubes (Masterflex, Cole Palmer) from a reservoir by a peristaltic pump (Cole Palmer) at a controlled flow rate and passed through one pulse dampeners before entering the flow chamber, where the surface of ECs were exposed to FSS (Fig. 4.2. A). Flow rate and the distance between the parallel plates controls the FSS exerted on the EC surface [9, 17]. For steady laminar flow of a Newtonian fluid, mean FSS is calculated by the following formula:

$$FSS = \tau_{\omega} = \frac{6\mu Q}{h^2 b}$$

where μ= viscosity, Q=flow rate, h=chamber height, and b=chamber width. ECs were exposed for either 20 hours (Aim 3 & 4) or 24 hours (Aim1) to fully-developed, laminar flow at FSS of 12.5 dyne/cm^2. The FSS was slowly ramped up in 5 minute increments over 30 minutes starting at 2.5 dynes/cm^2.

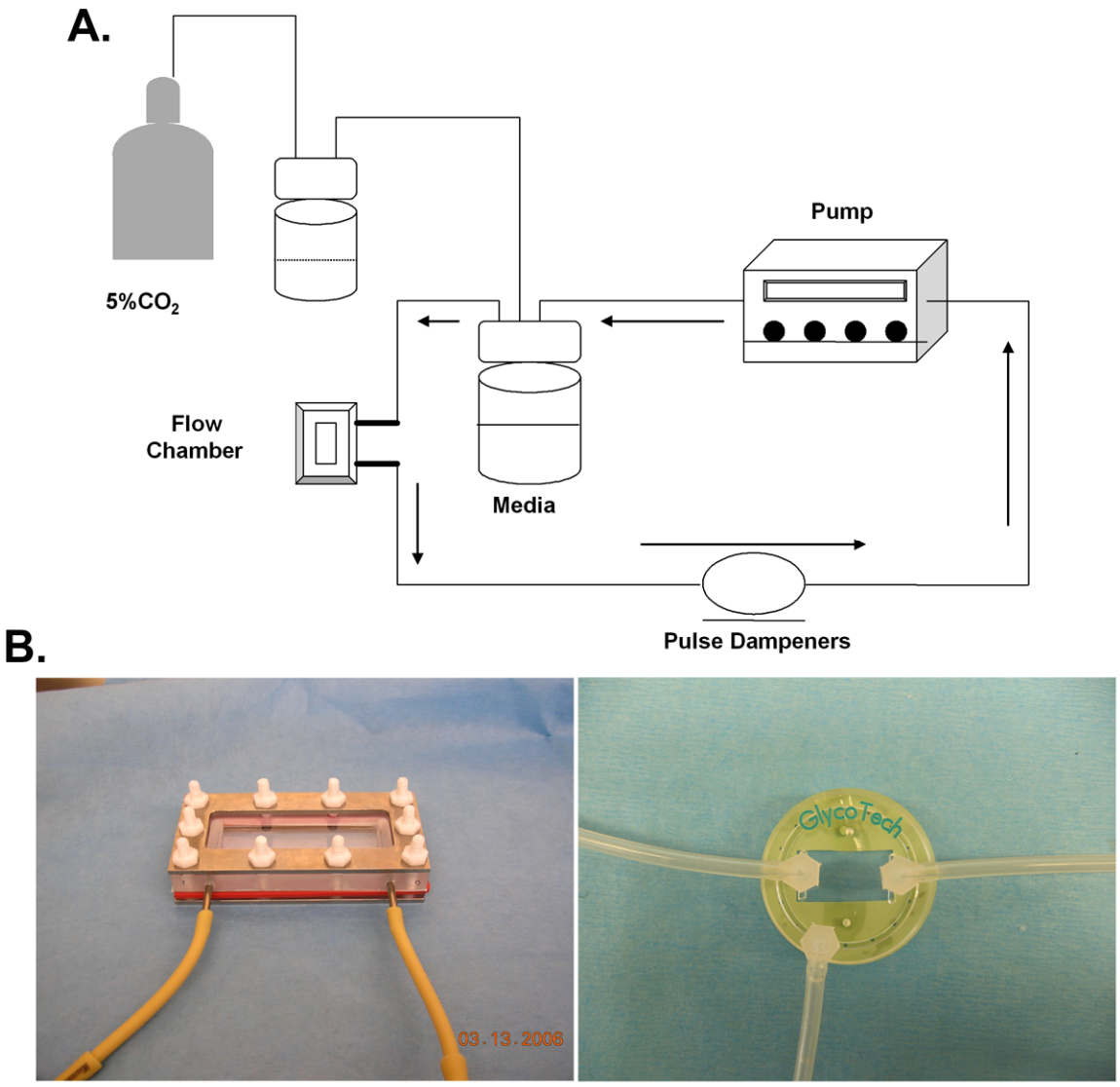

Figure 4.2. Diagram and images of flow chamber setup. **A.** Diagram of flow loop used in flow studies. The media, CO_2 container, flow chamber, and pulse dampener were all in an incubator maintained at 37^{o}C and 5% CO_2 for the duration of the study. **B.** Images of the two flow chambers used in this research. Left: Parallel plate flow chamber designed in the lab to accommodate rectangular slides. Right: Parallel plate flow chamber purchased from Glycotech used for circular slides. The third port located on the edge of the chamber with connected tubing is for is attachment to an external vacuum to maintain a seal between the flow chamber and slide containing the ECs.

4.7. Shape Index

Microscopy images of ECs were quantified using NIH Image J. ECs were outlined to obtain pixel measurement of the perimeter and the cell was filled in to obtain the number of pixels that made up the surface area. At least 10 cells were measured in each image and at least three images were measured for each condition. The shape index, a measure of cell shape, was calculated using the following formula:

$$ShapeIndex = \frac{4\pi SA}{p^2}$$

where SA= surface area, and p=perimeter. A shape index of 1 represents a circle while a shape index of zero represents a line.

4.8. Immunofluorescent Staining

ECs were fixed in 3.7% paraformaldhyde (PFA) for 10 minutes, blocked with FX enhancer (Invitrogen) for 30 minutes and with 10% Goat Serum for 30 minutes. If necessary, ECs were permeabilized prior to blocking with 0.1% Triton in PBS for 5 minutes. ECs were rinsed several times with PBS. Mouse anti-human primary antibodies were diluted in PBS with 1% BSA to the desired titer and incubated for one hour, using mouse IgG1 (clone DAK-GO1, Dako) as a control. Rinsing was repeated and secondary goat anti-mouse Alexa Fluor antibodies (488 or 568, Invitrogen) were diluted 1:500 in the same buffer and incubated for 30 minutes. After repeating the rinsing step, DAPI nuclear stain was diluted to 300 nM and incubated for 5 minutes. ECs were rinsed a final time and the slide was sealed with coverslips using 10% glycerol:PBS. Images were taken at 40X on an inverted Nikon Eclipse Microscope.

4.9. Cytoskeletal Alignment Quantification

The cytoskeletal components actin and microtubules were visualized using immunofluorescent staining as described above including the permeabilization step. Primary antibody mouse-anti-human β-tubulin (Sigma) was used for microtubules with secondary Alexa Fluor 488. Following microtubule staining, actin was stained using Alexa Fluor 568 conjugated Phalloidin (Invitrogen). The stained ECs were imaged at 40X.

A custom Matlab image analysis program was used to quantify the alignment of the stained cytoskeletal components. The image was processed in two major steps: (1) Laplacian edge detection to highlight the cytoskeletal fibers, and (2) Radon transform to determine the distribution of fiber orientation angles.

Edge detection is a widely used form of image analysis used to determine the boundaries of objects. Edge detection is based on differentiation by determining changes (i.e., gradients) in gray scale values between neighboring pixels. Laplacian edge detection is commonly used because it is an isotropic neighborhood operator, meaning that the filter or kernel is designed to take neighboring pixels into account and it detects edges equally in both the -x and -y direction [93]. The Laplacian operator approximates the second derivative of the image [93, 94]. The second derivative method takes advantage of the fact that the inflection points in the original signal (which are representative of edges in the image) become zero in the second derivative of the signal. Therefore, Laplacian edge detection highlights regions in the original image that transition from dark to light. Compared to other edge detection methods, such as the single derivative gradient vector, Laplacian edge detection is preferable for detecting lines since the position of a line is characterize by extreme transitions from dark to light [93]. The Laplacian operator (see Appendix A for MATLAB code) was separately convolved with the original image in the –x and –y direction to create the Laplacian image (Fig. 4.3). However, this could have been accomplished in a single step using a 2-dimensional convolution filter [93].

A Radon transform method was used to determine the location and features of objects in the image. Radon transforms utilize projection beams oriented at a spectrum of angles θ and located at a series of distances from the origin r [93]. The Radon transform calculates the line integral by summing the pixel intensities along the length of the projection beam [93]. The result determines the location (r, θ) of features in an image [93]. A Radon transform was applied for angles ranging from -90^{o} to 90^{o} to the Laplacian image to determine the angles at which the cytoskeletal fibers were oriented. The results were plotted as total pixel intensity versus angle θ (the distance from the origin r is not a critical factor since we are only interested in the fiber angle and not spatial location) and normalized to the area under the curve to obtain the distribution of orientation angles found throughout the image. This plot is referred to as the probability density function, PDF (Fig. 4.3).

The PDF was used to quantify the degree of cytoskeletal alignment using two methods: (1) variance about the peak angle, and (2) signal entropy. Variance measures the distance between data points and their mean value [95]. In this case, the variance was calculated with respect to the peak angle, which was the maximum value in the PDF. The variance (σ) of the distribution was calculated as:

$$\sigma^2 = \sum_{i=1}^{N} \left(\theta_i - \theta_{peak}\right) P\left(\theta_i\right),$$

where θ is the angle and $P(\theta_i)$ is the probability of the edge being oriented at angle θ (Fig. 4.3). Entropy is a measure of the amount of disorder in a system and has only recently been described by Bercher and Vignat as a method to analyze continuous signals [96]. The entropy $H(x)$ of the PDF was calculated using the following formula:

$$H\left(x\right) = -\sum_i p_i \log_2 p_i \text{ , [96]}$$

where p_i is the PDF of angles ranging from -90 ^{o} to 90^{o}. Large values of entropy indicate more disorder in the signal and therefore more randomly oriented cytoskeletal structures (Fig. 4.3). Micropatterns were oriented horizontally, which was defined as 0^{o}.

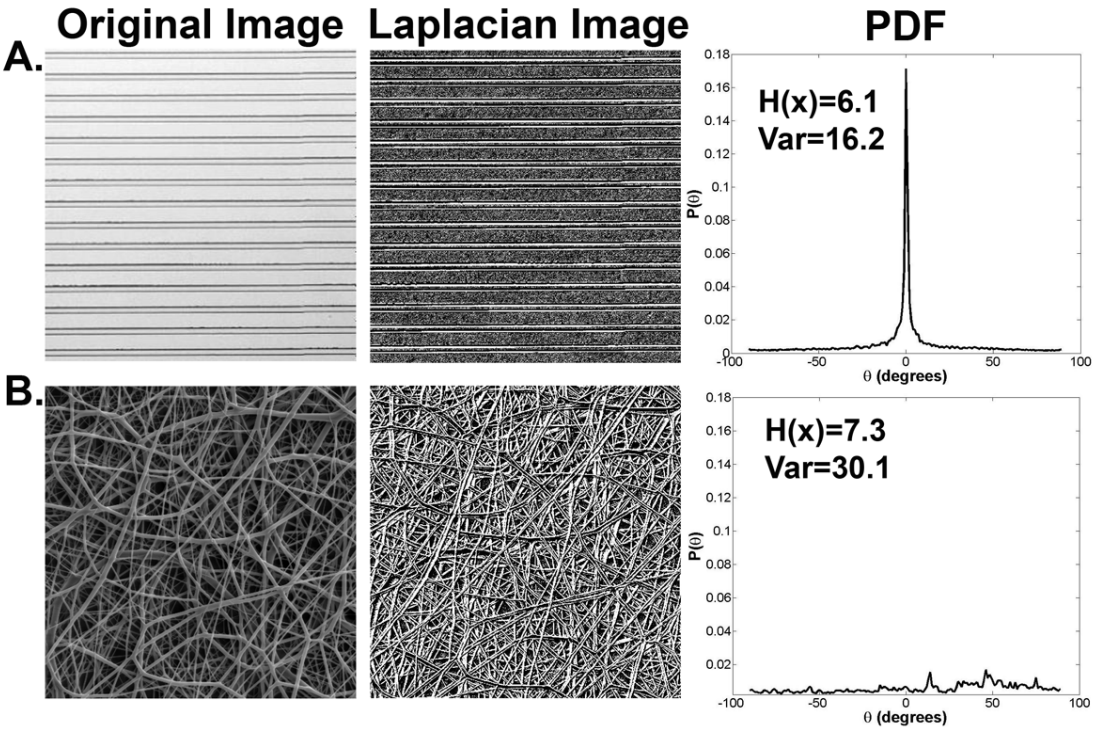

Figure 4.3. Matlab image analysis of feature orientation. Examples of the applied Matlab image analysis program designed to determine orientation angle of features in an image. **A.** Image of PDMS with 25 μm wide lanes with 100 μm spacing, representing aligned image features. **B.** Image of electrospun elastin (provided by Kathy McKenna), representing randomly oriented image features. *Left:* the original image for each example. *Middle:* the generated Laplacian image highlighting edges found in the original image. Edges are represented in white due to subtraction of the Laplacian image from the original image. *Right:* Normalized probability distribution function plotted as probability of the feature orientation versus angle. In example A the energy of the signal is found at 0^o while example B has low energy distributed throughout the full range of possible orientation angles. The entropy [H(x)] and variance [Var] was calculated for each example. Example A has low entropy of 6.1 and variance about the peak angle of 16.2^o compared to example B, which has entropy of 7.3 and variance about the peak angle of 30.1^o.

4.10. Quantitative Polymerase Chain Reaction (qtPCR).

Total RNA samples were obtained from cell lysates using an RNA Mini Isolation Kit (Zymo Research) followed by RNA Clean Up (Zymo Research) to remove any remaining genomic DNA. Reverse transcription was performed using SuperScript III Reverse Transcriptase (Invitrogen). PCR reactions were made using SYBR Greener PCR Master Mix (Invitrogen). The primers for the genes of interest are listed in Table 1. PCR reaction in the 7500 Fast System thermocycler was run at 95^{o}C for 2 min, for 40 cycles of the following sequence: 95^{o}C for 25 sec, T_m (melting point) of primer for 30 sec, and 72^{o}C for 30 sec. Finally, the temperature was held at 60^{o}C. Samples were run on 2% Agarose gels at 100-150 V to confirm specific DNA amplification. Quantitative results were obtained directly from the ABI 7500 Fast System using the ddCt method and taking primer efficiencies into account.

Table 4.1. Primer Sequences

Gene Name	Forward Primer 3'-5'	Reverse Primer 3'-5'	Amplicon Length (bp)
TF	caccgacgagattgtgaaggat	ttccctgccgggtaggag	69
TFPI	gactccgcaatcaaccaaggt	tgctggagtgagacaccatga	70
TM	gcattcgggcttgctcatag	caaaagcgccaccacca	61
vWF	cctattggaattggagatcgcta	cttcgattcgctggagcttc	97
eNOS	atctccgcctcgctcatg	agccatacaggattgtcgcct	64
MCP-1	cagcagcaagtgtcccaaag	gaatcctgaacccacttctgctt	93
E-Selectin	gatgagaggtgcagcaagaa	ctcacacttgagtccactgaag	147
ICAM-1	cggctgacgtgtgcaggctcg	cacctcggtcccttctgaga	127
VCAM-1	agtgatcccaacaggctcg	cagcgtttccagaggtgatac	123
KLF-2	caccgggtgtagagtagagg	aaatgccgcagacagtacaa	81
GAPDH	cctcaacgaccactttgtca	ttactccttggaggccatgt	104

CHAPTER V

Endothelial Cell Cytoskeletal Alignment Independent of Fluid Shear Stress on Micropatterned Surfaces

5.1. Abstract

ECs in athero-protective regions are elongated with actin and microtubule fibers aligned parallel to the direction of blood flow. Fluid shear stress (FSS) affects EC shape and functions, but little is known about shape-dependent EC properties, such as cytoskeletal structure, that are independent of FSS. To evaluate these properties, ECs were elongated on micropatterned 25 μm wide collagen-coated lanes (MPECs) and characterized by cell shape index, actin and microtubule alignment, and polarization of the microtubule-organizing center (MTOC). ECs on non-patterned surfaces were also exposed to FSS to induce elongated shape and alignment of the cytoskeleton. MPEC elongation was microtubule-dependent (and actin-independent); shape indices and cytoskeletal alignment were comparable to FSS-elongated ECs. Cytoskeletal alignment was lost when MPECs were exposed to perpendicular FSS, but not parallel FSS. MTOC polarization was FSS-dependent. Thus, by isolating EC elongation and cytoskeletal alignment from FSS, micropatterning creates a platform for studying EC shape-related cellular functions that are independent of FSS.

This research was originally published in Biochemical and Biophysical Research Communications. Vartanian, K.B., Kirkpatrick, S.J., Hanson, S.R., and Hinds, M.T., "Endothelial cell cytoskeletal alignment independent of fluid shear stress on micropatterned surfaces," *Biochemical and Biophysical Research Communications.* 2008;371(4):787-92.

5.2. Introduction

Vascular endothelial cells (ECs) may be characterized as either elongated or cobblestone. Elongated ECs have actin and microtubules aligned parallel to the cell's long axis and are found in athero-protected regions of the vasculature exposed to high, unidirectional FSS [16, 59]. In contrast, cobblestone ECs have randomly oriented actin and microtubules and are found in athero-prone vessels exposed to low, oscillatory FSS [61]. The overall goal of this research is to link EC shape and cytoskeletal structure to EC function independent of FSS. To do this, the cytoskeleton of ECs in the proposed model (micropatterned lanes) must be fully characterized to validate that the EC shape and cytoskeleton is comparable to ECs exposed to high, unidirectional FSS in vivo or in vitro. This aim investigates the major cytoskeletal components, actin and microtubules, of micropattern-elongated ECs (MPECs) compared to ECs elongated by exposure to FSS.

5.3. Background

5.3.1. The Cytoskeleton

The cytoskeleton is a dynamic structure comprised of actin, microtubules, and intermediate filaments that regulate mitosis, cell shape, migration, and spreading [97]. The profound EC shape difference seen in vivo between athero-protective and athero-prone regions, and in vitro under high, unidirectional or low, oscillatory FSS, indicates profound differences in cytoskeletal arrangement. The cytoskeleton translates mechanical forces from the external environment via transmembrane signaling [98-101]; ultimately leading to the remodeling of actin fibers and microtubules. Intermediate filaments are also influenced by FSS [60], but do not demonstrate FSS-induced alignment or regulation of EC shape [61]. FSS-induced EC elongation and cytoskeletal alignment has been extensively studied in vitro [60, 61, 102, 103].

5.3.2. Actin

Composition: Actin fibers are composed of a string of globular actin (G-actin) monomers wound together to form a tight, flexible two-stranded helix [104]. Actin fibers

polymerize through a fast growing plus end and a slow growing minus end [97]. This actin polymerization takes place in two steps: (1) nucleation, where three G-actin monomers come together to form a nucleation point, and (2) elongation, where ATP-bound G-actin monomers are added to the plus and minus ends [97]. Actin depolymerization occurs when ATP becomes hydrolyzed to ADP, which destabilizes the actin fiber [97]. Actin treadmilling occurs when steady state is reached, defined as identical on and off rates of G-actin, causing the actin fiber to maintain a constant length [104] . These highly dynamic actin fibers are critical in EC elongation since actin assembly has been shown to drive changes in cell shape [103].

Actin Response to FSS: Actin alignment is the most widely studied cytoskeletal component influenced by FSS. Subconfluent ECs rapidly undergo shear-induced elongation and actin alignment in approximately 2 hours. Subconfluent ECs mediate FSS-induced shape change by extending cdc-42 induced fillapodia and Rac-initiated lamellapodia, both of which are generated by actin assembly, to drive EC elongation [103, 105]. In contrast, studies investigating actin alignment in post-confluent ECs show dramatically different shape change mechanisms, independent of fillapodia and lamellapodia extension, that required much longer exposure to FSS to induce EC elongation and aligned actin fibers [102, 103]. Post-confluent ECs initially responded to FSS by depolymerizing their actin fibers [98]. After 8 hours, actin fibers reformed and actin assembly was concentrated at the ends of stress fibers, but at this point the actin fibers assembly was randomly oriented [98, 102]. By 16 hours of FSS, many ECs elongated and aligned with flow, and actin preferentially assembled in the upstream direction [102]. However, of the elongated ECs at 16 hours many did not yet demonstrate actin alignment parallel to flow [102]. Actin alignment was completed by 24 hours but actin polymerization continued throughout the 96 hours measured in this study [102]. Interestingly, Malek and Izumo showed that treating post-confluent ECs with phalloidin, an actin stabilizer, prior to exposure to FSS, did not prevent FSS-induced EC elongation and actin alignment, indicating that actin may not be the only cytoskeletal component that can drive cell shape change [61].

5.3.3. Microtubules

Composition: Microtubules are hollow, stiff, cylindrical tubes formed from the parallel assembly of 13 protofilaments [104]. Protofilaments are comprised of alternating α- and β- tubulin heterodimers [97, 104]. Microtubules are also dynamic structures that

polymerize through a fast growing plus end and a slow growing minus end, but assembly and disassembly is driven by GTP rather than the ATP for actin. The growing end of the microtubules contains a GTP cap, which increases microtubule stability. If GTP hydrolyzes quickly to form GDP, the microtubule becomes less stable and depolymerizes [97]. In contrast, if GTP hydrolysis is delayed, the microtubule undergoes dynamic instability, which is a period of rapid polymerization followed by rapid depolymerization [104]. Typically, in animal cells, the minus end of the microtubules are collected at a common nucleation point referred to as the microtubule organizing center (MTOC) and the plus end extends outward to the cell's periphery [104]. The microtubule network is crucial in cell signal transduction because it provides a highway for protein transport and delivery [103], affecting cell functions including gene transcription and actin assembly [106].

Microtubule Response to FSS: In vivo and in vitro evidence indicates that high, unidirectional FSS induces microtubule elongation and alignment parallel to the direction of flow [6, 30, 103]. The sequence of FSS-induced microtubule reorganization is not well documented, but microtubules have been reported as the first cytoskeletal component to align under FSS [61]. Evidence shows that treating ECs with the microtubule destabilizer nocodozale abolishes EC elongation and actin alignment under FSS [61]. Thus microtubule stability is crucial for EC elongation and actin assembly. FSS-dependent polarization of the MTOC has been documented in ECs, but whether the MTOC is upstream or downstream of the nucleus depends on animal age, EC type, and duration of FSS [27]. In general, in arterial ECs, the MTOC localized upstream of the nucleus after long term exposure to FSS [6, 27].

5.3.4. The Decentralization Model

Due to the anatomical location of ECs, the luminal cell surface is exposed to FSS. Despite extensive research, cell surface mechanosensors still have not been identified or implicated in FSS-dependent influences on ECs. Evidence suggests that many parts of a cell respond to the mechanical stimulation imposed by FSS including the cell surface, cell-cell junctions, focal adhesions, and the nucleus [26, 27, 101]. These cellular locations are connected by the cytoskeleton [26]. The decentralization model suggests that mechanotransduction is transmitted by the cytoskeleton throughout the cell, thus initiating the myriad of FSS-induced cell responses. Therefore, the highly dynamic cytoskeleton not only provides cell structure, but is also integral in cell

signaling. The importance of the dramatic reorganization of the cytoskeleton to an alignment network independent of FSS has not been previously investigated.

5.3.5. Summary

ECs in the vasculature have two distinct shapes, elongated and cobblestone, which are associated with athero-protected and athero-prone regions of the vasculature, respectively. EC shape is controlled by the cytoskeletal structure. Therefore, elongated ECs have aligned and elongated cytoskeletal components in the direction of the long axis of the cell and cobblestone ECs have randomly oriented cytoskeletal components. In vivo and in vitro studies indicated that FSS is a major regulator of EC shape and cytoskeletal structure. Under high, unidirectional FSS actin aligns over 24 hours while microtubules are the first component to align and the MTOC localizes downstream of the nucleus. The cytoskeleton has also been shown to mediate cell signaling, and therefore may play an important role in cell function, independent of the influence of FSS. In this study, ECs elongated on micropatterned lanes (MPECs) were quantified with respect to shape index, actin and microtubule alignment, and MTOC polarization to determine if the micropatterned surfaces can induce comparable EC elongation and cytoskeletal structure compared to FSS-induced EC elongation.

5.4. Materials and Methods

5.4.1. Experimental Design

Four conditions were used to fully characterize cytoskeletal structure: (1) ECs elongated on micropatterned lanes (MPECs), (2) ECs elongated by 24 hours of 12.5 dynes/cm^2 FSS, (3) ECs elongated on micropatterned lanes for 24 hours followed by exposure to 24 hours of 12.5 dynes/cm^2 FSS and (4) static cobblestone ECs. Micropatterning techniques, flow studies, quantification of cytoskeletal alignment, and shape index were all executed as described in Chapter IV: Common Materials and Methods. Methods specific to this aim are detailed below.

5.4.2. Surface preparation

The micropattern design of 25 μm wide lanes with 100 μm wide spaces was used for these studies. The microfluidic technique was utilized as described in Common Materials and Methods (Section 4.4).

5.4.3. Flow studies

ECs were incubated on micropatterned and non-patterned surfaces for 24 hours. The parallel-plate flow chamber designed in this lab (described in Common Materials and Methods Section 4.6) was used to apply 12.5 dynes/cm^2 FSS for 24 hours [17]. ECs on micropatterns were oriented either parallel or perpendicular to the direction of flow.

5.4.4. Shape Index and Cytoskeletal Alignment

MPEC shape index and cytoskeletal structure was quantified at 1, 2, 4, 8, 24, and 48 hours to define the sequence of elongation and alignment. Cytoskeletal alignment was also quantified (described in detail in Common Materials and Methods Section 4.9) at 48 hours for all four of the conditions listed in the Experimental Design above.

5.4.5. Cytoskeletal inhibitors.

MPECs were treated for 24 hours beginning at 1 hour or 24 hours after plating with either 1 μM Nocodazole (Sigma), 100 nM Cytochalasin D (Sigma), or the DMSO vehicle. IF staining was used to verify the disruption of the cytoskeletal components and shape index was quantified to determine their effects on micropattern-mediated cellular elongation.

5.4.6. MTOC quantification.

The method to determine the location of the MTOC was adapted from McCue, et al., [6]. Using this approach the ECs were sectioned into three regions with respect to the midpoint of the nucleus: 1 = downstream, 2 = centered, and 3 = upstream (Fig. 5.6 B). The location of MTOC was identified as the region of greatest staining intensity using the NIH Image J analysis program.

5.4.7. Statistical Analysis

All experiments were performed in triplicate; multiple images (N ≥ 3) per experiment were analyzed. Mean values ± standard error of the mean (SEM) are given with representative images. One-way analysis of variance (ANOVA) was used to make comparisons between 3 or more timepoints or conditions. Subsequently, Tukey post-hoc test was used to determine statistically significant differences between the groups analyzed in the ANOVA. Statistical significance required a $p < 0.05$.

5.5. Results and Discussion

5.5.1. Confirmation of EC Phenotype

The carotid phenotype of the baboon carotid ECs used throughout these studies was confirmed using IF. ECs were positive for all EC markers tested including AcLDL uptake, CD31, eNOS, VEGFR2, VE-CAD, vWF, and TM (Fig. 5.1).

5.5.2. MPEC shape index and cytoskeletal alignment

The shape index of MPECs was measured over 48 hours to quantify cell elongation (Fig. 5.2 A). At 1 hour, MPECs had the largest measured shape index of 0.61 ± 0.04 (Fig. 5.2 B), a value comparable to those reported for cobblestone-shaped ECs that have been observed in vivo [16]. After 1 hour, the shape index of MPECs began to decline as the cells elongated. The shape index significantly decreased to 0.35 ± 0.04 at 24 hours (Fig. 5.2 B), a value that is equivalent to the shape index of elongated ECs observed in vivo [16]. The shape indices at 24 and 48 hours were similar (Fig. 5.2 B), indicating that MPEC elongation was complete by 24 hours and maintained for an additional 24 hours.

Actin and microtubule structures were visualized using IF double staining. The actin fibers first formed a dense peripheral band (DPB) with central stress fibers at 1 hour. At 24 hours, most MPECs maintained a DPB, and many centrally-oriented actin stress fibers were present (Fig.5.3 A). In contrast, previous research showed that in FSS-induced EC elongation, early remodeling caused EC actin depolymerization and partial loss of the DPB [98, 102], but after 8-12 hours of FSS, actin fibers reformed and began orienting parallel to flow [98, 102]. In this study, MPEC and FSS-induced EC elongation utilized different actin remodeling strategies to create aligned and elongated

actin. The microtubules of MPECs showed signs of cytoskeletal alignment as early as 1 hour, and the actin and microtubules continued elongating and aligning as the shape index decreased with time (Fig. 5.2 B). This finding is consistent with the observed early alignment of EC microtubules under flow [61].

To quantify actin and microtubule alignment, the peak angle of fiber orientation and the variance about the peak angle were measured (Fig. 5.3 B). Since the micropatterned lanes and adherent ECs were oriented at 0^o, the peak angles for both actin and microtubule fibers were also close to 0^o, resulting in no significant difference between the peak angles over time (Fig. 5.3 B). However, the variance of fiber orientation did change over time. Both MPEC actin and microtubule variance declined significantly at 24 hours (Fig. 5.3 B), corresponding to the decrease in shape index (Fig. 5.2 B). MPEC actin and microtubule orientation maintained this level of variance at 48 hours, indicating that cytoskeletal elongation and alignment were largely complete by 24 hours. Additionally, at a timepoint as early as 1 hour, the variance of actin and microtubule alignment of MPECs was significantly lower than that of non-patterned ECs (ANOVA, $p<0.001$). Thus, the alignment of MPEC actin fibers and microtubules began almost immediately upon initial cell adhesion. In contrast, under FSS-induced elongation of confluent EC actin alignment does not begin until 8-12 hours after the onset of flow [98, 102].

5.5.3. Roles of actin and microtubules in EC elongation

To distinguish the roles of actin fibers and microtubules in MPEC elongation the cytoskeletal inhibitors cytochalasin D and nocodazole were used, which interfere with the polymerization of actin and microtubules, respectively. In particular, cytochalasin D caps the rapidly polymerizing plus end of actin fibers inhibiting further actin assembly and resulting in a net depolymerization of actin fibers [104]. Nocodazole binds the β subunit required for microtubule assembly, thereby sequestering one of the necessary building block required for microtubule formation [104]. The cytoskeletal inhibitors were added 1 hour after plating to determine their effects on MPEC elongation, and at 24 hours to determine their effects on the maintenance of the elongated cytoskeleton. Shape index was measured to determine the degree of elongation after treatment with each inhibitor. Actin and microtubules were stained to visualize cytoskeletal changes (Fig. 5.4 A & B). The addition of the inhibitors at 1 hour or 24 hours after cell plating resulted in comparable shape indices (Fig. 5.4 C). Cytochalasin D disruption of actin

fibers attenuated cellular elongation at 1 hour, and at 24 hours caused MPECs to become less elongated (shape indices of 0.51 ± 0.07 and 0.53 ± 0.02, respectively; Fig. 5.4 C). Structurally, the formation of central actin stress-fibers was eliminated. However, a DPB remained present in most MPECs (Fig. 5.4 A). The cytochalasin D concentration was not increased above 100 nM (e.g., in order to eliminate DPB) since these levels may be cytotoxic [32]. The microtubules in cytochalasin D treated ECs remained intact. Thus, MPECs elongated and maintained an elongated morphology without intact actin fibers, but to a lesser extent than when both actin and microtubules were present. Interestingly, previous studies of EC elongation under FSS have been unsuccessful in demonstrating an effect of cytochalasin D on EC elongation since ECs treated with even low levels of cytochalasin D (40 nM) were unable to resist FSS [61]. However, in an investigation of the role of actin in FSS-induced EC elongation, Osborn, et al., showed that FSS first causes actin depolymerization [98], which was a necessary step for the reformation, remodeling, and alignment of actin fibers that occurs hours later. Taken together, this indicates that actin fibers may not be required for the *initiation* of either MPEC or FSS-induced EC elongation.

Nocodazole treatment at 1 hour completely prevented MPEC elongation, while treatment at 24 hours completely reversed elongation, with resulting shape indices of 0.68 ± 0.06 and 0.69 ± 0.06, respectively (Fig. 5.4 C). These shape indices are similar to the shape index of untreated MPECs at 1 hour after adhesion (0.61 ± 0.04). Structurally, microtubule formation was completely abolished with only diffuse cytosolic staining (Fig. 5.4 B). However, some actin fibers were still present in the form of a DPB and dim central fibers (Fig. 5.4 B). These findings suggest that the presence of actin fibers alone is not enough to promote and maintain cellular elongation; rather, MPEC elongation and maintenance of the elongated structure are dependent upon microtubules. This result confirms previous observations that FSS-induced EC elongation was dependent on the presence of intact microtubules [61].

5.5.4. The effect of FSS on MPECs and non-patterned ECs

To determine the effect of FSS on MPECs, 12.5 dynes/cm^2 FSS was applied for 24 hours. FSS was oriented either parallel or perpendicular to the MPEC long axis. The resulting FSS-dependent cytoskeletal remodeling was compared to that of non-patterned ECs elongated by FSS (Fig. 5.5 A). Both parallel and perpendicular FSS had no significant effect on actin peak angle and angle variance compared to static MPECs (Fig.

5.5 B), a finding that is particularly interesting in the case of perpendicular flow where the direction of FSS opposed the MPEC actin fiber orientation. Many MPECs exposed to perpendicular flow could not resist the FSS and detached, a finding similar to that reported previously in studies with HUVECs on micropatterned lanes exposed to 12 hours of perpendicular FSS [31]. Actin staining of the remaining MPECs exposed to perpendicular FSS indicated maintenance of the DPB, which may have helped resist FSS, as well as condensation of the centralized actin, seen as bright punctuate staining suggesting the formation of globules of actin monomers (Fig. 5.5 A). The formation of globular actin is a marker of apoptosis [32, 107], confirming that even those MPECs remaining after 24 hours of perpendicular FSS may not have survived at much longer experimental times. Therefore, perpendicular FSS had a dramatic affect on actin structure, causing depolymerization and formation of globular actin, but those actin fibers that did remain intact (i.e. the DPB) remained aligned and resisted FSS-induced reorientation. MPECs exposed to parallel FSS maintained the same actin structure as exhibited by ECs elongated on the micropatterned lanes under static conditions (Fig. 5A & B). There was no evidence of increased stress fiber formation. Actin stress fiber induction has been previously reported in HUVECs grown on micropatterned lanes and exposed to parallel FSS for 12 hours [31]. However, in that study, the HUVECs were elongated on 15 μm wide micropatterned lanes, which induced apoptosis under static conditions after only 12 hours [31]. The application of parallel FSS to HUVECS on the micropatterned lanes prevented apoptosis, and ultimately led to an increased number of actin stress fibers [31]. In contrast, under static conditions, MPECs on 25 μm wide micropatterned lanes survived for 48 hours. Increased EC survival and greater lane width, with increased surface area and cell-cell contacts, may explain the increased presence of actin stress fibers under static conditions, in which case FSS was not needed for actin fiber formation. Parallel FSS-exposed MPECs had the same actin fiber alignment as ECs on non-patterned surfaces elongated by FSS.

Perpendicular FSS also had a dramatic affect on microtubules. MPECs exposed to perpendicular FSS showed a significant increase in alignment variance compared to static MPEC controls, and compared to both MPEC and non-patterned ECs exposed to parallel flow (Fig. 5.5 A & B). Under perpendicular flow, MPEC microtubules remained intact, unlike the actin fibers, and therefore were able to undergo FSS-induced reorganization. Under parallel FSS, variance in microtubule orientation angle was not significantly different between MPECs and non-patterned ECs (Fig. 5.5 B). Moreover,

static MPEC actin and microtubule alignment were not significantly different than the alignment resulting from the imposition of FSS on non-patterned ECs (Fig. 5.5 B). Therefore, micropattern-induced EC elongation alone creates equivalent cytoskeletal alignment as FSS-induced EC elongation.

5.5.5. FSS-dependent MTOC localization

To determine the role of micropattern-induced versus FSS-induced EC elongation on MTOC polarization, MTOC location was quantified relative to the cell nucleus for MPECs under static flow, parallel FSS, or perpendicular FSS and compared to non-patterned ECs exposed to FSS (Fig. 5.6). Elongation alone on micropatterned lanes did not influence the position of the MTOC (Fig. 5.6 C). The average percentages of MPECs with the MTOC in positions 1, 2, or 3 were 47 ± 1 %, 17 ± 3 %, and 35 ± 4 %, respectively (Fig. 5.6 C). There was no significant difference between values at positions 1 and 3 for MPECs grown under static conditions (Fig. 5.6 C). No trend was observed in MTOC location per individual lane, even though MPECs had numerous cell-cell contacts. Under parallel flow, both MPEC and non-patterned ECs had significantly greater percentages of cells with MTOC in position 1, upstream of the nucleus (Fig. 5.6). Overall, MPECs and non-patterned ECs exposed to parallel flow had no significant differences in the average number of cells with MTOC located in positions 1, 2, or 3 (Fig. 5.6 C). However, results with static MPECs differed significantly from both MPECs and non-patterned ECs exposed to parallel flow (Fig. 5.6 C). Thus, MTOC polarization cannot be communicated by cell-to-cell contact through elongation alone, a finding consistent with the observed dependence of MTOC polarization on FSS [6]. These results are also consistent with observations of MTOC localization in vivo, where the MTOC is typically found upstream of the nucleus in arteries [6, 108]. However, results from in vitro studies of EC polarization vary with EC source and duration of FSS [6, 27]. The present findings indicate that either the microtubules of MPECs exposed to parallel FSS underwent further remodeling to re-position the MTOC upstream of the nucleus, or that MPECs with the MTOC positioned upstream of the nucleus prior to the imposition of FSS had better survival rates. Examining the MTOC location of MPECs exposed to perpendicular FSS was more difficult since cellular elongation did not match the direction of flow. In this case MPECs were sectioned as shown in Fig. 5.6 B to determine whether the MTOC became centralized towards the nucleus. MPECs exposed to perpendicular

FSS had no effect on MTOC location compared to static MPECs (Fig. 5.6 B), even though perpendicular FSS caused microtubular filaments to reorganize.

5.5.6. Limitations

The area of the micropatterned surfaces is approximately 1 cm^2 with 25 μm wide lanes with 100 μm wide spacing. The total number of ECs that adhere and elongate on the micropatterned lanes averages approximately 1000 – 3000 cells. This cell number is insufficient for analysis of the presence and activity of regulators of cytoskeletal dynamics, such as Rho A. Furthermore, this study analyzes actin and microtubule structure as snap shots at a variety of timepoints. To fully understand cytoskeletal remodeling of micropattern-induced elongation, and polarization of the MTOC in MPECs exposed to FSS, live fluorescent imaging of ECs transfect with labeled actin or microtubule monomers is required.

The pulsatile nature of blood flow can also affect cytoskeletal dynamics and EC function. High, unidirectional pulsatile flow can be approximated using steady, laminar FSS. For consistency, the same FSS of 12.5 dynes/cm^2 FSS was used in all of the studies that examined FSS-dependent EC shape and functions (Chapters VII, VIII, and IX). However, comparisons between the cytoskeletal structure and function of ECs exposed to non-reversing, pulsatile flow compared static MPECs would also be valuable.

5.5.7. Conclusion

Micropattern-induced EC elongation produces microtubule-dependent shape change and cytoskeletal alignment with a final morphology and cytoskeletal conformation equivalent to FSS-induced elongation of ECs. MTOC polarization was dependent on parallel FSS, not elongation alone, and perpendicular FSS ultimately disrupted both actin fiber formation and microtubule orientation. Micropattern-induced EC elongation allows cell shape and cytoskeletal alignment to be dissociated from FSS variables, thereby permitting discrimination of shape-dependent and FSS-dependent effects on EC phenotype and functions.

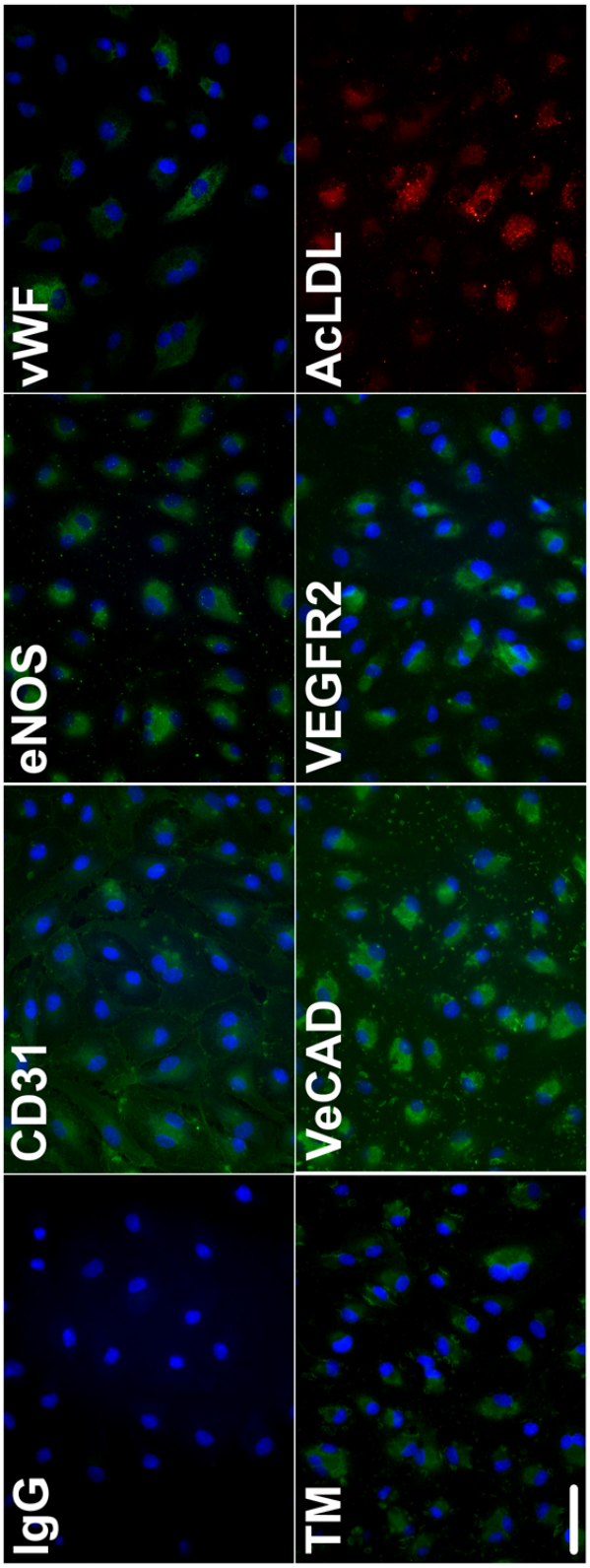

Figure 5.1. Confirmation of EC phenotype. IF staining of mature ECs isolated from baboon carotid areteris, images taken at 40 X. Staining pattern indicates that ECs are positive for the EC markers CD31, eNOS, vWF, TM, VECAD, VEGFR2, and AcLDL uptake. Scale bar = 50 µm.

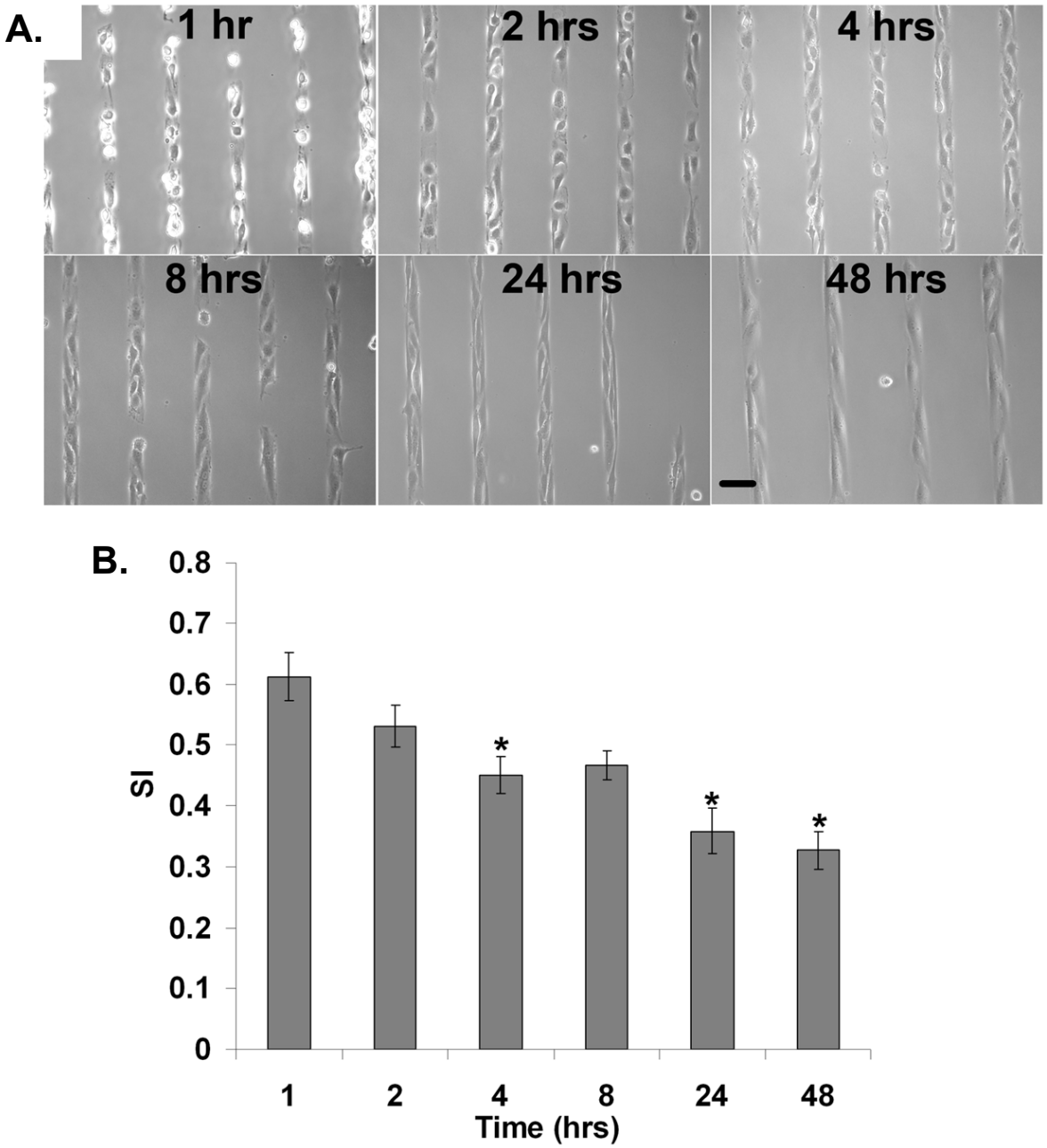

Figure 5.2. ECs on micropatterned lanes elongate and decrease shape index with time. **A.** Representative 20 X images of MPECs at select timepoints, Scale Bar = 50 μm. **B.** Shape index measurements over 48 hours with representative images of MPECs at 2 and 48 hours. * = ANOVA, Tukey's, $p<0.05$, compared to 1 hour.

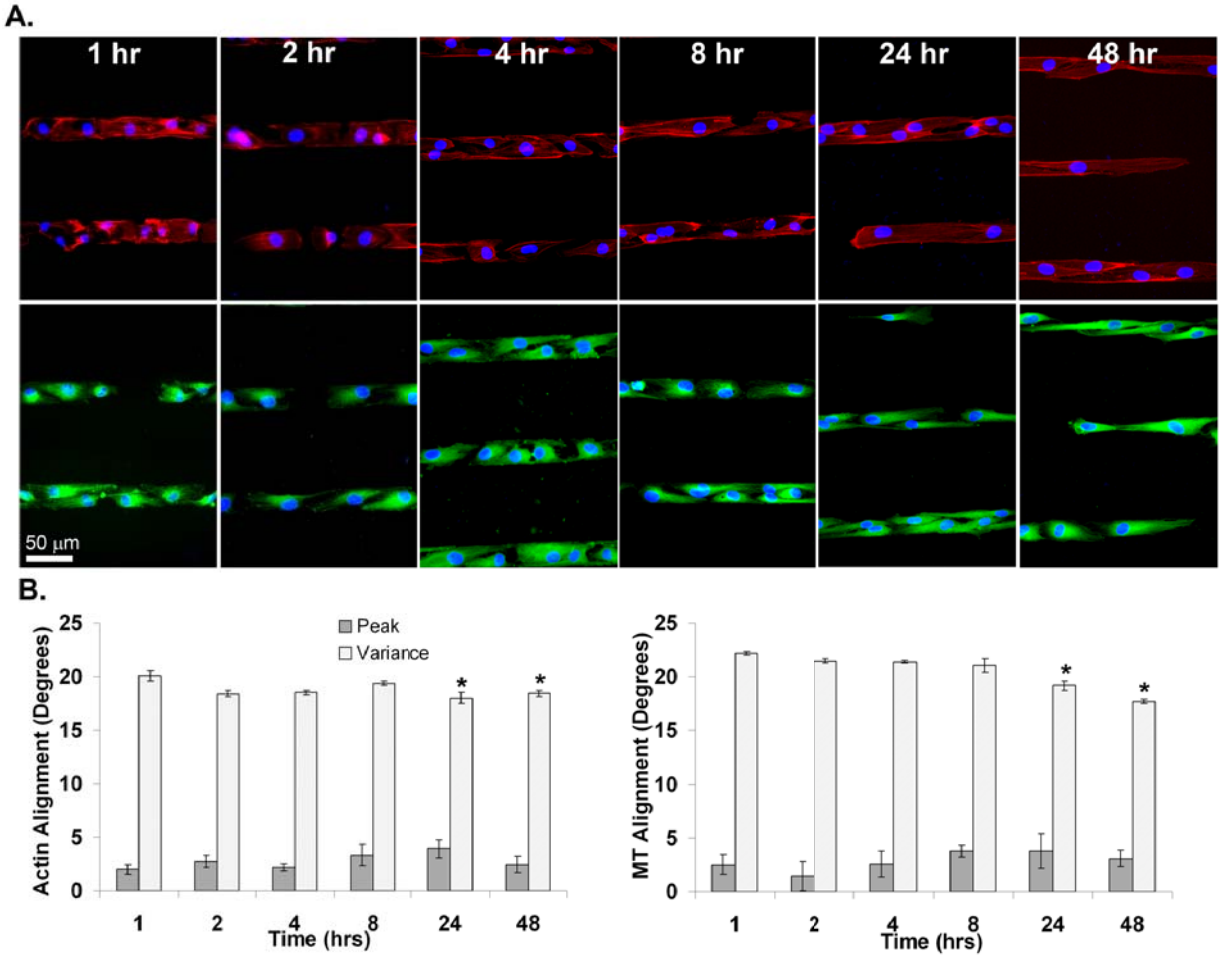

Figure 5.2. MPEC actin and microtubule alignment. **A.** Representative images of actin (top) and MT (bottom) stained MPECs at select timepoints showing cytoskeletal alignment. **B.** Peak and variance about the peak for quantified actin (left) and microtubules (MT,right) alignment over time. * = ANOVA, Tukey's, $p<0.05$, compared to 1 hour.

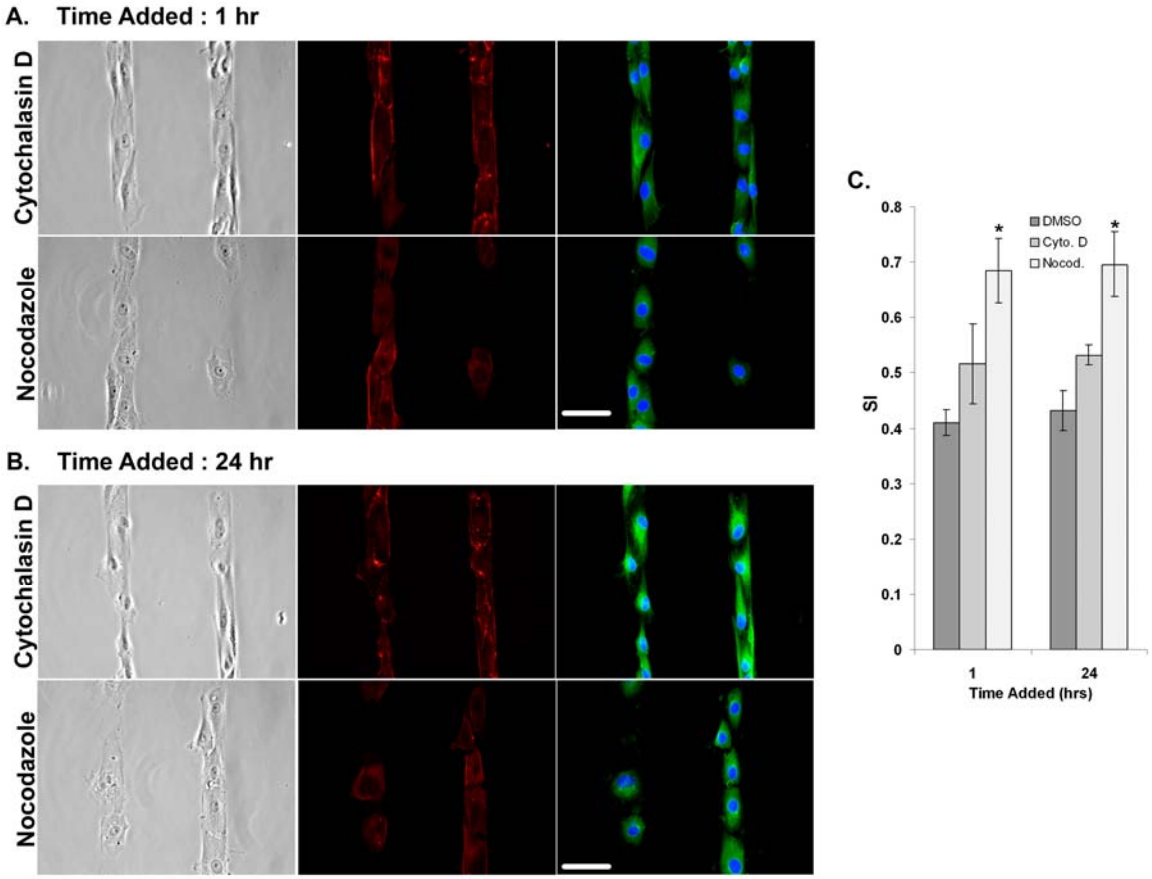

Figure 5.3. Isolation of the roles of actin and microtubules (MTs) using cytoskeletal inhibitors. **A.** Representative matched 40 X phase image and fluorescent actin and MT staining of MPECs treated with 24 hours of cytochalasin D and nocodazole added 1 hour after EC adhesion. **B.** Representative matched 40 X phase and fluorescent actin and MT images of MPECs treated for 24 hours with cytochalasin D or nocodazole added 24 hours after EC adhesion to micropatterned lanes. Scale bar = 50 μm. **C.** Shape index of MPECs treated with cytochalasin D and nocodazole for 24 hours. * = ANOVA, Tukey's, $p<0.001$, compared to DMSO.

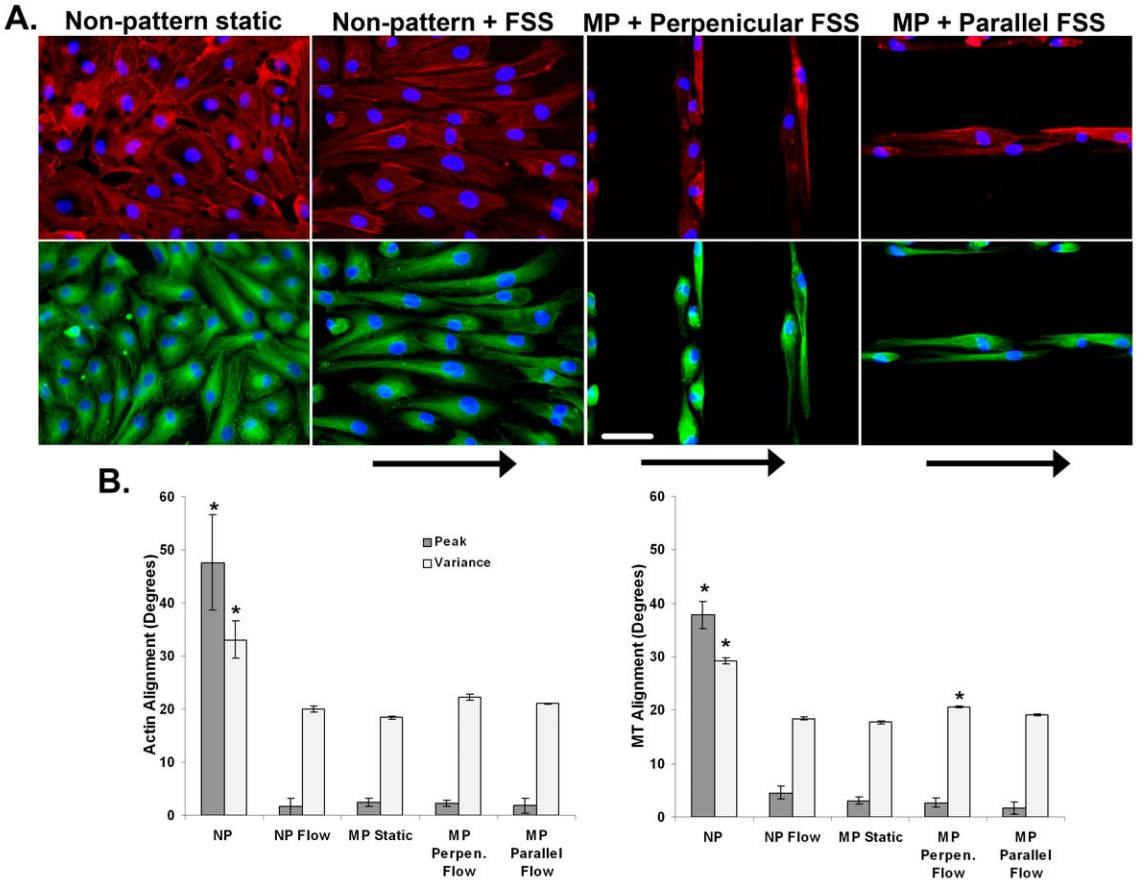

Figure 5.5. MPECs and non-patterned (NP) ECs exposed to FSS. **A.** Representative 40 X fluorescent images of actin (top) and microtubule (bottom) staining of MPECs and non-patterned ECs exposed to parallel and perpendicular FSS. Scale bar = 50μm. Arrows indicate the direction of FSS. **B.** Peak and variance about the peak of actin (left) and microtubules (MTs, right) to quantify alignment of MPECs and non-patterned ECs exposed to 24 hours of parallel or perpendicular flow compared to static conditions. * = ANOVA, Tukey's, $p<0.05$, for either peak or variance compared to all other conditions.

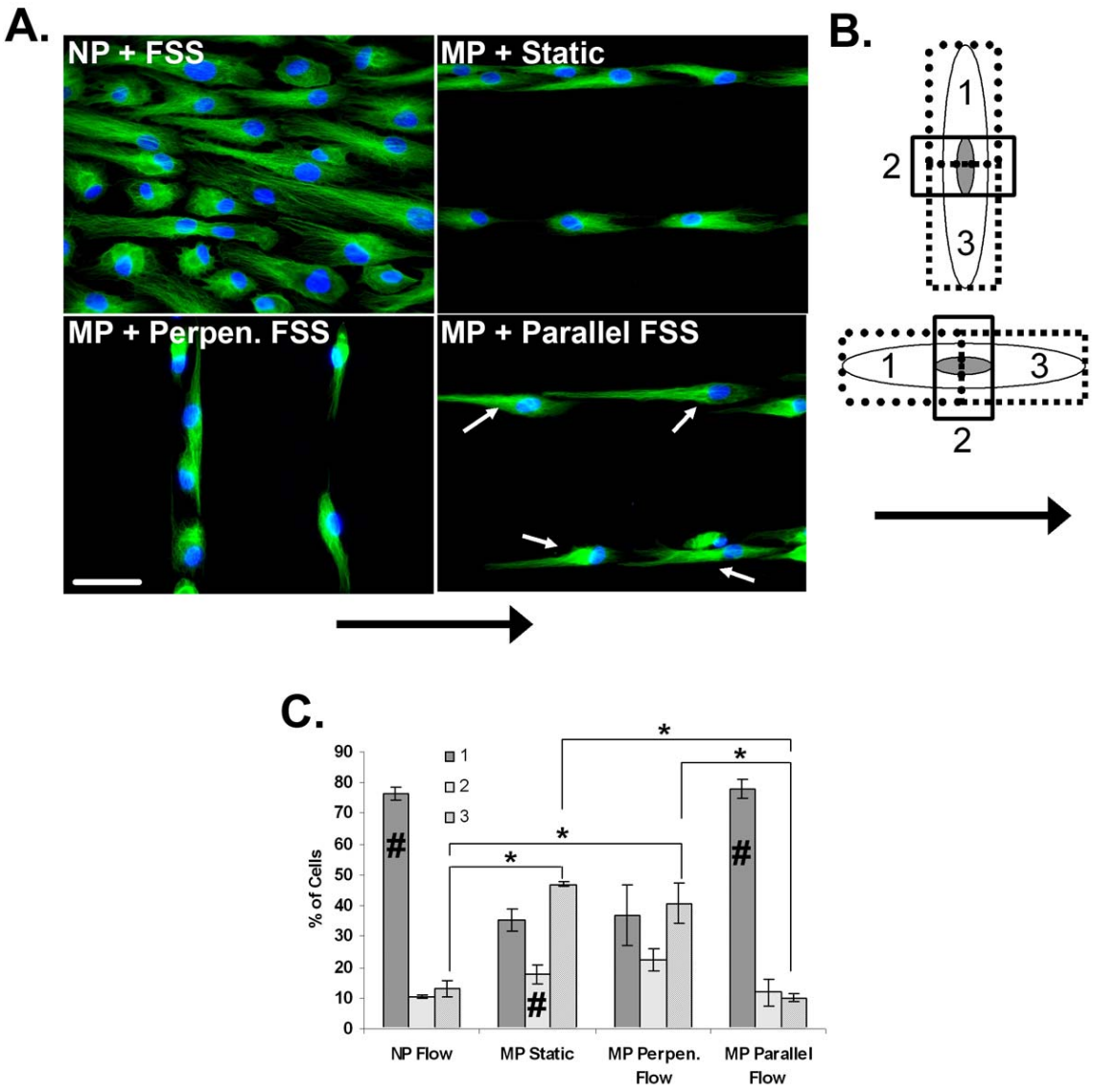

Figure 5.6. Polarization of MTOC in MPECs under static and flow conditions. **A.** Representative images of each condition in which MTOC location was measured. Arrow indicates FSS direction, Scale bar = 50 μm. **B.** Schematic describing how the MTOC location of the ECs were sectioned and scored in respect to the direction of FSS (indicated by the arrow) **C.** Average percent of MPECs with MTOC in specified location. * = ANOVA, Tukey's, $p<0.01$, NOTE: Location 1 & 3 have the same statistical significance between conditions, stars shown for location 3 only. # = ANOVA, $p<0.01$, compared to other locations within condition.

Chapter VI

Distinct extracellular matrix microenvironments of progenitor and carotid endothelial cells

6.1. Abstract

ECs produce and maintain the local extracellular matrix (ECM), a critical function that contributes to EC and blood vessel health. This function is also crucial to vascular tissue engineering, where endothelialization of vascular constructs require a cell source that readily produces and maintains an ECM. In this study, mature carotid EC and baboon endothelial progenitor cell (EPC) deposition of ECM (laminin, collagen IV, and fibronectin) was characterized for both elongated and cobblestone morphologies typically found in vivo. Microfluidic micropatterning was used to create 15 μm wide adhesive lanes with 45 μm spacing to reproduce the elongated EC morphology. Both EPCs and ECs elongated on micropatterned lanes had aligned actin cytoskeleton and readily deposited ECM. EPCs deposited and remodeled the ECM to a greater extent than ECs. Since a readily produced ECM can improve graft patency, EPCs are an advantageous cell source for endothelializing vascular constructs. Furthermore, mature EC deposition of ECM was dependent on cell morphology, where mature elongated ECs deposited more collagen IV and less fibronectin compared to matched cobblestone controls. Thus micropatterned surfaces controlled EC function of ECM deposition, which ultimately has implications for the design of tissue-engineered vascular constructs.

This research was originally published in *Journal of Biomedical Materials Research A*. Vartanian, K.B., Kirkpatrick, S.J., McCarty, O.J.T., Vu, T.Q., Hanson, S.R., and Hinds, M.T., "Progenitor and carotid endothelial cells elongated on micropatterned surfaces exhibit distinct and shape-dependent extracellular matrix microenvironments," *J Biomed Mater Res*.

6.2. Introduction

There have been extensive in vitro investigations into the functions of endothelium. However, there is limited research exploring the role of the distinct elongated EC morphology with aligned actin cytoskeleton found in vivo [16, 109], independent of external forces. Functional evaluation of ECs on micropatterned surfaces has demonstrated that cell shape, independent of the influence of FSS, plays a role in migration [36], apoptosis [33, 34], proliferation [34, 110], differentiation [28], nitric oxide production [29], ICAM-1 production [39], and ECM remodeling [28]. The composition of ECM also can influence EC functions including adhesion, proliferation, and permeability [111-114]. However, the influences of EC shape on ECM deposition are unknown. As shown in Aim 1, micropatterning can be used to replicate in vivo EC elongated morphology to study the role of cytoskeletal alignment on EC functions in vitro. This aim will evaluate ECM deposition of ECs on micropatterned lanes (elongated ECs) and on non-patterned surfaces (cobblestone ECs) using mature ECs and endothelial progenitor cells (EPCs).

6.3. Background

6.3.1. The Basement Membrane

The basement membrane ECM is an intricate molecular meshwork situated beneath the endothelium. Physically, the basement membrane acts a structural scaffold and sieve. Biochemically, interactions between ECM and ECs are required for cell survival, spreading, proliferation, migration, and morphogenesis [115]. ECM interaction with a cell is translated to the cytoskeleton via mechanical and biochemical linkages [35, 109, 115, 116]. The types of interactions formed between the ECM and the cytoskeleton are dependent on the composition of the ECM. The major ECM components of the basement membrane produced by ECs are collagen IV, laminin, and fibronectin. Research has shown that hemodynamics affects the composition of the ECM basement membrane. This correlates to altered ECM environments associated with atherosclerotic plaques.

6.3.2. Collagen IV

The collagens are a family of fibrous proteins that make up the most abundant protein found in mammals. Collagen is made of α chains wound tightly together to form long, stiff triple helical coils. Unlike other collagens, collagen IV is exclusively expressed in basement membranes [104, 117]. Collagen IV is referred to as a “network collagen” because it is flexible and is able to associate to form sheets [117]. Collagen IV has some unique structural properties that allow for the formation of these networks. First, the intermittent replacement of glycine with another amino acid in the characteristic Gly-X-Y (where X and Y are normally proline and hydroxyl-proline) repeats causes looser molecular interactions within the helical coil increased flexibility [117, 118]. The triple helical coils are more weakly associated with each other in the collagen IV network compared to other collagens. Second, the long carboxy-terminal noncollagenous (NC1) domain forms end-to-end interactions of two NCI trimers [117, 118]. Third, the amino-terminal domains bind each other through hydrophobic interactions and the cysteine and lysine rich domain promotes disulfide crosslinking between multiple triple helical coils [117, 118]. The resulting collagen IV network acts as a scaffold for the basement membrane and is required for maintaining structural integrity under mechanical stress [119].

6.3.3. Laminin

Laminin is a large, flexible cross-shaped protein that associates to form a lattice network within the basement membrane. Laminin is made of α1, β1, and γ1 chains, connected by disulfide bonds, that individually form the three short arms of the cross-shaped protein and wind together to form the long, helical fourth arm of the cross [104]. The lattice network of laminin molecules is formed through spontaneous self-assembly by calcium-dependent interactions between the three short arms [118, 120]. The long, fourth arm is believed to interact with the cell surface [120, 121]. The assembly of laminin promotes the recruitment of other matrix molecules to the basement membrane, and therefore laminin is crucial for basement membrane construction. The importance of the basement membrane and its dependence on laminin has been demonstrated through the embryonic lethality of laminin γ1 chain knockout mice due to their inability to form basement membrane [120, 122], while the basement membrane was able to form in embryonic knockouts of other matrix molecules (e.g. collagen IV) [120].

6.3.4. Fibronectin

While collagen IV and laminin are the major ECM proteins typically found in the basement membrane, EC fibronectin deposition was investigated in this study for several reasons: (1) it is abundantly secreted by ECs in vitro, (2) it plays a major role in cell adhesion, and (3) it is associated with the basement membrane of atherosclerosis prone regions of the vasculature. Fibronectin is secreted by ECs as soluble plasma protein that is found in circulating blood and as insoluble fibronectin that is associated with the basement membrane [104]. Insoluble fibronectin consists of two large disulfided bonded ~250 kDa subunits, which can assemble to form fibronectin fibrils [104, 123]. The two large subunits consist of long amino acid chains that fold to form functional domains separated by flexible polypeptide chains [104]. One highly specialized region of fibronectin is the Arg-Gly-Asp (RGD) repeat that mediates cell adhesion through integrin binding [114]. Integrins, a family of receptors found on the cell surface, connect the fibronectin ECM to the actin cytoskeleton [114] and act as a site for extracellular signal transduction due to physical (e.g. tension) or biochemical (e.g. ECM composition) cues [100].

6.3.5. The Influence of FSS on the ECM

While much effort has been spent on investigating regulation of ECM in vivo and in vitro, little is known about the effect of FSS on the actual composition of the basement membrane. The limited in vitro studies investigating the influence of high, unidirectional and low, oscillatory FSS are reviewed in the following paragraphs. These studies utilized either steady (30 dynes/cm^2) or oscillatory (0.2 ± 15 dynes/cm^2 and 40 mmHg hydrostatic pressure) FSS to determine the effects on organization and deposition of ECM by bovine aortic ECs (BAECs) [66, 67].

ECM Organization: BAECs in static culture deposited ECM in a granular pattern within the cytosol and a randomly oriented fibrillar pattern in the subendothelium. Under both steady and oscillatory FSS, collagen IV, laminin, and fibronectin all formed thicker fibers compared to static culture [66, 67]. ECM under steady and oscillatory FSS differed in organization. BAECs exposed to steady laminar FSS organized the fibronectin fibrils parallel to the elongated cell, but collagen IV and laminin remained

randomly oriented [66, 67]. The alignment of fibronectin fibrils is likely due to the direct link between fibronectin and the actin cytoskeleton (which aligns under steady FSS) [123]. Under oscillatory FSS, BAECs organization of all ECM components remained randomly oriented [67].

ECM Protein Deposition: Collagen IV protein deposition was not measured in these studies since the antibody was not available for Western blotting. Under steady laminar FSS, fibronectin levels at 12, 24, and 48 hours were 0.4, 1.2, and 1.8 of static controls, respectively [66]. Levels of fibronectin compared to static control deposited by BAECs exposed to oscillatory FSS were 1.68, 1.38, and 2.96 at 12, 24, and 48 hours, respectively [67]. Under steady FSS, laminin levels at 12, 24, 48 hours were 1.3, 1.8, and 2.3 of static controls, respectively [66]. BAECs deposition of laminin under oscillatory FSS compared to static controls were 2.39, 1.36, and 5.67 at 12, 24, and 48 hours, respectively [67]. Both steady and oscillatory FSS increased deposition of fibronectin and laminin (except the initial decrease of fibronectin seen at 12 hours). Oscillatory FSS appeared to increase the levels of fibronectin and laminin compared to static controls to a greater extent than steady FSS, but these results were from separate studies and therefore statistical comparison was not available.

6.3.6. The Basement Membrane and Atherosclerosis

The organization and composition of the basement membrane has been implicated in several vascular diseases including diabetes mellitus, which is characterized by thickening of capillary basement membrane [124]. Common complications of diabetes mellitus are atherosclerosis and myocardial infarction [124], linking dysregulation of the basement membrane to these vascular pathologies. Changes in ECM during atherosclerosis is most often associated with smooth muscle cells (SMCs), in particular SMC's robust synthesis of collagens and other matrix molecules [13, 125]. Recent investigations also implicate ECs in increased synthesis of ECM molecules associated with atherosclerosis [126]. Since the composition of the basement membrane affects EC function, the pathogenesis of atherosclerosis may be regulated, in part, by the EC microenvironment. Research suggests that EC-matrix interactions regulate EC immunogenicity, which is one of the earliest and most prolonged processes involved in the development of atherosclerosis [111-113]. For example, atherosclerotic regions of the vasculature have fibronectin-enriched basement

membranes, which induced increased EC permeability through increased activation of p21-activated kinase (PAK) [111]. In vitro, increased activation in PAK also occurred under oscillatory FSS (atheroprone FSS) and in ECs plated on fibronectin coated dishes [111]. The composition of ECM deposited by ECs and cell-matrix interactions are important for understanding EC regulation of functions that contribute to atherosclerosis and could be used in vascular tissue engineering applications.

6.3.7. Extracellular Matrix and Vascular Grafts

Synthetic vascular grafts require sufficient mechanical strength to resist in vivo internal pressure and a luminal surface that supports EC attachment, retention, and function. In native vessels, ECM molecules support both of these requirements. Vascular tissue engineering has employed a variety of techniques to utilize the mechanical and biological properties of ECM. L'Heureux, et al., was the first to use sheets of naturally produced collagen from SMCs to make a vascular graft with sufficient mechanical strength to withstand in vivo pressure [127, 128]. Other methods have included combining matrix scaffolds and elastin to improve the elastic properties of the engineered vessel while maintaining sufficient burst pressures [128, 129]. To improve EC retention, a variety of ECM coatings have been applied to the lumen of vascular grafts including collagen, laminin, fibronectin, and fibrin [45, 130]. Fibronectin coating has been most successful, showing significant improvement in EC attachment and retention [131, 132] compared to uncoated grafts and grafts coated with other ECM-based coatings including collagen IV, laminin, poly-lysine, and gelatin [130]. Using combinations of fibronectin with other ECM molecules, such as fibronectin and collagen, performs better by increasing EC adhesion compared to fibronectin coating alone [130]. Once ECs are attached they produce and maintain their own ECM, and the composition of this microenvironment is important to the long term structural and functional integrity of the endothelium. As discussed above, the composition of the basement membrane ECM has functional consequences that contribute to EC pathological states. Thus, EC deposition of ECM and the ultimate composition of ECM are of the utmost importance for maintaining a functional endothelium, which is crucial for improved vascular graft patency.

6.3.8. Endothelial Progenitor Cells

Autologous EC sources for vascular graft applications include veins, arteries, omental fat, and subcutaneous fat [130]. Harvesting cells from these sources all require either an additional surgical site or an entirely separate surgical procedure. Recently, peripheral blood-derived endothelial progenitor cells (EPCs), accessible through venopuncture, have been identified as a promising autologous cell source. EPCs were identified in 1997, and their harvesting from peripheral blood described in 2000 [133]. EPCs have subsequently been the source of intense interest due to their remarkably diverse and beneficial roles in therapeutic processes of hemostasis, angiogenesis, and tissue repair [134-136]. The outgrowth of EPCs cultured in vitro is primarily from marrow-derived cells that have a high proliferative rate, indicating that these cells are derived from circulating angioblasts [137]. Conversely, ECs in fresh blood that originate from vessel walls have limited growth capability. EPCs play a pivotal role in repairing damaged endothelium in vivo by localizing to areas of vascular damage [138-141]. EPCs are recruited to sites of ischemic tissue injury (e.g., acute myocardial infarction) and circulate in increased numbers in multiple disorders [142]. Following surgical procedures, EPCs have been found to increase in number, localize to implanted synthetic grafts [143] and balloon denuded arteries [144], and inhibit neointimal hyperplasia [144-147]. EPCs capacity to promote rapid reendothelialization of denuded arteries and prosthetic grafts [146, 147] has presented them as a promising cell source for tissue engineered vascular grafts. However, EPC production of ECM molecules has not been established. In this study, ECM deposition by EPCs and mature ECs in elongated and cobblestone morphology was characterized without the influence of FSS.

6.3.9. Summary

The local ECM environment produced and maintained by a cell critically influences cell fate. The EC-associated ECM is the basement membrane, of which the major components are collagen IV, laminin, and fibronectin. These components are uniquely suited for basement membrane assembly and function. The composition of the basement membrane varies in vivo, and of particular interest, is dysregulated in athero-prone regions. The athero-protective and athero-prone regions of the vasculature are made up of dramatically differing EC morphology, where ECs are elongated or cobblestone, respectively. Whether EC shape alone affects the composition of ECM deposited by a cell has not been previously investigated. Furthermore, for tissue

engineering applications, naturally produced ECM is advantageous due to biocompatibility and mechanical strength [148]. Thus, EPC, a potential autologous cell source for endothelializing vascular grafts, deposition of ECM was also characterized.

6.4. Materials and Methods

6.4.1. Experimental Design

Experiments in this aim were designed to quantify ECM deposited by EPCs and mature ECs in both elongated and cobblestone morphologies. Surface micropatterning was used to create elongated EC shapes (independent of FSS). ECM analysis included comparing: (1) micropattern-elongated EPCs and mature ECs, (2) cobblestone EPCs and mature ECs, and (3) micropattern-elongated mature ECs and cobblestone mature ECs. Further comparisons between EPCs and mature ECs were made describing cell surface area, proliferation rates, and adhesion. EPC and mature EC spreading on micropatterned surfaces and resulting actin structures were also quantified and compared. Micropatterning techniques, IF, and quantification of actin structures are described in Common Materials and Methods (Chapter IV). Methods specific for this aim are detailed below.

6.4.2. Cells and culture conditions

Mature ECs were isolated from baboon carotid arteries as previously described in Common Materials and Methods Section 4.1 [149]. EPCs were isolate from whole blood drawn from male baboons. The blood was diluted 1:1 with warm HBSS and gently layered on 12 mls Histopaque density gradient and centrifuged at 400xg for 30 minutes to separate the blood into layers of red blood cells, buffy coat, and plasma (Fig. 6.1 A). The buffy coat layer was removed, diluted 1:1 with HBSS, and centrifuged at 250xg for 10 minutes. After aspirating the supernatant, the pellet was washed two times by resuspension in 20 mls HBSS and centrifugation at 250xg for 10 minutes. The final cell pellet was resuspended in EGM-2 supplemented with 18 % FBS (Hyclone) and plated on 50 µg/ml fibronectin (Sigma) coated 12-well plates at $1x10^7$-$1x10^8$ cells/well [91, 147, 150]. EPCs were incubated at 37^{o}C and 5% CO_2 and treated with EGM-2 media with 20% FBS (Hyclone). EPC outgrowth was typically seen after three weeks of culture, at which time the EPCs were expanded onto collagen I coated TCP flasks and maintained

in EGM-2 with 10% FBS through passage 6. Endothelial phenotype was confirmed for EPCs as described in Common Materials and Methods Section 4.2 [151]. In all experiments, cells were plated on micropatterned lanes and non-patterned surfaces at $4x10^4$ cells/cm^2 in EBM-2 media supplemented with Single Quots (Lonza).

6.4.3. Surface Preparation

Two micropatterned designs were used in this aim: (1) 15 μm wide lanes with 45 μm spacing, and (2) 5 μm wide lanes with 20 μm spacing. The silicon templates containing these designs were made at Boston University (BU) and provided by Tania Vu, PhD (OHSU) and Joe Tien, PhD (BU). In this aim, FITC-collagen I (50 μg/ml, Sigma) was used as the substrate to make it possible to visualize the pre-adsorbed matrix. Micropatterning with 5 μm x 20 μm patterns utilized microcontact printing and the 15 μm x 45 μm patterns used microfluidic patterning. Microcontact printing is preferred when patterning designs with small features (5 μm or less) [152].

6.4.4. Cell crossing assay

Microscopy images of EPCs and ECs on micropatterned surfaces were imaged at 4 or 24 hours. The number of cells crossing non-adherent surfaces and total cell number were counted using NIH Image J, yielding the percent of cells crossing non-adherent regions.

6.4.5. Actin alignment

Actin structure was again quantified in this aim using MATLAB for both mature ECs and EPCs at 4, 24, and 48 hours. In this case, both variance and entropy were calculated to quantify actin structure.

6.4.6. ECM detection and quantification

ECM protein deposition by EPCs and ECs were compared on micropatterned collagen I, collagen I coated, and uncoated glass chamber slides at 4, 24, or 48 hours. IF (described in Common Materials and Methods Section 4.8) and colorimetric techniques were used for protein detection. Primary antibodies included anti-fibronectin (Sigma, 1:400), anti-collagen IV (Dako, 1:100), anti-laminin (Dako, 1:100), and negative control anti-IgG (Dako, 1:100). The secondary antibody Alexa Fluor 568 goat anti-mouse was used exclusively to not interfere with the FITC-collagen I substrate.

Remodeling of the FITC-collagen I lanes was evaluated using FITC images. Fluorescent microscopy images of ECM deposited by EPCs or ECs were analyzed using MATLAB to quantify the intensity of staining present in the image and NIH Image J to count cells in the DAPI stained images. The intensity of fluorescent ECM staining per cell was calculated.

For colorimetric detection, EPCs and ECs were incubated on 96-well TCP plates for 4 or 24 hours. Cells were fixed with 3.7% PFA and stained using the previously described ECM antibodies and the Mouse/Rabbit Polydetector HRP DAB (BioSB, Santa Barbara, CA). HRP was developed using TMBE substrate (Chemicon), followed by 0.5 M HCl, and read at 450 nm on a plate reader (M200, TECAN).

6.4.7. Surface area, adhesion, and proliferation assays

Surface area: EPC and EC surface areas were measured (n=180) using microscopy images in NIH Image J. Adhesion: EPCs and ECs were plated on two different surfaces, glass 8-well chamber slides and 96-well TCP, with the following treatments: (1) 50 μg/ml collagen I for 1 hour and 5 mg/ml BSA for 1 hour, (2) 5 mg/ml BSA for 1 hour, and (3) uncoated. Cells were plated for 1 hour, rinsed, fixed, and stained with 1 μM SYTOX (Invitrogen). Five fields of view per well were imaged at 10X and counted using NIH Image J. Proliferation: EPCs and ECs were plated on 96-well collagen I coated TCP plates. BrdU (10 μM, Roche, Indianapolis, IN) was added to the media 2 hours after plating and replaced every 24 hours. BrdU was detected at 24, 48, and 72 hours using a BrdU Colorimetric kit (Roche).

6.4.8. Statistical analysis

Statistical analysis was performed using SPSS version 15. All experiments were performed in triplicate with N≥3. The data are represented as mean ± SEM (when data represented the average of averages obtained from multiple samples in each experiment) except when indicated as mean ± standard deviation (when one data point collected from each experiment was averaged). Student's t-test and paired Student's t-test were used when comparing two conditions for unmatched or matched samples, respectively. ANOVA with Tukey post-hoc tests were used when comparing more than two conditions. Significant results required $p \leq 0.05$.

6.5. Results

6.5.1 EPC isolation and confirmed endothelial phenotype

EPCs isolated from baboon blood were successfully isolated as described in the Materials and Methods Section 6.4.2 and diagrammed in Figure 6.1 A. Outgrowth EPCs expressed the common EC markers CD31, eNOS, TM, VEGFR2, vWF, and showed uptake of AcLDL (Fig. 6.1 B).

6.5.2. Cell crossing on micropatterned lanes

EPCs and ECs plated on micropatterned surfaces of 15 μm wide lanes with 45 μm spacing had no evident differences in adhesion or spreading at 4 hours (Fig.6.2 A). At 24 hours, EPCs and ECs elongated and remained confined to the micropatterned lanes, but EPCs had a significantly greater percentage of cells crossing non-adherent regions than ECs, 22.93 ± 10.93% and 4.08 ± 3.32%, respectively (Fig. 6.2 B, $p<0.01$). At 48 hours, ECs were confined to the micropatterned lanes, while EPCs crossed the non-adhesive regions between lanes to form small confluent patches with cobblestone morphology (Fig. 1A). On 5 μm wide lanes with 20 μm spacing, a similar trend was seen at earlier timepoints. At 4 hours, EPCs (69.8 ± 7.3%) had a significantly greater percentage of cells crossing non-adherent regions compared to ECs (24.6 ± 4.6%). At 24 hours, EPCs began to form a confluent monolayer (data not shown).

6.5.3. Actin alignment

The actin filaments of EPCs and ECs aligned parallel to the direction of the cell's long axis on the micropatterned surface at 4 and 24 hours (data not shown). At 48 hours, ECs maintained this aligned and elongated actin cytoskeletal structure (Fig. 6.3), with thick actin fibers at the cell edges. The peak angles of actin orientation were in a narrow range of 2^{o} to 4^{o} with a variance range of 17.5^{o} to 18.8^{o} and the average entropy of H = 6.8 ± 0.09 (Table 6.1). In contrast, at 48 hours EPCs that spread onto non-adhesive regions between micropatterned lanes, began to lose their actin alignment, and had actin filapodia extended onto non-adherent regions (Fig. 6.3). The peak angle of EPC actin remained oriented with the horizontal at -3^{o} to 2^{o} but the variance increased to 19.9^{o} to 21.1^{o} and the entropy increased to H = 7.2 ± 0.05 (Table I). EPCs remaining on the micropatterned lanes maintained some visible actin alignment with thick actin fibers

at the cell edges. EPCs and ECs on non-patterned surfaces had randomly oriented actin profiles with comparable average entropy values of H = 7.4 and a wide range of peak angles with increased variance (Table 6.1). Images of the PDMS mold of the micropatterned lanes had the lowest entropy values of H = 6.1 ± 0.12 and the smallest variance about the peak angle (Table 6.1). Thus, this actin quantification confirmed actin alignment on micropatterned lanes and further established that EPCs were able to spread onto non-adherent regions of the micropatterns.

6.5.4. Micropatterned cell deposition of ECM

EPCs and ECs deposited limited amounts of laminin at 48 hours, but EPCs had more prominent staining of collagen IV and fibronectin on both the micropatterned lanes and on the non-adhesive regions between the lanes compared to ECs (Fig. 6.4). EPC versus EC staining intensities per cell were consistently greater for laminin (0.03 ± 0.01 vs 0.02 ± 0.01, $p < 0.05$), collagen IV (0.28 ± 0.15 vs 0.13 ± 0.08, $p < 0.001$), and fibronectin (0.13 ± 0.05 vs 0.04 ± 0.03, $p = 0.05$) at 48 hours. A similar staining trend in ECM deposition was seen on the micropatterned lanes at 24 hours (data not shown). Control experiments staining the micropatterned lanes prior to cell adhesion determined that the fibronectin, collagen IV, and laminin antibody did not cross-react with collagen I and that incubation with EGM-2 alone did not result in positive staining on the micropatterned lanes (data not shown). Thus the ECs were the source of the deposited ECM on the micropatterned lanes.

Fluorescent microscopy images suggest that EPCs incorporated and mobilized the underlying FITC-collagen I micropatterned lanes. Bright punctate FITC deposits were visualized within the cytosol of EPCs (Fig. 6.5). Interestingly, these FITC-collagen I molecules were seen in the cytosol of EPCs that had spread onto the non-adhesive regions (Fig. 6.5, arrows). The presence of punctate FITC-collagen I in mature ECs was dramatically reduced compared to EPCs and was limited to the micropatterned lanes (Fig. 6.5).

6.5.5. Cobblestone cell deposition of ECM

On collagen I coatings, EPCs consistently deposited more collagen IV ($p<0.05$) and fibronectin ($p \leq 0.06$) compared to ECs at 48 hours (Fig. 6.6 A). Fold increases in EPC staining intensity per cell compared to EC were 3.67 ± 0.53 for collagen IV and

1.71 ± 0.08 for fibronectin. EPC laminin deposition was variable with an average fold increase of 1.62 ± 0.09. A similar trend in staining was seen at 24 hours, but at 4 hours only fibronectin was present for EPCs (data not shown). On uncoated glass, EPCs and ECs deposited collagen IV and fibronectin as early as 4 hours after plating, at which time EPCs had more positive staining (data not shown). At 24hours, EPC deposition of all ECM proteins on glass was more prominent than ECs (Fig. 6.6 B). On glass, fold increases in EPC staining intensity per cell compared to ECs were 2.02 ± 0.48 for collagen IV, 2.49 ± 1.56 for fibronectin, and 1.47 ± 0.85 for laminin; in this case significance was variable and could not be established. On TCP, EPC and EC deposition of ECM was determined using an ELISA colorimetric detection. EPCs put down significantly more collagen IV and fibronectin at 4 hours (Fig. 6.6 C, $p<0.01$) and significantly more fibronectin at 24 hours compared to ECs (Fig. 5C, $p<0.05$). Both fibronectin and collagen IV colorimetric intensity was significantly greater than IgG at all time points (ANOVA, Tukey's, $p<0.05$).

6.5.6. Cell surface area, adhesion, and proliferation rate

The surface areas of confluent monolayers of EPC (1164.83 ± 358.35 μm^2) and EC (1109.62 ± 339.35 μm^2) isolations used in this study were not significantly different (Fig. 6.7 A). As expected, cell adhesion between surface type and protein coatings was notably different [130]. However, on all substrates (glass or TCP, both uncoated, coated with BSA, or coated with collagen I) EPC and EC adhesion was not significantly different (Fig. 6.7 C), thus assuring that comparable cell numbers were present in each experiment for the particular surface and substrate tested. Proliferation rates of EPCs and ECs in EGM-2 supplemented with 2% FBS on collagen I coated TCP (Fig. 6.7 B) and uncoated TCP (data not shown) were not significantly different for the 72 hours measured. In EGM-2 supplemented with 10% FBS, EPCs proliferated faster than ECs (data not shown).

6.5.7. Mature EC Shape dependent ECM deposition

Staining intensity of ECM deposited by mature ECs on micropatterned and non-patterned FITC-collagen I was quantified per cell (Fig. 6.8). The staining intensity of collagen IV, fibronectin, and laminin per cell of ECs elongated on micropatterned lanes at 48 hours were 0.162 ± 0.028, 0.054 ± 0.016, and 0.020 ± 0.004, respectively (Fig. 6.8 B). Matched non-patterned cobblestone ECs had collagen IV, fibronectin, and laminin

staining intensities per cell of 0.072 ± 0.018, 0.097 ± 0.030, and 0.018 ± 0.004, respectively (Fig. 6.8 B). Elongated ECs on micropatterned lanes laid down significantly more collagen IV (paired Student's t-Test, $p<0.01$) and less fibronectin (paired Student's t-Test, $p=0.05$) compared to cobblestone controls. Laminin production per cell was not significantly different between ECs on micropatterned and non-patterned surfaces. Therefore, mature EC deposition of collagen IV and fibronectin was dependent on cell shape.

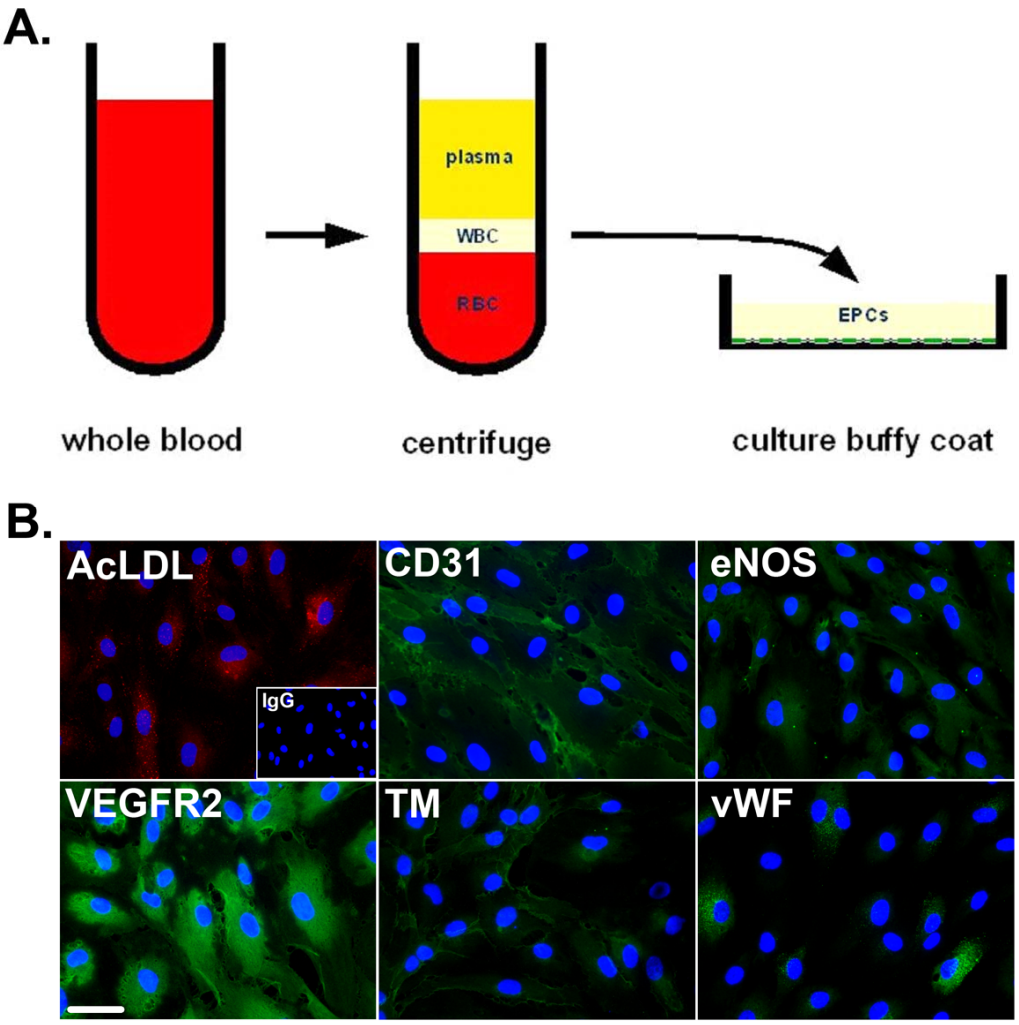

Figure 6.1 EPC isolation and staining of EC markers. **A.** Diagram of EPC isolation procedure. **B.** Representative IF 40 X images of positive EPC staining for endothelial markers. Scale Bar = 50 µm.

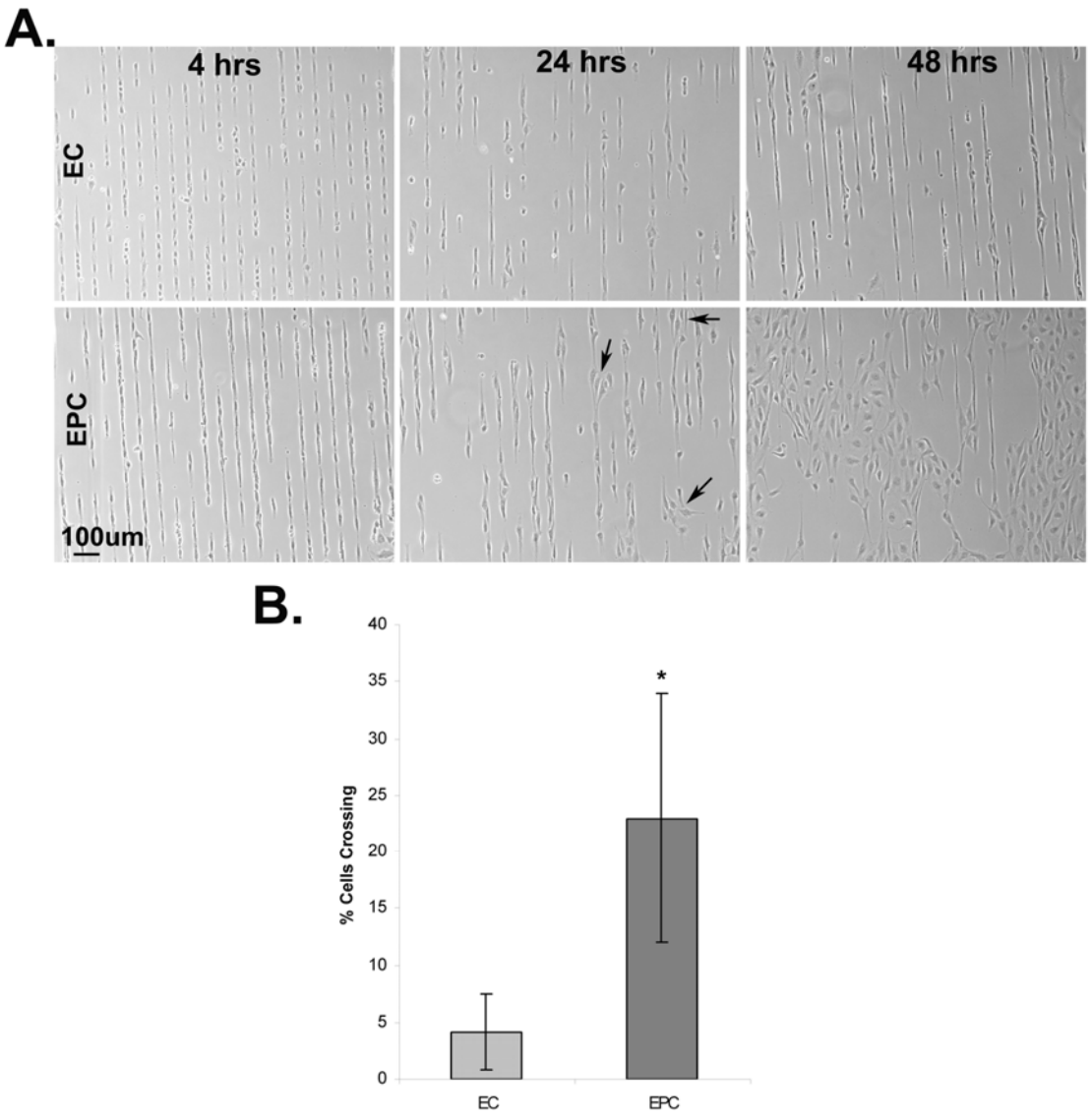

Figure 6.2. Spreading properties of EPCs and mature ECs on micropatterned lanes. **A.** Mature ECs and EPCs plated on micropatterned 15 μm collagen I lanes with 45 μm spacing. Images taken at 10X at 4, 24, and 48 hours. EPCs spread between lanes onto non-adhesive regions at 48 hours while ECs remained confined to the micropatterned surfaces. **B.** Percent of cells crossing the non-adhesive regions at 24 hours (arrows in A, Student's t-test, *$p < 0.01$).

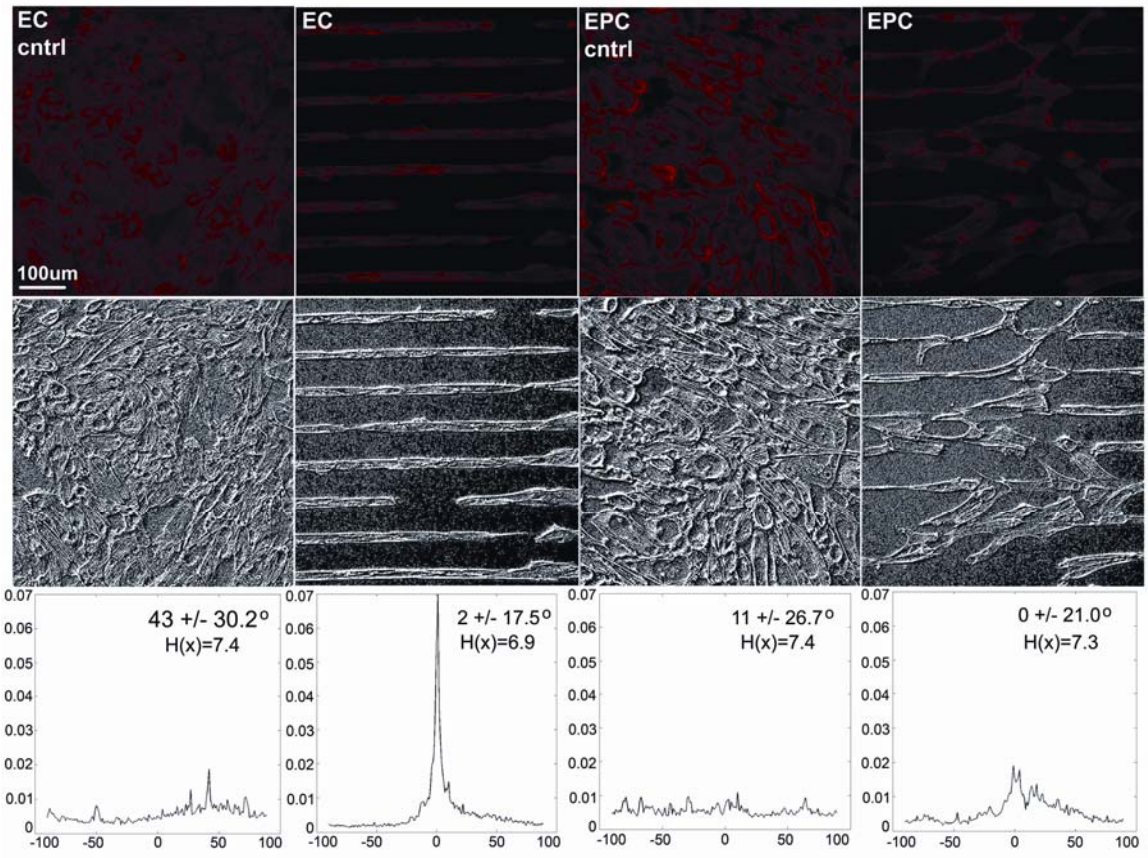

Figure 6.3. Quantified micropatterned mature EC and EPC actin structure. Actin staining and analysis confirm cytoskeletal alignment and EPC spreading onto non-adherent surfaces at 48 hours. Top: Alexa Fluor 568-phalloidin. Middle: Laplacian image (edge detection). Bottom: Normalized probability distribution of orientation angles with peak angle ± variance and entropy (H).

Table 6.1. Quantification of Actin Alignment

	Peak (degrees)	+/- Variance (degrees)	Entropy H(x)
Micropattern			
EC	2 – 4	17.5 – 18.8	6.8 ± 0.09
EPC	-3 – 2	19.9 – 21.1	7.2 ± 0.05
Control			
EC	15 – 43	24.9 – 30.22	7.4 ± 0.02
EPC	-55 – 63	25.5 – 39.6	7.4 ± 0.03
Aligned			
PDMS lanes	1	14.1 – 16.3	6.1 ± 0.12

Table 6.1. Quantification of alignment. The table lists the range of peak angles and variance about the peak angle in degrees for the mature ECs and EPCs on micropatterned lanes compared to mature ECs and EPCs on non-patterned control surfaces. Average entropy is also listed for each condition. The PDMS lanes represents the peak, variance, and entropy for completely aligned image features.

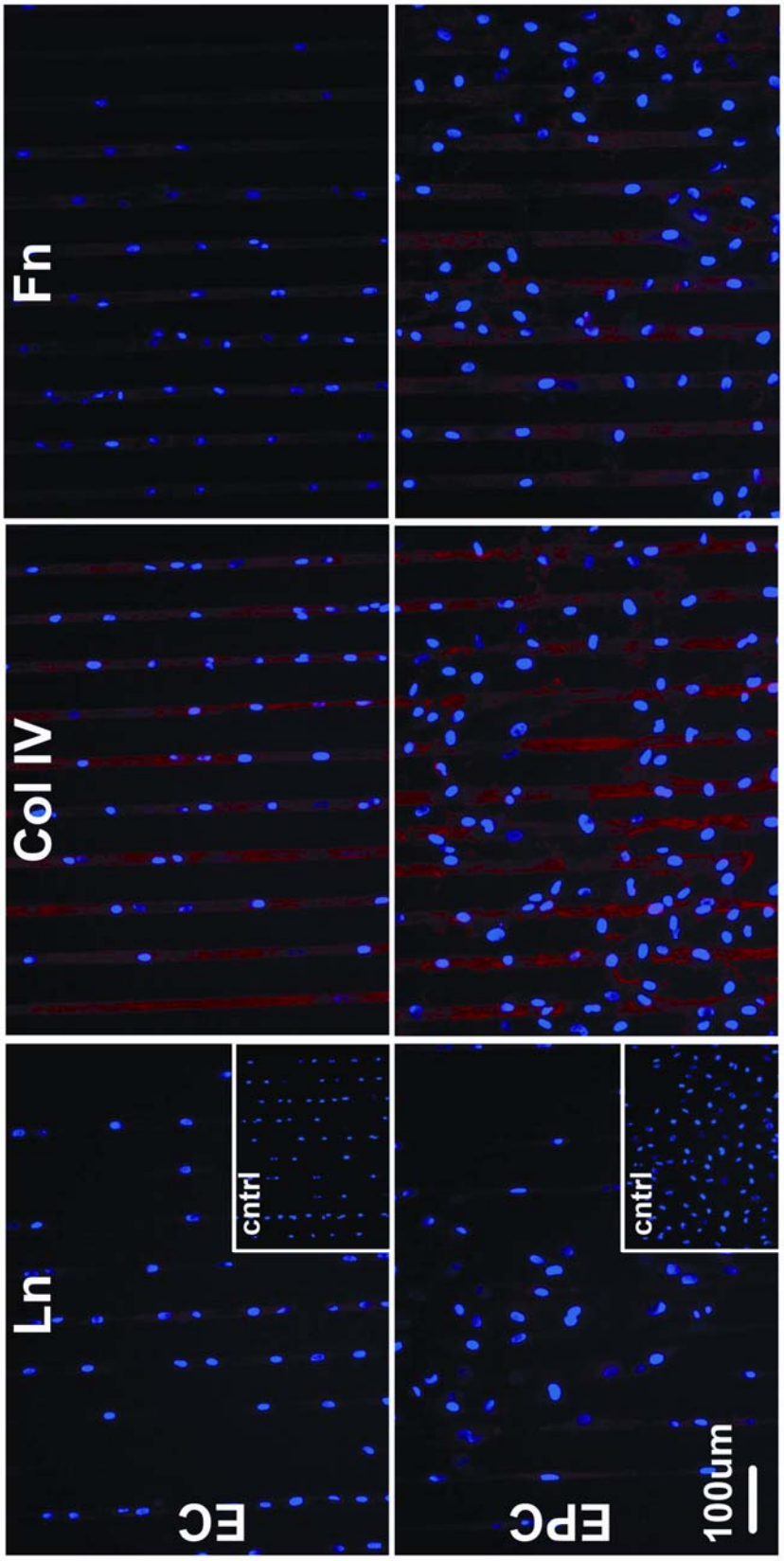

Figure 6.4. Mature EC and EPCs staining of ECM on micropatterned lanes. EPCs demonstrated more prominent staining of ECM compared to mature ECs. Left: Laminin (Ln) Center: Collagen IV (Col IV). Right: Fibronectin (Fn) staining of ECs and EPCs on 50 µg/ml collagen I micropatterned lanes incubated for 48 hours. Top: ECs, Bottom: EPCs. Control mouse IgG. DAPI stained nuclei are blue. Images taken at 20 X.

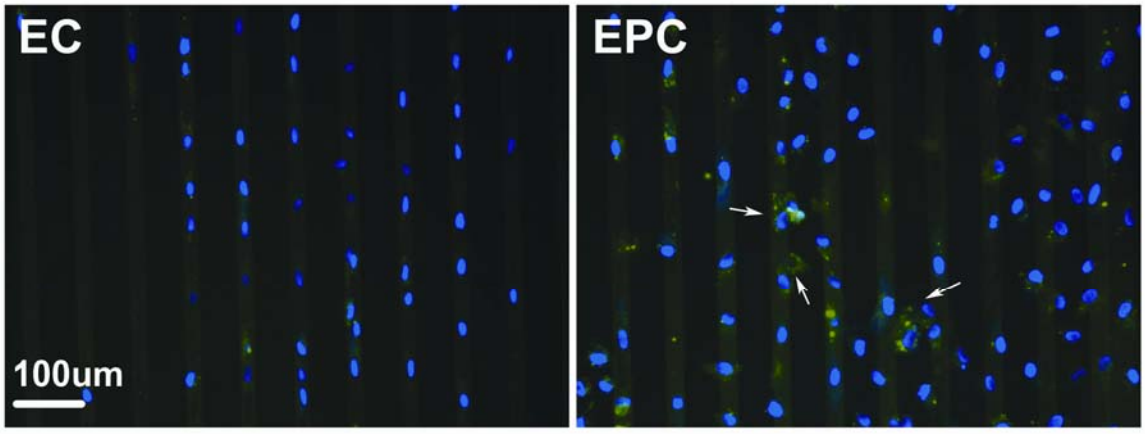

Figure 6.5. EPCs and mature ECs on micropatterned FITC-collagen I lanes. EPCs incorporated FITC-collagen I and mobilized it onto non-adhesive regions between micropatterned lanes. Arrows indicate cells that incorporated FITC-collagen I on non-adhesive regions between lanes.

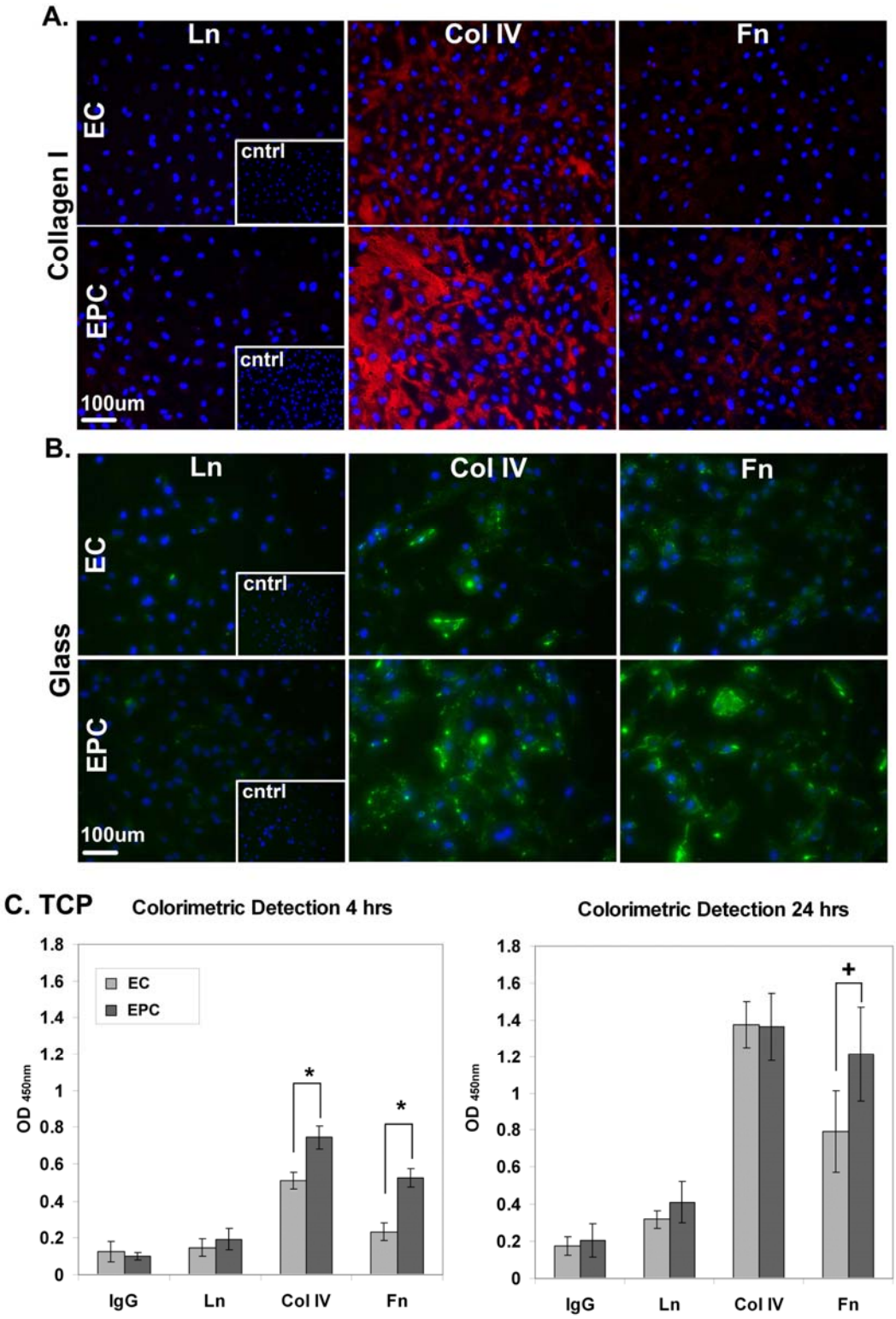

Figure 6.6. Mature EC and EPC staining of ECM proteins on non-patterned surfaces. Laminin (Ln), collagen IV (Col IV), fibronectin (Fn), and control IgG for EPCs and mature ECs plated on: **A.** collagen I at 48 hours, **B.** glass 8-well chamber slides at 24 hours, and **C.** TCP colorimetric detection of HRP-labeled ECM proteins at 4 and 24 hours. (Student's t-test, *$p < 0.01$ and $^{+}p<0.05$).

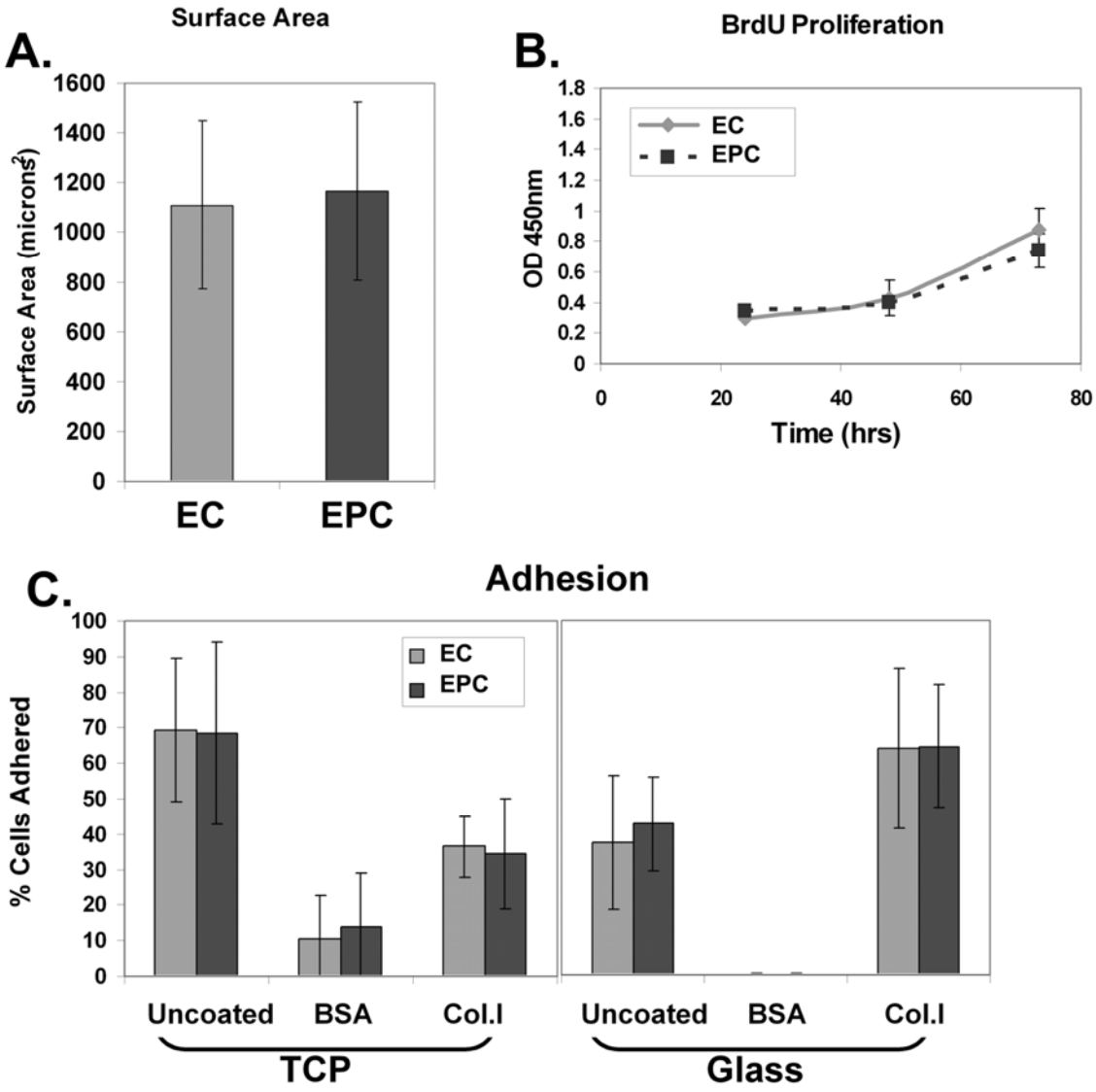

Figure 6.7. Quantification of EC and EPC surface area, proliferation rate, and surface adhesion. **A.** Surface area measurements (mean ± SD) of confluent EPC and mature EC isolations yield similar mean surface areas (Student's t-test, $p > 0.05$). **B.** BrdU proliferation assay. EPCs and ECs treated with 10 μM BrdU proliferate at the same rate on Col I coated TCP at 24, 48, and 72 hours in EGM-2 (Student's t-test, $p > 0.05$). **C.** Percent of cells adhered to the surface. Left: TCP surface. Right: Glass surface. (Student's t-test, $p > 0.05$).

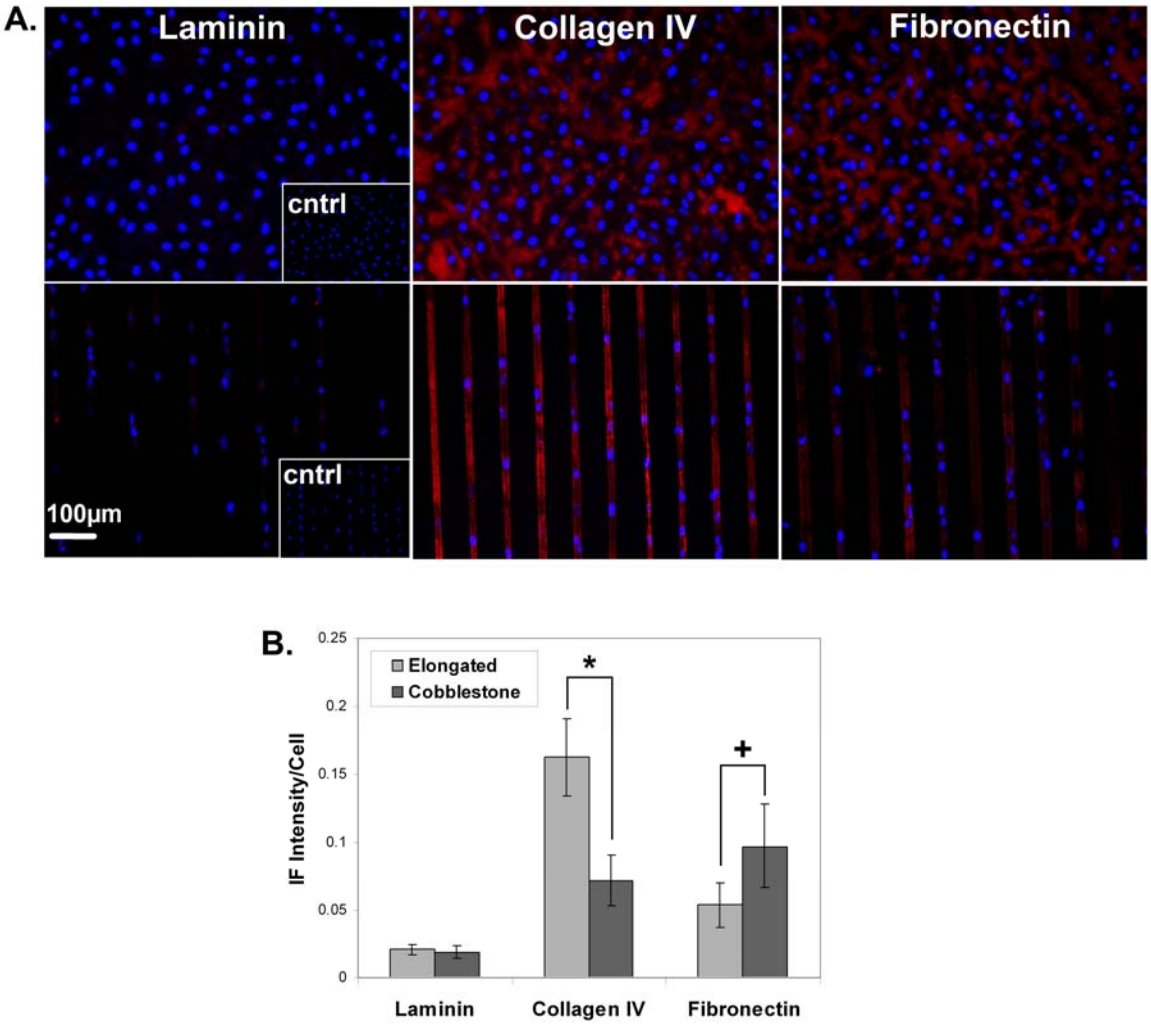

Figure 6.8. Shape-dependent mature EC deposition of ECM proteins. Relative levels of mature EC deposition of ECM proteins per cell. **A.** Representative 20X images of fluorescently stained ECM of matched mature cobblestone ECs and mature micropattern-elongated ECs at 48 hours. **B.** RGB image analysis of staining intensity per cell of ECs on micropatterned or non-patterned collagen I at 48 hours. Paired Student t-test, $^{*}p < 0.01$, $^{+}p = 0.05$

6.6. Discussion

EPCs and mature ECs represent a potential cell source for endothelialization of tissue engineered vascular constructs. One important aspect required of these endothelial cells is deposition of ECM to promote cell survival and function. Therefore, this study was undertaken to quantify EPC and EC deposition of ECM, in both elongated and cobblestone morphologies found in vivo, without the influence of FSS.

EPCs and mature ECs seeded on micropatterned surfaces preferentially adhered to and elongated on the FITC-collagen I coated lanes within the first hour after plating. The major difference observed between EPCs and mature ECs was at later timepoints, when EPCs spread onto the non-adhesive regions between the lanes and formed confluent cell patches, while ECs remained confined to the adhesive lanes. The time required for this EPC inter-lane spreading was dependent on the width and spacing of the micropatterned lanes. It took 48 hours for EPCs to overtake the micropatterned lanes with larger 15 μm lane widths and 45 μm spacing compared to 24 hours on narrower 5 μm lane widths with 20 μm spacing. Therefore, decreasing the width of the adhesive lane and spacing caused EPCs to spread onto non-adherent regions at early timepoints.

Actin alignment is a key feature of cellular elongation. Micropattern-induced actin alignment was fully characterized in Chapter V. The actin cytoskeleton was examined in this study to confirm actin alignment of the elongated cells on the 15 μm x 45 μm micropattern and to make structural comparisions between mature ECs and EPCs. Actin alignment was seen at 4, 24, and 48 hours on 15 μm lanes. EPC and EC actin fibers were observed primarily along the cell edges, forming a dense peripheral band (DPB), as previously reported in other cell types on micropatterned lanes [30, 149]. These DPBs are structural components seen in static EC cultures [102, 109]. Mature ECs elongated by the imposition of FSS demonstrate actin remodeling that includes partial loss of their DPB and elongated morphology after 8 – 24 hours of FSS [98, 102]. In contrast, EPCs and ECs elongated immediately after cell adhesion and the DPB was maintained throughout actin remodeling on micropatterned surfaces up to 48 hours. Thus actin cytoskeletal remodeling due to micropatterned lanes possibly utilized different mechanisms to achieve aligned actin structures and elongated morphology compared to remodeling due to FSS, which is consistent with previous research [149]. The EPCs and mature ECs confined to the micropatterned lanes at 48 hours had aligned actin fibers in

the cytosol. EPCs that spread between the micropatterned lanes at 48 hours had randomly oriented cytosolic stress fibers and filapodia extensions into the non-adhesive regions. To quantify the actin alignment and the degree of randomness in the orientation, the peak angle of the actin orientation, variance about the peak angle, and the entropy in the probability density function of angle orientations were determined. This analysis confirmed the higher degree of alignment (i.e smaller variance about the peak angle) and uniformity (lower entropy) of the actin of mature ECs compared to EPCs at 48 hours. Mature ECs remained aligned for the entire 48 hours. EPCs on micropatterned lanes had aligned actin at 4 and 24 hours, but at 48 hours some alignment was lost due to inter-lane spreading. Rho GTPase, a known regulator of actin dynamics, has been shown to contribute to actin stress fiber formation in ECs on micropatterned surfaces. In previous studies, HUVECs on 15 μm micropatterned lanes transfected with RhoV14, constitutively active, showed actin stress fiber induction in the cytosol [31]. However, RhoV14 activity did not cause HUVECs to spread off of the adhesive lanes at 12 hours. Rho activity in EPCs has not been characterized so it is unknown if it plays a role in EPC spreading off of the micropatterned lanes

Cell adhesion and spreading requires the presence of an underlying ECM. The deposition of ECM by micropatterned cells has never been characterized. Laminin, collagen IV, and fibronectin were stained to do the following: (1) characterize the ECM deposited by EPCs and mature ECs elongated on micropatterned lanes, and (2) determine if EPCs deposited ECM in non-adhesive regions allowing inter-lane spreading. EPCs and ECs deposited primarily fibronectin and collagen IV on the micropatterned lanes. Interestingly, fibronectin and collagen IV appeared in bright fibers along the lane edges, which corresponded to the dense actin bands also seen at the cells edges. There was minimal laminin present at all time points. On the micropatterned surface, EPCs deposited more laminin, fibronectin, and collagen IV than mature ECs at 24 hours and 48 hours. EPCs also deposited fibronectin and collagen IV on the non-adhesive regions between the micropatterned lanes. EPCs were observed to uptake the FITC-collagen I as seen by the presence of punctate FITC molecules within the EPC cell body. This suggests that EPCs were able to actively mobilize the underlying FITC-collagen I micropatterned lane, but it is unclear whether the FITC-collagen was re-deposited, contributing to EPC inter-lane spreading. Remodeling of micropatterned substrate has also been shown in bovine capillary ECs that remodeled micropatterned fibronectin lanes into thick fibers [28]. Taken together, this data

suggests that elongated EPCs deposit more ECM molecules on micropatterned lanes than mature ECs and that EPCs can generate and maintain ECM on unfavorable surfaces.

To determine whether EPC's increased deposition of ECM was limited to elongated cells on micropatterned surfaces, the deposition of ECM by cobblestone EPCs and mature ECs onto three different non-patterned surfaces: FITC- collagen I coated glass, glass, and TCP was evaluated. On all substrates cobblestone EPCs deposited more collagen IV and fibronectin than mature cobblestone ECs, similar to the elongated cells on the micropatterned surfaces. Laminin levels were again minimal on all surfaces; the most visible laminin was deposited by EPCs on uncoated glass at 24 hours. On the uncoated glass and TCP, the production of ECM molecules was detected as earlier as 4 hours. On both of these surfaces EPCs had more ECM molecules at 4 and 24 hours. On glass, both fibronectin and collagen IV were present in granular and randomly oriented fibrillar staining patterns, which has been previously reported [66]. Interestingly, EPCs had more fibronectin fibers compared to ECs, suggesting that EPCs readily deposit and remodel ECM to a greater extent than ECs. On collagen I, less ECM production was seen at 4 hours. The availability of collagen I upon adhesion may have delayed the immediate need for ECM production seen at earlier time points on uncoated surfaces. At 24 and 48 hours, EPCs deposited more collagen IV and fibronectin on the collagen I surface compared to ECs. Thus cobblestone-shaped EPCs deposit more ECM molecules on a variety of surfaces compared to cobblestone-shaped mature ECs. EPC increased capacity for ECM deposition possibly explains EPC's spreading onto the non-adhesive surface between the micropatterned lanes.

Additional explanations for the observed disparity in EPC and mature EC deposition of ECM and behavior on micropatterned surfaces include differences in cell size, adhesion, or proliferation rates. While larger cells have been shown to be capable of crossing wider non-adherent distances on micropatterned surfaces [34], EPCs and ECs had comparable surface areas in measured confluent monolayers. EPCs and ECs also had comparable adhesion on all of the tested non-patterned surfaces, including uncoated, collagen I coated, and BSA coated glass and TCP. Interestingly, on BSA-coated glass there was almost no cell adhesion, confirming that EPCs and ECs did not initially adhere to the BSA coated regions between the micropatterned lanes. Finally, EPCs characteristically have a high proliferative rate [133], but the low level of FBS (2%) in the media induced equivalent proliferation rates for EPCs and ECs. However,

proliferation rate was not measured for elongated cells on micropatterned surfaces. EPCs that were not confined to the micropatterned lanes likely had an increased proliferation rate compared to ECs and EPCs that were restricted to the micropattern. Therefore, cell surface area, adhesion, and proliferation are comparable under these conditions and do not account for the differences in EPCs and EC deposition of ECM and spreading on micropatterns.

While EPC's enhanced capacity for creating an ECM has been demonstrated, the mechanism regulating this function is not known. Two possible mechanisms for the EPC increased ECM deposition compared to ECs are: (1) increased ECM production, or (2) decreased ECM degradation. TGF- β is a known mediator of ECM production in vivo and in vitro [153, 154]. Recently, TGF-β was shown to stimulate ovine EPCs to produce significantly more fibronectin and laminin on tissue engineered scaffolds [155]. EPCs production of TGF-β could play a role in the observed increased ECM deposition, but whether EPCs inherently produce more TGF-β than ECs remains to be determined. Matrix metalloproteinases (MMPs) are major regulators of ECM degradation. In particular, MMP-2 and MMP-9, expressed by ECs, break down the basement membrane [156]. Tissue inhibitor metalloproteinases (TIMPs), also produced by ECs, are endogenous deactivators of MMPs [156]. A balance between MMPs and TIMPs largely regulate ECM maintenance, but EPC expression and activation of these molecules remains undefined.

Finally, mature EC deposition of ECM was shape dependent at 48 hours. Elongated ECs deposited more collagen IV and less fibronectin per cell compared to matched mature cobblestone ECs. Previous studies showed that bovine aortic ECs (BAECs) elongated by the imposition of 30 dynes/cm^2 laminar FSS for 48 hours first demonstrated a decrease in fibronectin production followed by a gradual increase peaking at almost twice the level of static cobblestone controls at 48 hours [66]. Under these conditions, BAECs laminin production showed continuous significant increases beginning at 24 hours and peaking at over twice the level of the controls at 48 hours [66]. In contrast, in this study the elongated ECs on micropatterned lanes deposited more collagen IV, less fibronectin, and the same amount of laminin per cell at 48 hours compared to cobblestone ECs. This suggests that either ECs elongated on micropatterned lanes follow a delayed timecourse of fibronectin and laminin production, or that the FSS is able to compensate for the diminished fibronectin and laminin production caused by elongated morphology. A direct comparison of ECs elongated by

micropatterns versus FSS is needed to fully characterize shape versus shear induced ECM production. However, this EC shape-dependent deposition of fibronectin and collagen IV could have interesting functional implications. Both in vivo and in vitro, fibronectin-rich ECM has been shown to increase EC permeability, which is a complication associated with atherosclerotic plaque development [157]. In vivo, this fibronectin-rich ECM occurs in athero-prone regions of the arterial vessels, which house cobblestone ECs [157]. This EC-shape dependent deposition of ECM has interesting mechanistic implications, suggesting that cytoskeletal structure contributes to the composition of the ECM environment that may be athero-protective or athero-prone. Furthermore, this indicates that the elongated ECs deposition of a fibronectin-depleted ECM could be advantageous for tissue engineered constructs to promote the much needed EC barrier-function during endothelialization. Overall, in the absence of FSS, EPCs and mature ECs elongated on micropatterned lanes are capable of depositing collagen IV, laminin, and fibronectin. Whether EPC deposition of ECM was shape-dependent was not investigated since EPCs did not remain confined to the micropatterned lanes. This evidence suggests that EC morphology plays a role in the production and maintenance of ECM.

6.6.1 Limitations

ECM matrix proteins were quantified using IF staining. Further protein analysis using Western blot for detection of secreted ECM molecules on the surface and in condition media was not possible due to low cell numbers on micropatterned-surfaces. The low cell numbers also prevents analysis of MMP and TIMP activity through such methods as zymography. However, the role of MMPs and TIMPs could be elucidated by treatment with inhibitors (see Chapter XI: Future Work). Shape-dependent EPC deposition of ECM could not be determined since the EPCs did not remain confined to the micropatterned surfaces for extended periods of time.

6.6.2. Conclusion

Micropatterning techniques were used to model in vivo EC elongated morphology to characterize the role of cell source and cytoskeletal alignment on ECM deposition. Micropatterned lanes successfully controlled mature EC and EPC shapes, creating an elongated actin cytoskeletal structure at early timepoints, but EPCs were able to overtake these micropatterned surfaces at 48 hours, spreading onto non-adhesive

regions. This observed inter-lane spreading correlated to ECM deposition in the non-adhesive regions between lanes and enhanced uptake and mobilization of the underlying micropatterned FITC-collagen I substrate. Furthermore, cobblestone EPCs deposited more ECM, in particular collagen IV and fibronectin, than cobblestone ECs on all tested surfaces. Thus EPCs readily generated ECM, which could be advantageous for tissue engineering applications, since EPCs represent an easily accessible autologous cell source. Strikingly, EC deposition of ECM was dependent on cytoskeletal alignment, where elongated ECs produced more collagen IV and less fibronectin than cobblestone ECs. The precise control of cell morphology on micropatterned-substrates may allow for manipulation of EC deposition of ECM and could prove useful for tissue engineering applications.

CHAPTER VII

Endothelial Cell Shape-Dependent Immunogenicity

7.1. Abstract

High, undirectional FSS causes EC elongation with aligned cytoskeletal components and anti-inflammatory EC function. In contrast, low, oscillatory FSS is associated with cobblestone-shaped ECs with a randomly oriented cytoskeleton and pro-inflammatory EC function. Whether EC shape plays a role in EC inflammatory function, independent of FSS, has not been previously determined. The goal of this aim is to determine the effect of EC elongation and cytoskeletal alignment on the expression of inflammatory genes and on EC inflammatory functions. Using micropatterned lanes (25 μm wide with 100 μm spacing) EC elongation and cytoskeletal alignment can be achieved in the absence of FSS. EC gene expression of key inflammation markers (E-selectin, VCAM-1, ICAM-1, and MCP-1) was determined for micropattern-elongated ECs (MPEC) and FSS-elongated ECs. Gene expression was determined with respect to non-patterned cobblestone ECs. MPEC inflammatory activity was evaluated by perfusing monocytic U937 cells over the MPEC surface and quantifying rolling and attachment. MPECs and FSS-elongated ECs both significantly downregulated VCAM-1, indicating decreased inflammation. Interestingly, FSS-elongated ECs significantly upregulated ICAM-1, which increases inflammation, while MPECs did not significantly change ICAM-1 expression. E-selectin expression was downregulated in FSS-elongated ECs and was highly variable in MPECs. MCP-1 expression was also highly

variable in both MPECs and FSS-elongated ECs. U937 adhered to both the MPECs and non-patterned cobblestone ECs surface, but U937 formed weaker interactions on MPECs. Therefore, the cellular elongation and cytoskeletal alignment of MPECs regulated immunogenic gene expression and functions and may act synergistically with FSS to create an EC surface with reduced inflammatory capability.

7.2. Introduction

Inflammation is associated with all stages of atherosclerotic plaque development; hence, atherosclerosis is often viewed as an inflammatory disease. Atherosclerosis occurs when ECs become activated resulting in dysregulation. ECs regulate the inflammatory response through the expression of important inflammatory molecules. Both chemokines and FSS regulate ECs predilection towards pro-inflammatory function [158, 159]. As previously discussed, in vivo and in vitro FSS induces dramatic changes in EC shape and cytoskeletal organization. Little is known about the role of EC shape and cytoskeleton organization as a mediator of EC inflammation, independent of FSS. Research using micropatterned surfaces to control EC shape have shown shape-dependent regulation of EC function, including effects on ICAM-1 gene expression in HUVECs [39]. This aim characterizes the MPEC and FSS-elongated EC expression of the key inflammatory molecules E-selectin, MCP-1, VCAM-1, and ICAM-1 compared to non-patterned cobblestone ECs. Shape dependent inflammatory function was also evaluated by measuring leukocyte interactions (rolling and adhesion) with ECs.

7.3. Background

7.3.1. Inflammation

Inflammation is a complex biological response designed to eliminate infectious or injurious agents. Chronic inflammation is associated with many diseases including ischemic heart disease and atherosclerosis [160]. The inflammatory response is initiated by recruitment of leukocytes to the site of injury. In the vasculature, ECs mediated leukocyte recruitment [161].

7.3.2. The Three Steps in EC-mediated Leukocyte Recruitment

ECs mediate the inflammatory response through expression of molecules that attract, tether, and adhere leukocytes to the EC surface and molecules that facilitate leukocyte movement across the endothelium. This occurs in a sequential three step process (Figure 7.1): (1) leukocyte tethering and rolling, (2) firm adhesion, and (3) transmigration [161-163].

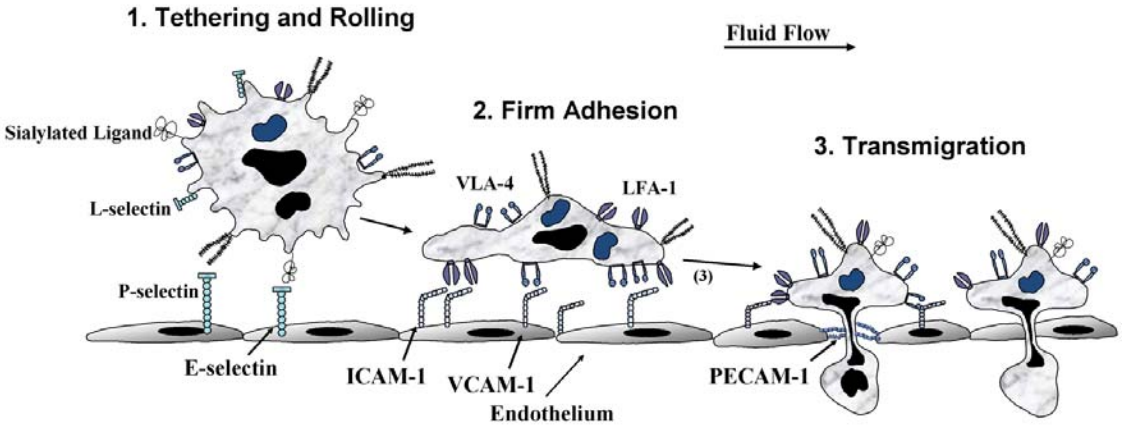

Figure 7.1. Schematic of leukocyte adhesion to the EC surface. Leukocytes adhere to the EC and transmigrate across the endothelium in three steps. **(1)** Tether and Rolling: P-selectin and E-selectin on the EC surface weakly interact with leukocytes. **(2)** Firm Adhesion: leukocytes form firm adhesion with VCAM-1 and ICAM-1 on the EC surface. **(3)** Transmigration: Leukocytes cross the endothelium either through paracellular (via cell-cell junctions, i.e. PECAM-1) or transcellular (directly through the EC surface, mediated by ICAM-1 and VCAM-1) migration. (Figure adapted from Burdick, et al., [4].)

Tethering and Rolling: Flowing leukocytes come in close contact with the ECs by margination, the process by which large red blood cells form a central stream that pushes smaller cells (platelets, leukocytes) towards the endothelial wall. Initially, leukocytes form weak, reversible interactions with ECs referred to as “tethering.” The weakly attached leukocytes roll along the EC surface at or below the velocity of free-flowing cells. Leukocyte tethering and rolling is mediated by selectins [162, 164].

Selectins are family of three transmembrane, adhesion proteins. These proteins have a conserved structure characterized by an NH_2-terminal Ca^{2+} dependent lectin-like

domain, an epidermal growth factor-like domain, a series of repeat sequences similar to the complement binding proteins, a hydrophobic transmembrane region, and a short cytoplasmic domain [160, 163, 164]. L-selectin is found exclusively on leukocytes, E-selectin is found on ECs, and P-selectin is found on both platelets and ECs. On ECs, P-selectin and E-selectin have some functional redundancy, but P-selectin has been observed to play a more prominent role in early rolling while E-selectin promotes slow rolling and adhesion [164, 165]. Furthermore, P-selectin is constitutively expressed and stored by ECs, while E-selectin expression is associated with an activated endothelium [163]. This research of EC regulation of selectins focuses solely on E-selectin.

E-selectin is a 155 kDa protein with a three conserved positively charged amino acids that form the ligand binding domain consisting of arginine 97, lysine 111, and lysine 113 [163]. Common ligands for E-selectin contain sialylated and fucosylated glycan motifs called sialyl Lewis x (SLe^x), sulphated (instead of sialylated) Lewis x (Le^x) [163, 165], or other related structures. Ligands containing these motifs that have been shown to bind E-selectin include L-selectin, CD66, and β_2 integrins [163]. E-selectin ligand binding facilitates leukocyte capture, slow rolling, and may initiated firm adhesion [164, 165].

Firm Adhesion: The initial attachment of leukocytes to ECs is rendered irreversible through leukocyte activation by chemokines, e.g. monocyte chemoattractant protein -1 (MCP-1), and by selectin-dependent activation of β_2 integrins [161]. Arrest of leukocytes and firm adhesion involves integrin binding to immunoglobulin (Ig)-like proteins expressed on the EC surface.

The Ig superfamily contains many cell-surface proteins with multiple Ig-like domains comprised of β sheets joined by disulfide bonds [166]. Ig proteins are involved in antigen binding, complement-binding, or cell adhesion [163]. Relevant Ig-like proteins expressed on the EC surface that are involved in firm leukocyte adhesion are vascular cell adhesion molecule-1 (VCAM-1) and intracellular adhesion molecule-1 (ICAM-1). One of the chemokines involved in the leukocyte activation step, MCP-1, and both VCAM-1 and ICAM-1 involved in firm adhesion are focused on in this research due to their prominent role in atherosclerosis and will be further discussed below.

MCP-1, also known as CCL2, is a 9 to 15 kDa protein in the C-C chemokine β subfamily. MCP-1 present on the EC surface activates leukocyte integrins through local triggering of G-coupled protein receptors [158]. This integrin activation is referred to as “inside-out” signaling, altering integrin conformation to increase leukocyte adhesiveness

[158, 163]. MCP-1 activation of rolling leukocytes facilitates slow rolling and the initiation of firm adhesion via E-selectin [159].

VCAM-1 is a 110 kDa protein with six or seven extracellular Ig-like domains. The most common ligand for VCAM-1 is leukocyte $\alpha_4\beta_1$ integrin, also known as VLA-4. VCAM-1 is almost exclusively expressed by activated ECs [166]. ICAM-1 is an 85-110 kDa protein with five extracellular Ig-like domains. Functional domains include the primary leukocyte binding site on the NH2 terminal 1st domain and a cytoplasmic lysine and arginine rich domain that can bind the cytoskeleton through α -actinin [163, 167]. The major leukocyte ligands for ICAM-1 are β_2 integrins, also known as LFA-1 [161]. ICAM-1 is basally expressed throughout the endothelium, but it is upregulated in activated ECs [161]. Both VCAM-1 and ICAM-1 are regulated by EC gene transcription, which is induced by inflammatory stimuli such as chemokines [161].

Transmigration: Leukocyte transmigration is characterized by the movement of leukocytes from the apical side of ECs to the subendothelial space (SES). Transmigration occurs through two pathways: (1) transcellular, and (2) paracellular [168]. Transcellular migration involves the transport of leukocytes directly through the cytosol of the EC. Paracellular migration utilizes EC cell-cell junctions, e.g. PECAM and VECAD, to move leukocytes to the SES. Most leukocytes have been shown to transmigrate through the paracellular pathway [168]. However recent evidence indicates that the transcellular pathway is highly orchestrated by coordination of the cytoskeleton, ICAM-1, and VCAM-1 [169], suggesting that it may be utilized more frequently in vascular beds with increased endothelial ICAM-1 and VCAM-1 expression [168]. While this research does not directly investigate leukocyte transmigration, the influence of ICAM-1, VCAM- 1, and the cytoskeleton in transcellular migration will be discussed in further detail due to their relevance to the nature of these studies.

Carman and Springer suggest that transcellular migration is coordinated through the assembly of a transmigratory “cuplike” structure [169]. The “transmigratory cup” is formed by ICAM-1 and VCAM-1 rich microvilli projections that can assemble within minutes and surround the site of transmigration. The “transmigratory cup” is also highly composed of cytoskeletal components, verified by the reduction of microvilli projections by inhibition of Rac and CDC42 (known regulators of cytoskeletal dynamics). ICAM-1 and VCAM-1 on the microvilli projections act to organize leukocytes into clusters through integrin binding (discussed above in *Firm Adhesion*). Transcellular migration is facilitated through the vertical alignment of these microvilli projections perpendicular to

the plane of the endothelium, which physically provides a pathway for the oriented migration of leukocytes through the EC body and into the SES, where it can target a site of infection. When this leukocyte transmigration is dysregulated, pathological states can develop and, in particular, contribute to fatty plaque formation in atherosclerosis.

7.3.3. FSS-regulation of EC Immunogenic Response

FSS is a known modulator of EC expression of inflammatory molecules. In vitro studies indicate that high, unidirectional FSS and low, oscillatory FSS can exhibit distinct immunogenic responses from ECs. Regulation of E-selectin by FSS is somewhat controversial, with conflicting reports indicating that steady FSS induces both EC downregulation and no effect on E-selectin gene and protein expression [68]. Steady FSS reduced gene and protein expression in TNF- α stimulated ECs [68]. In contrast, another study demonstrated that mRNA levels of E-selectin of TNF- α treated ECs were unaffected by steady FSS, but protein levels were diminished [170]. In particular, ECs exposed to 12 dynes/cm^2 steady FSS and treated with TNF- α had comparable levels of E-selectin mRNA compared to static TNF- α treated EC cultures, indicating that FSS does not affect EC transcription of E-selectin [170]. However, E-selectin protein expression was reduced 50% by steady FSS suggesting regulation at the protein translation level [170]. ECs expression of MCP-1 when exposed to sustained steady FSS initially increased followed by subsequent return to basal levels at 4 hours, while low, oscillatory FSS maintained upregulated EC expression of MCP-1 [19, 76-78]. EC expression of VCAM-1 is inversely related to FSS [19]. VCAM-1 was downregulated in response to high, steady FSS and upregulated in response to low and oscillatory FSS [19, 63]. Additionally, in the presence of TNF-α stimulation, steady FSS decreased EC mRNA and protein expression of VCAM-1 [68]. FSS-dependent EC regulation of ICAM-1 expression has been more variable. In general, EC expression of ICAM-1 has been shown to increase under high FSS [19, 74, 75]. Yet low and oscillatory FSS have both upregulated and downregulated EC expression of ICAM-1 gene and protein expression [9, 19]. Furthermore, the combination of steady FSS and TNF- α stimulation on EC expression of ICAM-1 is synergistic, resulting in augmented ICAM-1 expression [68]. This FSS-dependent EC regulation of inflammation is also seen in vivo and the functional consequences are most apparent in atherosclerosis.

7.3.4. Inflammation and Atherosclerosis

Athero-prone regions of the vasculature are typically exposed to low, oscillatory FSS. Vascular beds prone to or containing atherosclerotic lesions are associated with EC expression of E-selectin, MCP-1, VCAM-1, and ICAM-1 [171]. In human arteries, E-selectin is expressed by ECs covering the surface of early and late plaques [160, 171]. MCP-1 expression is highest in plaques with areas of flow recirculation, where FSS is low but there is a high shear stress gradient [9, 76]. These areas have increased monocyte recruitment and activation. MCP-1 has been reported to accelerate atherosclerotic plaque development [172, 173]. Mice deficient in MCP-1 had decreased monocytes and lipids in atherosclerotic lesions [174] and overall decreased lesion size [175, 176]. VCAM-1 is critical in early plaque development while ICAM-1 has been attributed to elaboration of "mature" atherosclerotic plaques [177]. In vivo, VCAM-1 is expressed in athero-prone ECs and in the developing plaque. The importance of VCAM-1 in plaque development was demonstrated in a transgenic LDL-receptor null mouse model homozygous for domain 4 deficient VCAM-1 (VCAM-$1^{D4D/D4D}$), which reduced VCAM-1 mRNA and protein [177]. The mice were fed a cholesterol rich diet for 8 weeks [177]. Significant reduction in the area of aortic atherosclerotic plaques was measured in VCAM-$1^{D4D/D4D}$ mice, but the plaque area in mice with ICAM-1 deficiency (ICAM-$1^{-/-}$) was not altered [177]. This indicates that VCAM-1 and ICAM-1 do not have redundant functions and that VCAM-1 facilitates the formation of early plaques. Long term studies of ICAM-$1^{-/-}$ mice crossed into an ApoE$^{-/-}$ background showed a decrease in atherosclerositic plaque area at 20 weeks [137, 177]. Histopathological analysis of ICAM-1 deficient plaques showed the presence of foam cells, ECM, and cholesterol clefts but no calcification [137], indicating a role for ICAM-1 in atherosclerotic elaboration of plaques, but not the late stages of plaque maturation associated with calcification, necrosis, and lumen narrowing [13].

7.3.5. Inflammation and Vascular Grafts

Vascular graft disease and rejection, particularly in the case of allografts, is the result of a robust immune response at anastomosis sites that results in intimal hyperplasia, the buildup of SMC-like cells and ECM [178]. Intimal hyperplasia is formed through a process similar to that of atherosclerotic lesions, except intimal hyperplasia formation can occur rapidly (within months) and is characterized by concentric intimal thickening. In vascular grafts, EC injury and activation can be triggered by all of the

following: (1) the host immune response, (2) ischemia during transplantation, or (3) by re-perfusion [178]. Activated ECs in vascular grafts express E-selectin, MCP-1, VCAM-1, and ICAM-1, all of which play a similar role in intimal hyperplasia as they do in atherosclerosis (discussed above). Interestingly, ICAM-1 deficiency decreased vascular graft disease [178]. Thus, vascular graft patency requires ECs that have anti-inflammatory function to promote long term function and compliance.

7.3.6. Summary

Inflammation is a complex process that becomes dysregulated in atherosclerosis leading to plaque development. Pro-inflammatory function is mediated by ECs in a three step process involving leukocyte tethering and rolling, firm adhesion, and transmigration. ECs in athero-prone regions of the vasculature, with cobblestone morphology, have increased inflammatory function compared to ECs in athero-protective regions of the vasculature, where ECs are elongated. The possible role of EC shape on regulation of EC inflammatory function has not been defined. Furthermore, EC mediated inflammation is also one of the major causes of vascular graft failure to due intimal hyperplasia, which is instigated by the immune response. Thus, determining the underlying cause of EC-mediated inflammation and learning to control it is critical to the understanding and treatment of atherosclerosis.

7.4. Materials and Methods

7.4.1. Experimental Design

The experiments in this aim were designed to assess EC shape-dependent immunogenic gene expression and function. The following three conditions were used: (1) micropattern-elongated ECs (MPECs), (2) ECs plated for 4 hours on non-patterned surfaces and elongated by 20 hours of 12.5 dynes/cm^2 FSS, and (3) static cobblestone ECs on non-patterned surfaces. Micropatterning, shape index measurements, cytoskeletal structure, flow studies, and qtPCR were all carried out as described in the Common Materials and Methods (Chapter IV). Methods specific to this aim are detailed below.

7.4.2. Cells and Culture Conditions

Mature carotid ECs were used in these studies up to passage 5. U937 cells, a monocytic, suspension cell line (a generous gift from Dr. McCarty), were maintained in RPMI 1640media (Gibco) supplemented with 10% FBS, 1% Penicillin/Streptomycin, and weekly addition of L-glutamine (2mM). U937 cells were plated in ultra-low attachment surface flasks (Corning) at $2x10^5$ cells/ml. U937 cells were fed every 2 days and were not allowed to exceed $2x10^6$ cells/ml. When U937 cell density exceeded the volume limits of the tissue culture flasks, the cells were counted and the appropriate cell number was pelleted at 250xg for 5 minutes for re-seeding. The pellet was resuspended in fresh media at $2x10^5$ cells/ml and re-plated. The U937 cells were maintained in normal tissue culture conditions at 37^{o}C and 5% CO_2.

7.4.3. Surface Preparation

The micropattern design of 25 μm wide lanes with 100 μm wide spaces was used for these studies. The microfluidic technique was utilized as described in Common Materials and Methods (Section 4.4).

7.4.4. Flow Studies

ECs were incubated on non-patterned surfaces for 4 hours prior to application of FSS. At 4 hours, the non-patterned ECs were placed in the Glycotech flow chamber and exposed to 20 hours of 12.5 dynes/cm^2 FSS (with FSS ramping described in Common Materials and Methods Section 4.6.).

7.4.5. Shape Index and Cytoskeletal Structure

The shape index and cytoskeletal structure of the ECs in each condition was measured at 24 hours. A minimum of 10 cells were measured in at least 3 images per condition. The cytoskeletal components actin and microtubules were visualized using IF as 24 hours.

7.4.6. qtPCR

RNA isolation and reverse transcription was performed on all samples at 24 hours. Primers for MCP-1, E-selectin, VCAM-1, ICAM-1, and GAPDH were used (Table 4.1). The amplified cDNA was run on 2% agarose gels with SYBR green for UV detection to confirm the amplicon length.

7.4.7. Leukocyte Rolling

For leukocyte adhesion assays, glass slides plated with ECs were carefully assembled onto a flow chamber (GlyoTech) connected to a Harvard PHD22/200 syringe pump (Harvard Apparatus). Assembled flow chambers were mounted on the stage of an inverted microscope (Zeiss Axiovert 200M). U937 cells (1×10^6/ml) suspended in HBSS containing 2 mM Ca^{2+}, 2 mM Mg^{2+} and 0.1% BSA were perfused over ECs at $150s^{-1}$ (corresponding to a FSS of 1 dyne/cm^2) for 4 minutes. After 4 minutes buffer was flowed over the EC surfaces and the flow rate was double every 15 seconds for 1 minute to achieve shear rates of 300, 600, 1200, and 2400 s^{-1} (corresponding to 2, 4, 8, 16 dynes/cm^2) and then held for one additional minute at 4800 s^{-1} (32 dynes/cm^2).

U937 cell adhesion was imaged using brightfield microscopy with a Zeiss 10×, 0.25 NA A-plan lens on a Zeiss Axiovert 200M microscope (Carl Zeiss), and recorded using Stallion 4.0 (Intelligent Imaging Innovations, Inc). Imaging a graticule under the same conditions allowed conversion of pixel size to micrometers.

7.4.8. Statistical Analysis

SPSS version 15.0 was used for statistical analysis. For each set of experimental conditions at least 3 samples were tested. Data represented as mean ± SEM except when indicated as mean ± SD. Shape index comparisons between the three tested conditions employed ANOVA with Tukey post hoc test. Statistical analysis of gene expression was performed on dCt values, calculated in reference to GAPDH, using paired Student's t-test, since the samples were matched. Analysis of U937 cell rolling and attachment utilized paired Student's t-test to determine significant differences for the matched samples. Significance for all statistical tests required $p \leq 0.05$.

7.5. Results

7.5.1. MP- and FSS- Induced EC Shape and Cytoskeletal Alignment

MPEC shape index at 24 hours was 0.37 ± 0.01 which was comparable to FSS-elongated ECs with shape index of 0.39 ± 0.06, (Fig. 7.2). The shape index of ECs that were plated for 24 hours and then exposed to 24 hours of FSS (condition used in Chapter V) was also comparable, with a shape index of 0.36 ± 0.01. Both MPECs and

FSS-elongated ECs had significantly different shape indices compared to non-patterned cobblestone ECs, which has a shape index of 0.72 ± 0.12 (Fig. 7.2).

IF staining and variance measurements confirmed that actin and microtubules of both MPECs and FSS-elongated ECs were elongated and aligned parallel to the direction of FSS (Fig. 7.3 A & B). Actin and microtubules of non-patterned cobblestone ECs remained randomly oriented.

7.5.2. MPECs Regulated Gene Expression

Fold changes in gene expression were calculated compared to non-patterned cobblestone ECs to determine the effect of cellular elongation (induced either by micropatterned surfaces or by FSS) on gene expression. MPECs and FSS-elongated ECs both significantly downregulated VCAM-1 with a fold changes of 0.59 ± 0.2 and 0.11 ± 0.8, respectively (Fig. 7.4). ICAM-1 expression by MPECs did not significantly change while FSS-induced EC elongation significantly upregulated ICAM-1, represented by fold changes of 1.33 ± 0.47 and 1.54 ± 0.38, respectively (Fig. 7.4). MPEC expression of E-selectin was highly variably with fold changes of 0.42 ± 0.58, while FSS-elongated ECs significantly downregulated E-selection expression with fold changes of 0.19 ± 0.07 (Fig. 7.4). It should be noted that the significant downregulation in FSS-elongated ECs was dependent on confluence, where the increased confluence of ECs exposed to FSS resulted in decreased E-selectin. Both MPECs and FSS-elongated ECs had highly variable MCP-1 expression, with fold changes of 2.63 ± 2.07 and 3.26 ± 2.37 (Fig. 7.4). Electrophoresis gels indicated that the appropriate size transcript was amplified by the qtPCR for each corresponding gene (Fig. 7.5).

7.5.3. U937 Cell Rolling and Attachment on MPECs

EC inflammatory function was evaluated by quantifying the attachment of perfused monocytic U937 cells. The surface of MPECs and non-patterned ECs both facilitated U937 rolling and attachment. U937 attachment strength was determined qualitatively by ramping shear stress after U937 attachment. The highest measured shear stress (32 dynes/cm^2) promoted U937 detachment from MPECs and non-patterned ECs. A significantly larger percent of U937 cells detached from MPECs compared to non-patterned ECs. The percent of U937 cell detachment was calculated by dividing the number of U937 cells attached after exposure to the highest shear stress (32 dynes/cm^2) by the number of U937 cells initially attached after flowing the U937 cells

for 4 minutes at 1 dyne/cm^2. The percent of U937 cells that detached from the MPEC and non-patterned cobblestone EC surface were 42.63 ± 7.43 and 18.76 ± 2.55 %, respectively. This implies that the U937 cells formed weaker attachments on the MPEC surface compared to non-patterned cobblestone ECs.

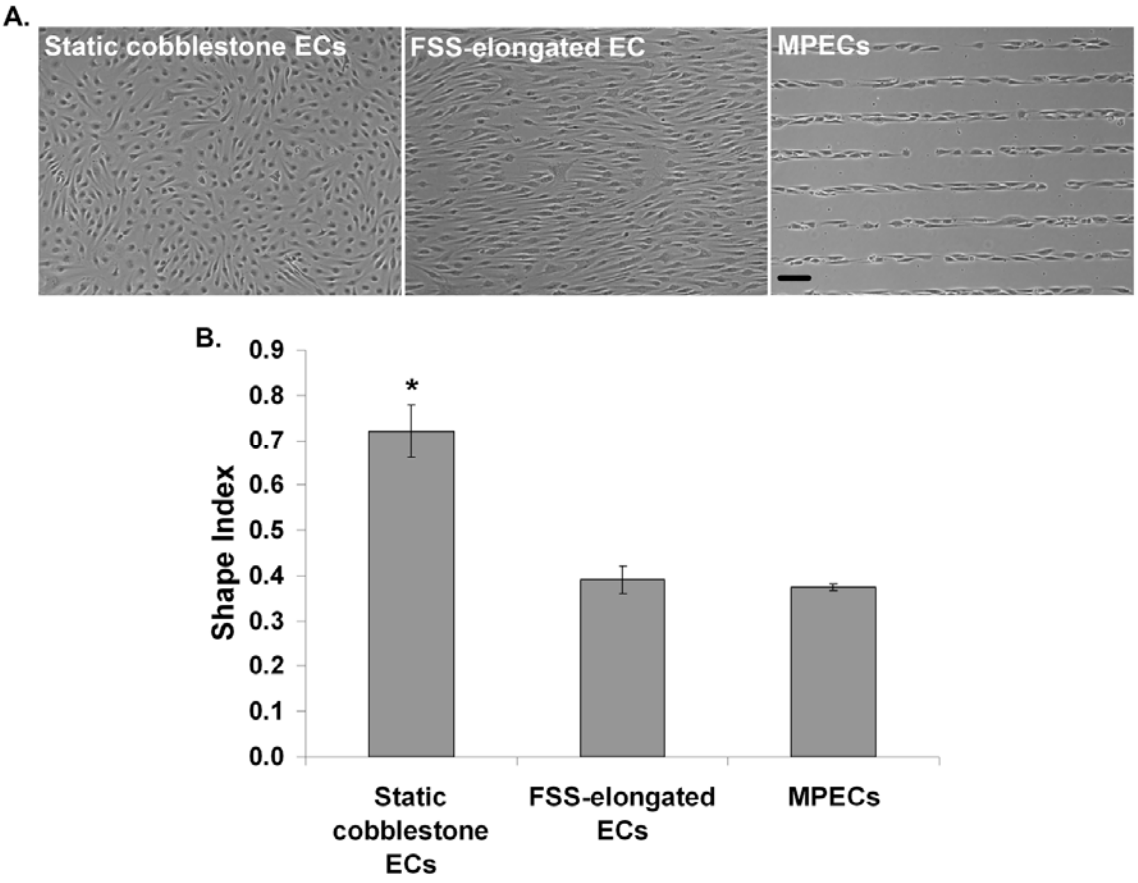

Figure 7.2. MPEC and FSS-elongated EC have comparable shape indices. **A.** Representative EC images of the three conditions used in this chapter (10 X). Scale bar = 100 μm. **B.** Shape index measurements of ECs in each condition. *$p<0.05$, ANOVA, Tukey's. FSS-elongated EC and MPEC shape indices are not significantly different.

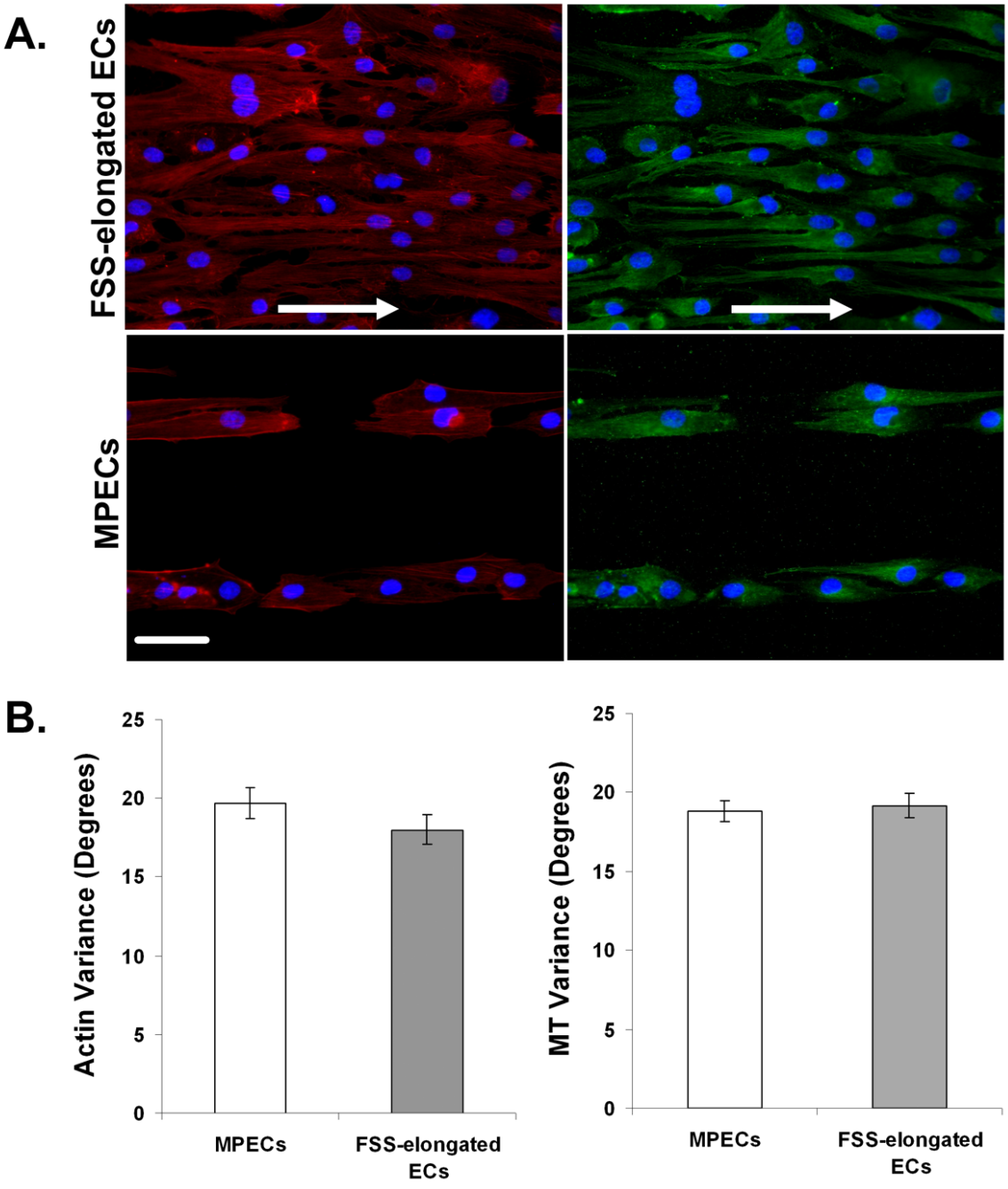

Figure 7.3. Comparable MPECs and FSS-elongated ECs cytoskeletal alignment. **A.** Representative 40 X images of MPECs and FSS-elongated EC actin (left) and microtubule (right) staining. Arrows indicate direction of FSS. Scale bar = 50 μm. **B.** Quantification of peak and variance of actin and microtubule alignment for the MPEC and FSS-elongated EC conditions used in this chapter.

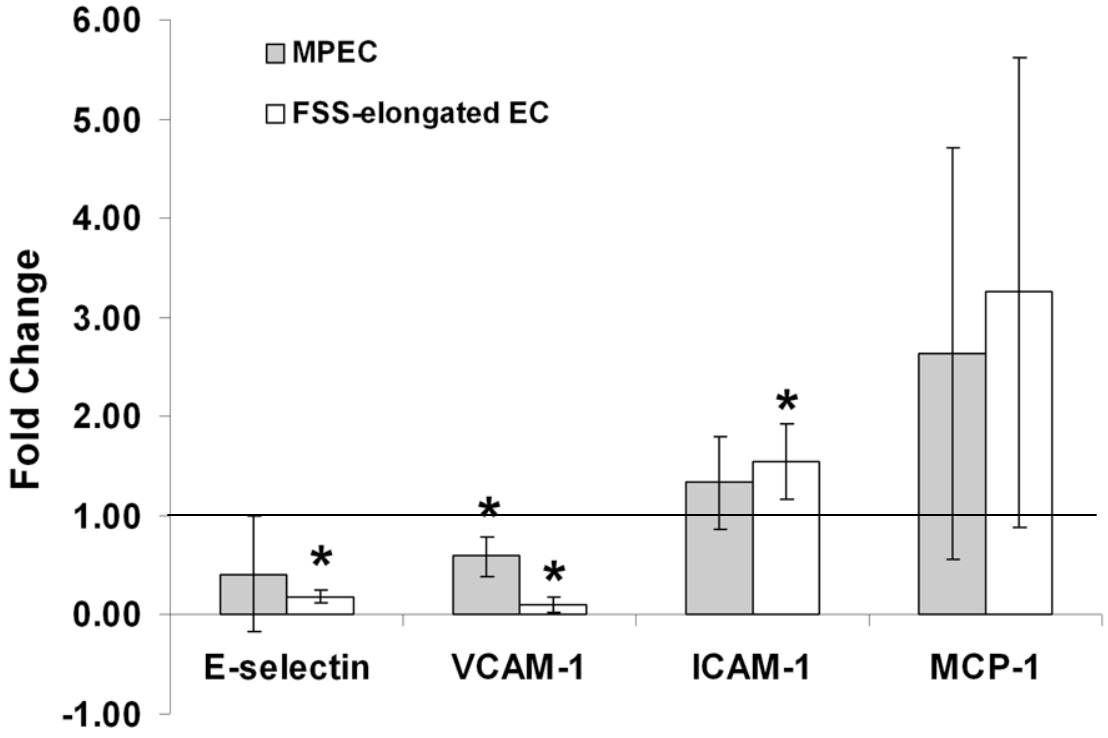

Figure 7.4. Gene expression of key EC markers of inflammation. Fold change in gene expression for MPECs and FSS-elongated ECs was calculated with respect to non-patterned cobblestone ECs to determine the role of cytoskeletal alignment (induced by micropatterned surfaces or by FSS) on EC expression of E-selectin, VCAM-1, ICAM-1 and MCP-1. Data represented as mean ± SD. The line at 1.00 represents the level of non-patterned cobblestone EC gene expression. *p≤0.05, Student's t-test, comparing dCt values.

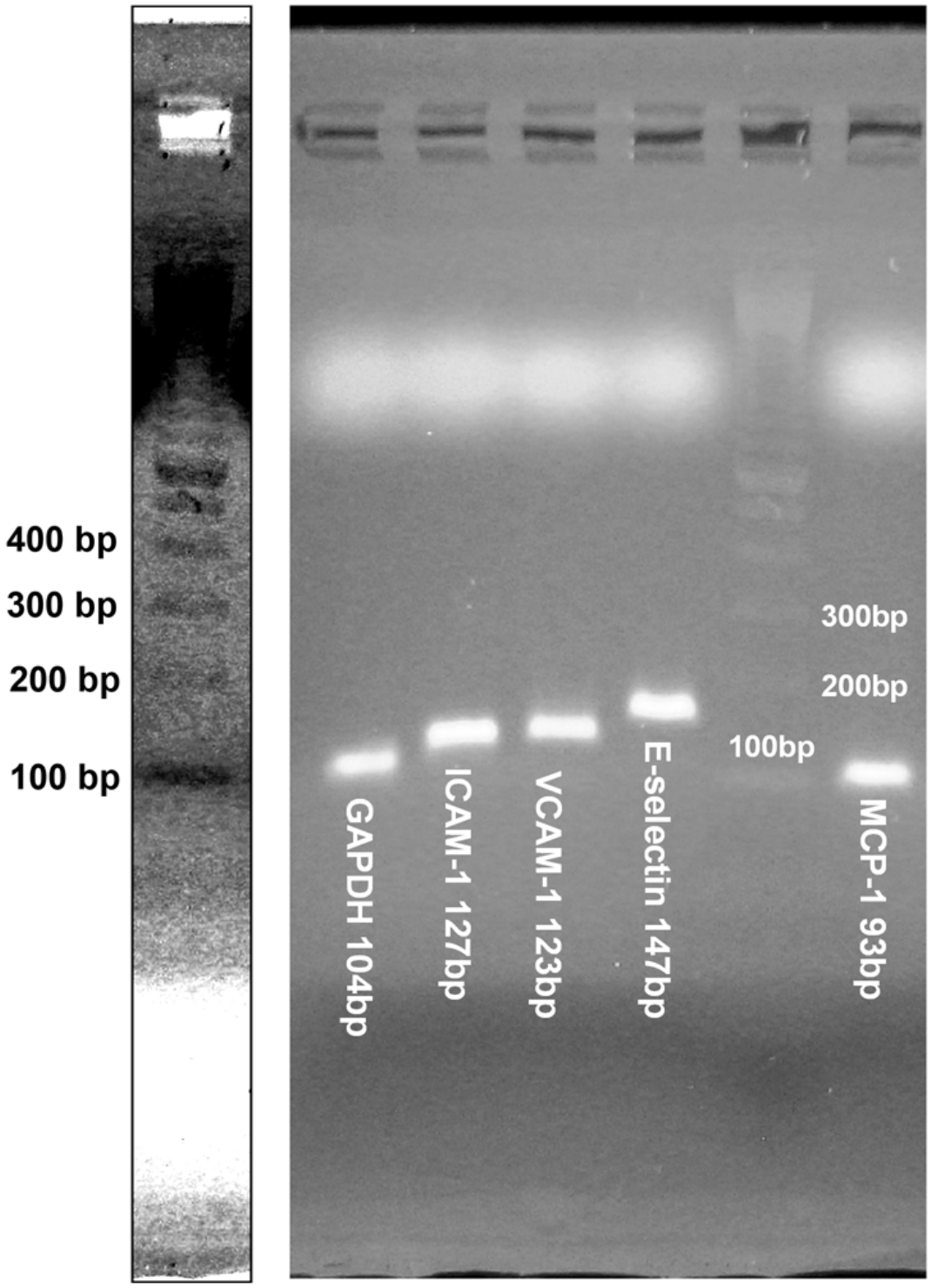

Figure 7.5. Electrophoresis gel of inflammatory genes. Validation of appropriate transcript size for each gene measured in this chapter. Standard for comparison used a 100 bp ladder. Left: Cropped and inverted ladder with adjusted brightness and contrast to aid in visibility of the ladder banding.

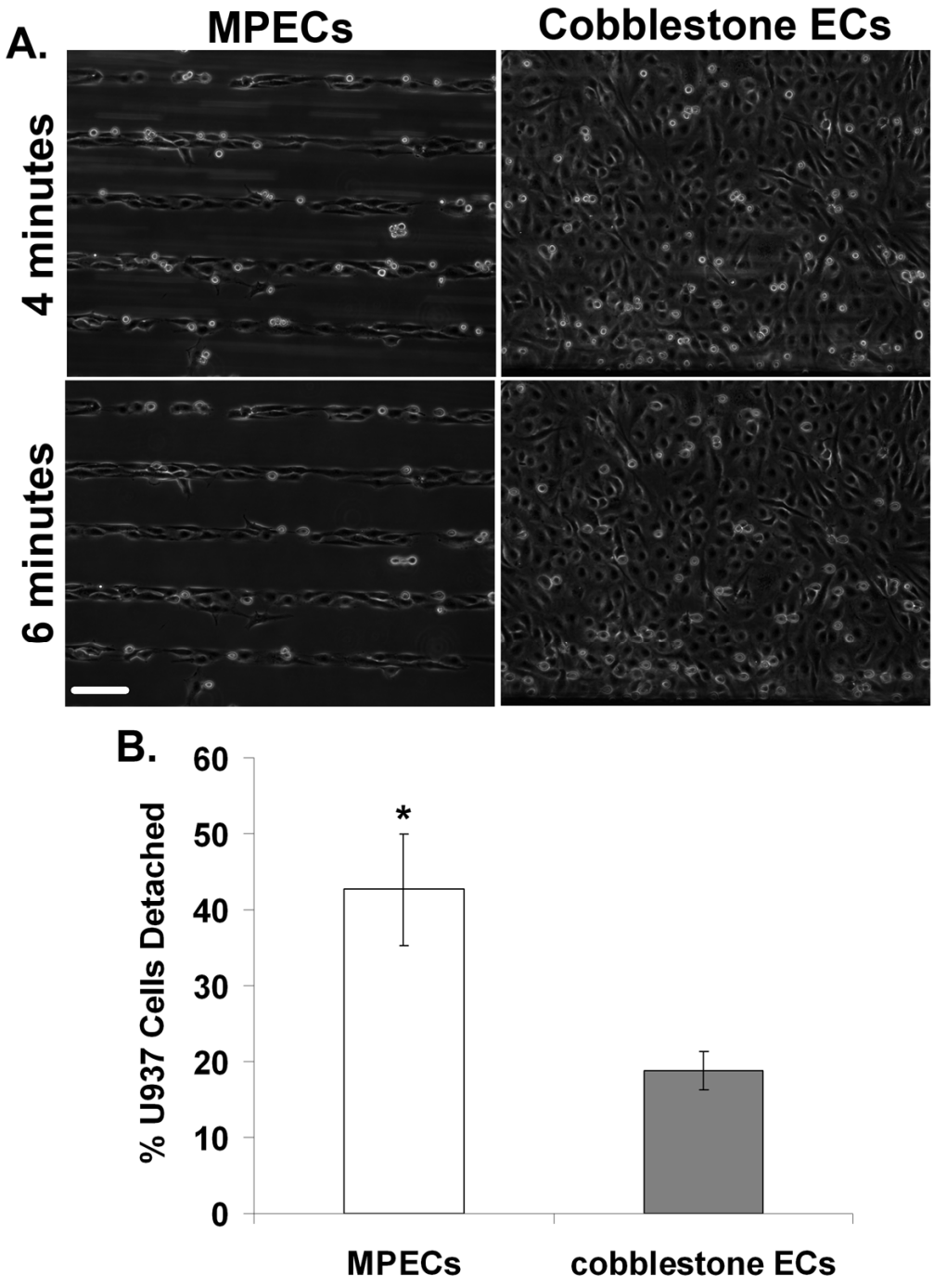

Figure 7.6. U937 attachment to the MPEC surface. **A.** Representative images of U937 cells attached to the MPEC (right) and non-patterned cobblestone EC (left) surface at the end of 4 minutes of U937 perfusion at 1 dyne/cm^2 and at the end of 2 additional minutes of shear stress ramping to 32 dynes/cm^2 at that 6 minute timepoint. Scale bar = 100 μm. **B.** Quantification U937 detachment from the MPEC and non-patterned cobblestone EC surface. A significantly greater percentage of U937 cells detached from the MPEC surface. Data represented as mean ± SD. *$p<0.05$, paired Student's t-test.

7.6. Discussion

Prior to beginning the gene expression and functional evaluation of MPECs, the shape index and cytoskeletal alignment were determined to confirm comparable cell shape and cytoskeletal structure as FSS-elongated ECs. This comparison was fully characterized in Chapter V; however, the conditions utilized in this aim were slightly different. In Chapter V, non-patterned EC were plated for 24 hours prior to commencing 24 hours of 12.5 dynes/cm^2 FSS and therefore final structural, comparisons to MPECs were made at 48 hours. In contrast, in this aim, non-patterned ECs were plated for only 4 hours prior to 20 hours of exposure to FSS, and therefore comparisons need to be made at 24 hours. In Chapter V, it was established that MPECs shape index and cytoskeletal alignment at 24 and 48 hours were not significantly different, but it was important to establish that 20 hours of FSS after only 4 hours of EC adhesion still induced comparable shape index and alignment. The conditions were changed in this aim, and in aim 4, for two reasons: (1) we were concerned that subjecting the ECs to 48 hours of media containing only 2% FBS would create conditions of stress that would alter the genetic profile, and (2) to ensure that both MPECs and FSS-elongated ECs would undergo the elongation process in a similar timeframe. As expected, 4 hours of EC adhesion prior to 20 hours of 12.5 dynes/cm^2 FSS induced EC shape index and cytoskeletal alignment that was comparable to MPECs at 24 hours. Therefore, these two conditions can be used to delineate the effects of EC elongation and cytoskeletal alignment, induced by micropatterned surfaces or by FSS, on EC immunogenicity.

High, unidirectional FSS, that induces EC elongation and cytoskeletal alignment, generally promotes a gene expression profile that is non-immunogenic. In general, steady FSS induces ECs to decrease expression of E-selectin and VCAM-1 and MCP-1, while expression of ICAM-1 is increased. In this study, FSS-elongated ECs decreased E-selectin and VCAM-1, which are characteristic of decreased inflammation. FSS-elongated ECs increased ICAM-1 and variably affected MCP-1, suggesting a somewhat pro-inflammatory profile. Interestingly, MPECs also had significantly decreased VCAM-1 expression but affected no significant change in expression of E-selectin, ICAM-1, or MCP-1. Taken together, this data suggests that EC elongation and cytoskeletal alignment can affect EC expression of inflammatory genes independent of FSS.

Previous research on the influence of steady FSS on E-selectin has been inconclusive. This study suggests a FSS-dependent downregulation of E-selectin.

Cytoskeletal alignment alone was unable to influence E-selection expression, suggesting that shape does not play a role in E-selectin expression. However, previous research on influence of steady FSS, in the presence of TNF-α, on E-selectin has demonstrated regulation of E-selectin at the translational level, even when mRNA levels were unaffected [170]. Therefore, even though MPECs appeared to have no effect on E-selectin mRNA expression, E-selectin protein expression may not have been fully realized due to protein translational effects. E-selectin expression can be elucidated from the functional studies of leukocyte rolling studies discussed later.

While E-selectin is involved in leukocyte rolling, VCAM-1 and ICAM-1 are required for firm adhesion that promotes irreversible leukocyte binding to the EC surface. In MPECs, VCAM-1 expression was significantly downregulated and ICAM-1 expression was unchanged compared to cobblestone ECs. This suggests a role for EC shape and cytoskeletal alignment in regulation of VCAM-1, but not ICAM-1. In agreement with previous studies [19, 68, 179], FSS-elongated ECs also downregulated VCAM-1, and did so to a greater degree than MPECs. Thus, FSS must also play a role in VCAM-1 regulation that is synergistic with cytoskeletal alignment. Interestingly, MPECs had no effect on ICAM-1 while FSS-elongated ECs had a significant increase in ICAM-1 expression compared to cobblestone ECs. This regulation of ICAM-1 further supports that cytoskeletal alignment, either induced by micropatterned surfaces or by FSS, does not play a role in regulation of ICAM-1. This suggests that other FSS-induced mechanisms, independent of cytoskeletal alignment, are required for ICAM-1 induction. Overall, MPECs gene expression of VCAM-1 and ICAM-1 favors a reduced inflammatory profile, while FSS-elongated ECs have conflicting anti- and pro-inflammatory gene expression corresponding to decreased VCAM-1 and increased ICAM-1, respectively. Importantly, ICAM-1 and VCAM-1 are the major adhesion molecules present in the transmigratory cup, of which, ICAM-1 is most often implicated. MPECs, FSS-elongated ECs, and cobblestone EC expression profiles suggest that MPECs may be less likely to have the ICAM-1 and VCAM-1 necessary for a successful transmigratory cup. Therefore MPECs likely have decreased EC permeability, a function that is considered athero-protective. Further investigation into MPEC formation of transmigratory cups and permeability are needed to determine the effects of MPEC gene expression on this function.

Surprisingly, both MPECs and FSS-elongated ECs had variable effects on MCP-1 expression. Previous investigations indicated that sustained steady FSS (6, 12, or 32

dynes/cm^2) induced downregulation of MCP-1after 5 hours [77]. Therefore, it was expected that the 12.5 dynes/cm^2 FSS used in these studies would be sufficient to suppress MCP-1 expression. FSS studies are normally preformed with media containing 10% serum. In contrast, we used only 2% serum in all of these studies since EC spreading off of the micropatterned lanes was enhanced by increased serum levels. Therefore, the low serums levels may support increased MCP-1 expression.

High, unidirectional FSS promotes an EC surface with reduced inflammatory capability and decreased leukocyte adhesion [19, 179]. Similarities in MPEC and FSS-elongated EC gene expression suggest that the MPEC surface may also be innately non-immunogenic. To functionally evaluate EC surface leukocyte adhesiveness, MPEC and non-patterned cobblestone EC surfaces were exposed to flowing U937 cells, which express integrins LFA-1 (CD11a/CD18), VLA-4, and SLe^x [180]. Both MPECs and cobblestone ECs surfaces promoted U937 rolling and adhesion, but U937s attachment to the MPECs surface was weaker. The decrease in firmadhesion may be due to changes in leukocyte affinity, the strength of adhesion to a single EC surface ligand, or avidity, the clustering of EC surface ligands that would increase binding strength. It is difficult to determine whether affinity or avidity has a more prominent role in U937 interactions with MPECs and non-patterned cobblestone ECs since the spatial geometry of these ligands (E-selectin, VCAM-1, ICAM-1) is unknown. However, this data is consistent with MPEC gene expression data where MPECs have less VCAM-1 and comparable levels of ICAM-1, both of which mediate irreversible firm leukocyte adhesion, compared to non-patterned cobblestone ECs. Thus, it is likely that the significant decrease in VCAM-1 mRNA expression correlated to a decrease in VCAM-1 on the MPEC surface. E-selectin levels were not significantly different between MPECs and cobblestone ECs. While E-selectin mediates leukocyte rolling, it also functions to initiate firm adhesion. Therefore, the arrest and subsequent detachment of some of the leukocytes on the EC surface may have been due to weak interactions with E-selectin.

7.6.1. Limitations

Quantification of total amounts of protein is required to determine whether the gene expression levels correspond to protein expression levels. This is particularly important in the case of E-selectin where high, unidirectional FSS has been shown to affect protein translation. Unfortunately, the number of cells on micropatterned surfaces is too low to provide adequate amounts of protein for analysis, such as Western Blots.

The functional analysis EC leukocyte adhesiveness provides insight into EC protein expression of the inflammatory genes measured in this aim, but the specific protein expression still cannot be quantified. Finally, whole field permeability measurements cannot be made on MPECs due to spaces between lanes, making it difficult to accurately investigate leukocyte transmigration and EC permeability at this point. Live microscopy might allow for visualization of movement of leukocytes transcellularly through the EC surface.

7.6.2. Conclusion

EC regulation of inflammation is critical to the maintenance of vascular health. ECs exposed to high, unidirectional FSS promote a reduced EC inflammatory state. These results suggest that cytoskeletal alignment alone can also promote reduced EC inflammatory functions. In particular, VCAM-1 is significantly downregulated by cytoskeletal alignment. ICAM-1 was not changed in MPECs but it was upregulated in ECs exposed to FSS. Functional evaluation of EC-mediated inflammatory responses showed that MPECs formed weaker interactions with flowing leukocytes compared to non-patterned cobblestone ECs, which supports the decreased VCAM-1 gene expression data. E-selectin and MCP-1 expression was more variable in MPECs. Taken together, these data suggest that cytoskeletal alignment is a mediator of EC inflammatory function.

CHAPTER VIII

EC Shape Affects Thrombogenicity Independent of FSS

8.1. Abstract

Atherosclerotic vascular disease and dysfunction of ECs preferentially develop in regions where blood vessels are bifurcated and curved, correlating to regions where ECs are exposed to low, oscillatory FSS, have cobblestone-like morphology, and have an athero-prone phenotype. In contrast, in regions where FSS is high and unidirectional, ECs are elongated parallel to the direction of flow and have an athero-protective phenotype. To determine the role of EC shape on cell function, EC hemostatic functions were investigated, an important measure of EC dysfunction and atherosclerosis, by elongated and cobblestone ECs (with shape either independent of- or dependent on-FSS). To separate EC shape from FSS-induced effects, surface engineering was used to create elongated ECs on micropatterned collagen I lanes (25 μm wide with 100 μm spacing), which created EC elongation and cytoskeletal alignment comparable to that induced in ECs elongated by FSS. qtPCR was used to determine the gene expression of the following markers of coagulant/hemostatic functions: tissue factor (TF), tissue factor pathway inhibitor (TFPI), endothelial nitric oxide synthase (eNOS), thrombomodulin (TM), and von Willebrand Factor (vWF). PCR results indicated that micropattern-elongated EC (MPECs) downregulated expression of TFPI and vWF compared to static cobblestone ECs. TF, eNOS, and TM expression by MPECs was comparable to static cobblestone ECs. FSS-induced EC elongation also downregulated

TFPI and vWF compared to static cobblestone ECs, but to a greater extent than MPECs. FSS-induced elongation also resulted in a significant decrease in TF and significant increased in TM. To determine whether MPEC induced changes in gene expression had functional consequences, platelet adhesion to the EC surface was quantified compared to cobblestone ECs. Overall, MPECs had comparable platelet adhesion compared to cobblestone ECs. These findings suggest that EC shape has limited potential to regulate cell hemostatic functions, such as thrombogenicity. In particular, EC elongation may play a regulatory role in vWF and TFPI expression. However, EC elongation and cytoskeletal alignment alone is not sufficient to fully promote a non-thrombogenic phenotype independent of FSS. Thus, both EC shape and FSS may play important roles in regulating EC hemostatic functions in the maintenance of vascular integrity**.**

8.2. Introduction

Proteins that regulate thrombosis and hemostasis, such as TF, TFPI,TM, vWF, and eNOS are linked to atherosclerosis and are influenced by FSS [9, 10, 24]. Microarray data of baboon aortic ECs under static or FSS (15 dynes/cm^2 for 24 hours) conditions demonstrated differential expression of thrombogenic-related genes [91]. Furthermore, endothelialized vascular grafts pre-conditioned for 20 hours with high FSS (15 dynes/cm^2) versus low FSS (1 dyne/cm^2) demonstrated significantly lower platelet adhesion in a baboon ex vivo shunt model [91]. In these and other studies, FSS had a significant effect on EC thrombogenic potential; however, it is also known that FSS changes EC shape. Since FSS studies have not controlled for EC shape, whether EC shape contributes to pro-thrombotic or pro-coagulant phenotype remains unknown. *This aim is designed to determine shape-dependent EC thrombogenic gene expression and function by isolating EC shape-dependent effects from changes induced by FSS.*

8.3. Background

8.3.1. Hemostasis and Thrombosis

Hemostasis is the complex pathway utilized to stop bleeding through the formation of blood clots. Under pathological conditions in blood vessels, the robust

hemostasis response to vessel injury can result in thrombosis, the formation of a large blot clot that restricts or even blocks blood flow. Thrombosis and hemostasis occurs through the coagulation cascade, of which the extrinsic pathway is largely mediated by ECs.

8.3.2. Coagulation Cascade

The coagulation cascade involves a series of interactions between protease zymogens, enzymes, cofactors, and platelets. Coagulation molecule interaction occurs through two pathways known as extrinsic and intrinsic [181, 182]. These pathways have traditionally been modeled using a "waterfall" cascade, but recent data suggests a more complex "network" cascade model that more accurately demonstrates the complex interplay and regulation, through positive and negative feedback, between these pathways [181, 182]. The positive feedback in this cascade generates large amounts of thrombin and ultimately results in the formation of a stable fibrin-rich blood clot. Negative feedback prevents the over-reaction of this system through anticoagulant pathways. Key pathways for the pro-coagulant and anti-coagulant systems investigated in this research are briefly summarized below followed by an in-depth discussion of each molecule of interest (Figure 8.1).

TF is the primary initiator of the extrinsic coagulation cascade, leading to activation of factor VII and factor X, which in turn catalyzes the conversion of pro-thrombin to thrombin [181, 183]. Thrombin then cleaves fibrinogen, leading to the formation of fibrin, the major component of a blood clot [184]. TFPI is an endogenous inhibitor of TF through the deactivation of FXa and the TF/FVIIa complex. Platelet adhesion is stimulated by vWF [10], which is stored in EC Weibel Palade bodies and secreted to promote thrombosis. Platelet activation is inhibited by nitric oxide (NO) produced by ECs. Deactivation of thrombin is promoted by TM, a surface receptor involved in activation of the protein C anticoagulation pathway [9].

8.3.3. Tissue Factor

Structure: TF, a class II cytokine receptor, is a 47 kDa transmembrane glycoprotein [181, 185]. Structurally, TF consists of an extracellular domain, a transmembrane domain, and a cytoplasmic tail [181, 185]. The extracellular domain is folded into two compact β-sandwiches and is responsible for TF activity. The

transmembrane domain provides stability and the short cytoplasmic tail is thought to play a role in targeting the TF to specific cellular regions [185] .

Function: TF was identified as the major initiator of the extrinsic coagulation cascade more than 100 years ago [185]. Recently, TF signaling activity was linked to inflammation, angiogenesis, and tumor growth [181, 185]; however, the mechanism of this signaling is largely unknown. Exposure of TF to flowing blood occurs in pathological states where ECs are activated. Exposed TF forms a complex with circulating FVII resulting in activation (FVIIa). The TF/FVIIa complex activates Factor IX (FIXa) and FX (FXa). At this point, trace amounts of present thrombin activates FV, the cofactor for FXa, and FVIII, the cofactor for FIXa. This phase is referred to as the initiation phase, and the next steps are referred to as the propagation phase [181]. FXa and FVa bind together to form the prothrombinase complex, which cleaves prothrombin to form thrombin. FIXa and FVIIIa bind to form the tenase complex, which activates more FX. This process results in the generation of large amounts of thrombin. Thrombin cleaves fibrinogen to form fibrin, resulting in the formation of a stable fibrin clot.

Expression: TF is expressed in many cells and organs including the astrocytes, adipocytes, brain, and lung [185]. In blood vessels, TF is predominantly found in the cells of the adventia including fibroblasts and pericytes [185]. Under normal conditions, SMCs and ECs do not express TF; however TF expression can be induced by TNF-α, IL-1β, lipoplysaccharide (LPS), and oscillatory FSS [185-187].

.

8.3.4. Tissue Factor Pathway Inhibitor

Structure: TFPI is a 34-40 kDa Kunitz-type serine protease inhibitor [181, 182]. TFPI consists of three tandem Kunitz-type domains and a carboxy-terminal domain [182]. The first two Kunitz-type domains are critical to TFPI's dual inhibitory function. The third Kunitz domain and the carboxy-terminal have heparin binding sites and also contribute to anti-coagulant activity [182].

Function: TFPI inhibits the FXa and the TF/FVIIa complex in a two step process that is most effective in the presence of FXa, thus robust TFPI inhibitory activity is not triggered until coagulation has been initiated [181, 182]. First, the second Kunitz domain binds FXa at or near the enzyme active site, which deactivates it [181, 182]. Binding of FXa is most effective when FXa is bound to its cofactor FVa in the prothrombinase complex [188]. Next, the first Kunitz domain binds the TF/FVIIa complex, preventing further FX and FIX activation [181]. The dual binding of the Kunitz domains to FXa and

TF/FVIIa forms a quaternary complex that is necessary for TFPI inhibitory function [181]. The carboxy terminal domain participates in anti-coagulant activity of TFPI by facilitating the rapid binding of the second Kunitz domain to FXa and the binding of heparin, which also enhances FXa inhibition [182]. A truncated version of TFPI lacking the carboxy terminal domain has decreased inhibitory activity [182].

Expression: TFPI is mainly synthesized and stored in ECs [181, 182], but can also be found in platelets. TFPI is either secreted by ECs or found bound to the membrane [189]. The normal circulating concentration of TFPI found in the plasma is 2 nM [182]. Stimulation with heparin promotes the release of TFPI stores, which can increase the circulating TFPI levels two- to four- fold [182].

8.3.5. von Willebrand Factor

Structure: vWF is a multimeric cysteine-rich glycoprotein formed by the assembly of pro-vWF ~250k kDa subunits [190]. In the endoplasmic reticulum, pro-vWF subunits dimerize “tail-to-tail” through disulfide bonding between carboxyl terminals [190]. The multimer is formed in the golgi apparatus through “head-to-head” disulfide bonding of the amino-termini. The result is a long chain of disulfide-linked vWF subunits that can reach sizes of >20,000 kDa [190]. Only the vWF multimers are hemostatically active, the vWF subunits do not retain any function [190]. Mature vWF is stored in ECs; however, the majority of vWF is constitutively secreted [190].

Function: Normal synthesis and secretion of vWF is critical to coagulation. Deficiency in vWF is one of the most common heritable bleeding disorders, known as vWF disease [190]. Secreted vWF associates with the subendothelial matrix and binds platelets and FVIII when exposed to flowing blood, e.g. through vascular injury. A two-step model of platelet binding to vWF has been proposed. First, vWF rapidly, but loosely binds glycoprotein Ib-IX-V (GP Ib) complex on non-activated platelets [190]. Second, platelet activation leads to the slow, irreversible binding of $\alpha_{IIb}\beta_3$ integrin. Platelet-vWF binding is optimum at high shear rates of >1,000 s^{-1} (found in 10-50 μm diameter arteries) [190]. In vWF binding of FVIII, vWF acts as a carrier of FVIII for delivery to the coagulation site to further propagate the coagulation cascade through FVIII activation [190, 191].

Expression: ECs are the primary source for vWF. Approximately 95% of vWF is secreted [190]. ECs store the remaining mature vWF in Weibel-Palade bodies, which are 0.1-0.2 μm wide rod-shaped organelles specific to the endothelium [190]. Stored

vWF is secreted upon EC activation in response to an agonist. In vivo agonists include adrenergic stress and thrombin generation, while some in vitro agonists include histamine, thrombin, and phorbol myristate acetate [190].

8.3.6. Thrombomodulin

Structure: TM is a 75 kDa integral membrane protein [191] made up of 5 distinct domains [192]. TM has a short cytoplasmic tail, a membrane spanning domain, a serine-threonine-rich domain, six epidermal growth factor-like repeats, and an N-terminus with a lectin-like domain [192]. The six epidermal growth factor-like repeats domain has thrombin binding sites and is critical for protein C activation [192].

Function: TM functions as an anti-coagulant by facilitating thrombin activation of protein C (APC). Thrombin activates protein C by cleaving the N-terminus domain. Thrombin bound to TM undergoes conformational changes that result in an increased affinity to protein C, and ultimately a >1000 fold increase in thrombin-mediated protein C activation [63, 191]. APC, with cofactor protein S, proteolytically cleaves and deactivates FVa and FVIIIa. Beyond mediating the generation of APC, TM competitive binding of thrombin suppresses pro-coagulant function through decreased FV and FVIII activation, decrease fibrin formation, and decreased platelet activation [63, 191].

Expression: TM was first identified on ECs, and since then TM has been found on a variety of cells including astrocytes, mesothelial cells, platelets, and monocytes [192]. Basally, ECs express approximately 30,000 – 100,000 TM molecules on the cell surface [191]. TM expression is transcriptionally regulated and is affected by TNF-α, IL-1β, endotoxin, and FSS [85, 191, 192].

8.3.7. Endothelial Nitric Oxide Synthase/Nitric Oxide

Structure: NO is a small, unstable gaseous molecule. Nitric oxide synthase (NOS) is a bifunctional enzyme present in three isoforms: neuronal (nNOS), inducible (iNOS), and endothelial (eNOS) [191]. The NOS family have a conserved carboxyl-terminal reductase domain and an N-terminal oxygenase domain containing a heme prosthetic group [191]. Both domains are required for efficient NO catalysis [191].

Function: NO is a potent vasodilator that also plays a role in platelet inhibition. NO inhibitory activity occurs through diffusion into platelets and activation of guanylyl cyclase, which inhibits platelet adhesion, activation, and aggregation [191]. The

biosynthesis of NO is catalyzed by endothelial nitric oxide synthase (eNOS) through NADPH-dependent conversion of L-arginine and O_2 to L-citrulline and NO [88].

Expression: Basally, eNOS is present in the endothelium of the vasculature in an inactive state [191]. Physiological agonists, such as VEGF, exercise, estrogen, and FSS, can activate eNOS increasing NO [191]. Transcriptional regulation of eNOS is controlled by mechanical and biochemical factors, of which FSS is considered the major regulator of sustained eNOS activity and NO synthesis [191].

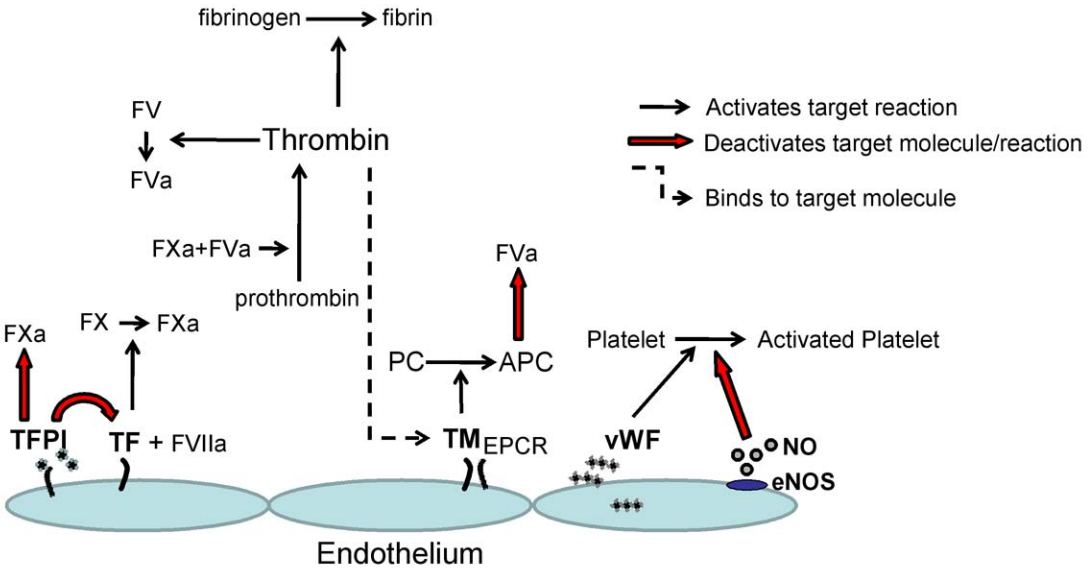

Figure 8.1. Extrinsic coagulation cascade. Schematic highlights the roles of the molecules of interest to this study in regulation of the extrinsic coagulation cascade. Red arrows indicate inhibitory activity

8.3.8. FSS Regulation of Thrombogenicity

EC expression and activity of coagulation factors has been linked to FSS. FSS-dependent expression of TF is controversial, with varying results as to regulatory effects. HUVECs exposed to 12 dynes/cm^2 steady FSS for varying time periods ranging from 20 minutes to 12 hours showed time-dependent transient increases in TF expression and activity compared to static controls [79]. Another study, using the human derived EC line EaHy 926 evaluated TF and TFPI expression and activity under unidirectional pulsatile or oscillatory flow compared to static controls [80]. Results of this study show a

significant 1.5 and 1.75 fold increase in TF mRNA and protein expression under oscillatory FSS (0 ± 3 dynes/cm^2), respectively. TFPI expression did not change and a 2 fold increase in TF activity was recorded. Under unidirectional, pulsatile flow (6 ± 4 dynes/cm^2), TF expression did not change, but TFPI mRNA and protein expression had significant 1.5 and 1.8 fold increases, respectively. These changes in protein levels, mediated by unidirectional FSS resulted in a decrease in TF activity [80]. Other studies have also confirmed that steady FSS-dependent increases in TFPI expression and secretion modulate TF activity [81, 82]. A recent study showed that expression of vWF is responsive to stimulation with FSS [83]. In this study, HUVECs exposed to 26 hours of 15 dynes/cm^2 steady FSS had a 1.8 fold increase in vWF mRNA expression compared to static controls [83]. Multiple studies have shown steady FSS-dependent regulation of TM [85, 86]. Malek, et al., investigated TM expression in bovine aortic ECs (BAECs) under physiological (15 dynes/cm^2), elevated (36 dynes/cm^2) and low (4 dynes/cm^2) steady FSS [85]. These results indicated early transient increases in TM followed by significant downregulation of TM in BAECs exposed to 15 and 36 dynes/cm^2 steady FSS. BAEC exposure to 4 dynes/cm^2 FSS did not alter TM expression. In contrast, Takada, et al., reported a 330% and 200% increase in TM mRNA expression in HUVECs exposed to 15 dynes/cm^2 steady FSS for 8 and 24 hours, respectively [86]. Steady FSS-dependent upregulation of eNOS expression has been well documented [19, 76, 87, 89, 193]. In particular, Davies, et al., have shown that upregulation of eNOS mRNA under laminar FSS involves binding of NFκB to eNOS promoter, resulting in upregulation and increased eNOS stability [88, 194] The importance of FSS regulation of EC-mediated expression of coagulation factors translates in vivo and is relevant to the pathological vascular environment.

8.3.9. Thrombosis and Atherosclerosis

EC expression of thrombotic proteins is generally associated with the late stages of atherosclerosis. ECs express TF almost exclusively in atherosclerotic regions of the vasculature [195], while TFPI is constitutively expressed in the endothelium. In atherosclerotic plaques, TF and TFPI can be found in ECs, SMCs, macrophages, and foam cells [196, 197]. Human autopsies reveal that in atherosclerotic plaques TF is mRNA and protein is expressed and TFPI mRNA and protein expression is increased [196]. In all plaques, TF and TFPI expression was co-localized and often found in fibrin-rich areas, indicating TFPI regulation of TF activity [196, 197]. The role of vWF in the

development of atherosclerotic plaques and occlusive thrombi was elucidated in a pig model of vWF disease [198]. While vWF was not required for the development of atherosclerotic plaques, mechanically-induced stenosis led to the formation of occlusive thrombi only in normal pigs [198]. This indicates that vWF has a critical role in the development of occlusive thrombosis in atherosclerotic plaques [198]. TM mRNA expression was not found in samples taken from atherosclerotic plaques from 8 human patients [199]. An in vitro study of endothelial TM expression found that uptake of oxLDL (a common component of atherosclerotic plaques) downregulated EC expression of TM [200]. Thus, the atherosclerotic environment may prevent TM expression in the endothelium of atherosclerotic lesions, promoting a pro-thrombotic EC phenotype. Loss of eNOS function is one of the earliest signs of EC dysfunction, and is considered to be a risk factor for atherosclerosis. In human tissue samples, the endothelium overlying atherosclerotic plaques had decreased EC expression of eNOS mRNA and protein in both early and late lesions compared to healthy vascular tissues [201]. Taken together, EC expression of thrombotic proteins is dysregulated in atherosclerotic plaques, creating a vascular environment prone to robust hemostatic response that can form occlusive thrombi, ultimately leading to heart attacks and strokes.

8.3.10. Thrombosis and Vascular Grafts

Synthetic small caliber (<6 mm diameter) vascular graft patency is severely limited by intimal hyperplasia (discussed in Section 7.3.5.) and thrombosis. Upon implantation, the uncoated surfaces of synthetic vascular grafts are coated with plasma proteins that present integrin bindings sites for platelet adhesion and activation [202]. Surface modifications have been developed to prevent blood contact-initiation of thrombosis [202, 203]. A variety of anti-coagulant molecules have been conjugated to the graft surface to limit platelet adhesion, e.g. heparin [204], resulting in decreases in platelet adhesion in the short term, but in vivo surface coating is short-lived and does not provide increased long term patency [205]. Anti-coagulant eluting vascular constructs [202, 206, 207], e.g. stents, to prolong the durations of therapy are being considered due to the current failure of anti-proliferative drug eluting stents due to delayed thrombosis [208]. As previously discussed, endothelializing the lumen of synthetic vascular graft surfaces can create non-thrombogenic surfaces; however, these ECs must be fully functional. In vivo, endothelialization of the graft surface is limited, resulting from pannus ingrowth from the anastomoses site that do not form complete endothelial coverage of

the graft surface. In vitro, surface coatings, e.g. fibronectin, and additional ex vivo manipulations, e.g. FSS, have been used to promote anti-thrombotic function in EC-seeded synthetic vascular grafts prior to implantation. The presence of functional ECs on the graft surface has demonstrated decreases in thrombogenicity, but this usually required additional ex vivo manipulation to promote an anti-thrombotic EC phenotype. Thus, understanding how to promote anti-thrombotic EC function is a critical design feature required for the success of vascular grafts.

8.3.11. Summary

Due to their anatomical location, ECs come in direct contact with flowing blood. Through a delicate balance of protein expression, ECs create a non-thrombogenic barrier between the blood and the vessels wall. Healthy ECs are equipped to handle minor vascular injury through a tightly regulated coagulation cascade that results in formation of a hemostatic fibrin plug. Under pathological conditions, in particular late stages of atherosclerosis, the balance of EC expression of pro- and anti- thrombotic proteins can become disrupted resulting in dysregulated coagulation, which promotes robust coagulation and the formation of occlusive thrombi. FSS is a known regulator of EC thrombogenicity, both in vivo and in vitro. However, whether the distinct EC shapes induced by FSS in athero-protective (elongated ECs) and athero-prone (cobblestone ECs) vascular beds play a regulatory role in EC expression of thrombotic markers, independent of FSS, has not been previously determined.

8.4. Materials and Methods

8.4.1. Experimental Design

The experiments in this aim were designed to determine whether EC elongated shape and cytoskeletal alignment affect thrombogenicity independent of FSS. The following three conditions used in this aim: (1) ECs elongated on micropatterned lanes for 24 hours (MPECs), (2) ECs plated for 4 hours on non-patterned surfaces and elongated by 20 hours of 12.5 dynes/cm^2 FSS, and (3) static cobblestone ECs on non-patterned surfaces. Micropatterning, IF, and qtPCR were performed as described in Common Materials and Methods (Chapter IV). Details of the methods used in this aim are described below.

8.4.2. Cells and Surface Preparation

Mature carotid ECs were used in these experiments through passage 5. Micropattern design of 25 μm wide lanes with 100 μm spacing were used, implemented using the microfluidic technique.

8.4.3. Flow Studies

ECs were incubated for 4 hours on non-patterned surfaces prior to the application of FSS. ECs slides were inserted in the GlycoTech flow chamber and exposed to 20 hours of 12.5 dynes/cm^2 FSS for 20 hours (with the ramping profile described in Common Materials and Methods Section 4.6.).

8.4.4. qtPCR

RNA isolation and reverse transcription were performed on ECs in each condition at 24 hours. Primers for TF, TFPI, vWF, TM, eNOS, and GAPDH were used for qtPCR (Table 4.1). The amplified cDNA was run on 2% agarose gels with SYBR green for UV detection to confirm the amplicon length.

8.4.5. vWF staining

IF staining, with permeabilization, for vWF was performed on MPECs and cobblestone ECs at 24 hours.

8.4.6. Platelet Adhesion and Quantification

Healthy human male volunteers (average age 26) donated 20 mls of blood, taken in syringes containing sterile 3.8% sodium citrate anticoagulant at 1:10. The blood was transferred into polypropylene tubes, equilibrated, and centrifuged at 200xg for 20 minutes at room temperature. After centrifugation, the platelet rich plasma (PRP) was removed and placed into 15 ml centrifuge tubes. A sample of the PRP was diluted 1:200 in Modified Tyrode's buffer (containing 129 mM NaCl, 20 mM HEPES, 12 mM $NaHCO_3$, 2.9 mM KCl, 1 mM $MgCl_2$, and 0.34 mM Na_2HPO_2:$12H_2O$ at pH 7.3) to count the platelets using a hemocytometer. The required volume of PRP was removed and the excess PRP was centrifuged at 1000xg for 10 minutes to create platelet poor plasma (PPP), which was carefully removed from the centrifuge tube to avoid disrupting the platelet pellet. The PRP was diluted with PPP to 8x10^7 platelets/ml. MPECs and non-

patterned static ECs were rinsed twice with PBS (without Ca^{+2} and Mg^{+2}) and incubated with one ml PRP for one hour at 37°C and 5% CO_2. After incubation, the ECs were gently washed three times with Modified Tyrode's buffer to remove unattached platelets. The ECs and platelets were fixed in 3.7% PFA and stained as described in Common Materials and Methods (Section 4.8), without permeabilization, using primary antibody anti-CP8, which identifies platelet GP IIb/IIIa, and secondary antibody conjugated with Alexa Fluor 488. DAPI was used to stain the nuclei of ECs. The IF staining was imaged at 40X.

Platelet adhesion to ECs and exposed ECM was quantified using NIH Image J. Phase and fluorescent images were overlaid by first converting the images to a stack followed by combining the image stack in a Z projection set at maximum intensity. Platelets were counted according to the following attachment location: exposed matrix only, cell edges, cell-cell junctions, and cell body. Total surface area of EC coverage and exposed matrix was quantified using NIH Image J to determine total pixel number in a manually traced area. The total number of platelets (at all measured cellular locations) attached to ECs or matrix only was calculated per mm^2. The percentage of platelets attached to a particular region of a cell was calculated by dividing the number of platelets counted in a particular EC region by the total number of platelets attached to ECs in that image. A minimum of 6 images were quantified for each MPEC sample and 3 images per image of static ECs on non-patterned surfaces.

8.4.7. PECAM-1 Staining

PECAM-1 was stained in MPECs and in non-patterned cobblestone ECs using IF, without permeabilizing. The PECAM-1 antibody (BioCare, clone JC/70A) was used at 1:50. Secondary antibody Alexa Fluor 488 was used for detection.

8.4.8. Statistical Analysis

SPSS version 15.0 was used for statistical analysis. At least 3 samples were tested in each experimental condition. Data represented as mean ± SEM unless indicated as mean ± SD. For gene expression, statistical analysis was performed on dCt values, calculated in reference to GAPDH, using paired Student's t-test for matched samples. For analysis of platelet adhesion, paired Student's t-test was used to determine significant differences in matched samples. Significance for all statistical tests required $p \leq 0.05$.

8.5. Results

8.5.1. EC Elongation Influences Thrombogenic Gene Expression

MPEC and FSS-elongated EC gene expression was compared to non-patterned cobblestone ECs to determine the effect of EC elongation induced by micropatterned surfaces or by FSS. PCR results indicated that MPECs significantly downregulated vWF and TFPI with fold changes of 0.65 ± 0.25 and 0.72 ± 0.24, respectively (Fig. 8.2). MPECs did not significantly affect expression of TF, TM, and eNOS, such that fold changes were 0.79 ± 0.34, 0.84 ± 0.30, and 0.78 ± 0.60, respectively (Fig. 8.2). FSS-dependent EC elongation also resulted in a significant downregulation of vWF and TFPI with fold changes of 0.15 ± 0.01 and 0.54 ± 0.2, respectively (Fig. 8.2). FSS-induced EC elongation also significantly downregulated TF and significantly upregulated TM, with fold changes of 0.33 ± 0.25 and 1.47 ± 0.35, respectively (Fig. 8.2). FSS-induced EC expression of eNOS was surprisingly variable, with fold change of 1.19 ± 0.62 (Fig. 8.2). Gel electrophoresis confirmed that size of the transcript amplified by qtPCR transcript was appropriate for the corresponding gene (Fig. 8.3).

8.5.2. MPECs and Static Cobblestone ECs vWF Protein Expression

Protein levels of vWF were assessed using IF since the gene expression data indicated significant downregulation of vWF by MPEC compared to non-patterned cobblestone ECs. Both MPECs and non-patterned cobblestone ECs stained positively for vWF with no observed differences in expression (Fig. 8.4).

8.5.3. Platelet Adhesion on MPECs and Static Cobblestone ECs

To assess MPEC thrombogenicity, platelet adhesion was evaluated compared to cobblestone ECs. Platelets adhered to both MPECs and static cobblestone ECs. There was no significant difference in platelet adhesion per mm^2 between the exposed matrix of MPECs and cobblestone EC samples, resulting in 4609 ± 1324 and 3146 ± 557 platelets/mm^2, respectively (Fig.8.5). The majority of platelets adhered to MPECs edges, which were exposed to BSA. These platelets were counted, but since cobblestone ECs did not have a comparable “edge” surface, these platelets were not included in total platelet calculations. Overall, platelet adhesion to MPECs per mm^2 of

EC surface area was comparable to their adhesion to cobblestone ECs, where platelet adhesion to MPECs and cobblestone ECs were 1118 ± 160 and 1149 ± 180 platelets/mm^2, respectively (Fig. 8.5). The percent of platelets adhered at cell-cell junctions and on the cell surface were also comparable between MPECs and non-patterned cobblestone ECs. The percentages of platelets adhering to the cell-cell junctions of MPECs and non-patterned cobblestone ECs were 80.35 ± 3.21 % and 78.84 ± 4.18 %, respectively (Fig. 8.5). On the cell surface, platelets adhered to MPECs and non-patterned cobblestone at 19.65 ± 3.21 % and 21.15 ± 4.18 %, respectively (Fig. 8.5).

8.5.4 PECAM-1 Expression

Due to platelet adhesion at cell-cell junctions, and on the exposed edges of MPECS, platelet cell adhesion molecule -1 (PECAM-1) expression was determined using IF. Both MPECs and non-patterned cobblestone ECs stained positive for PECAM-1 at cell-cell junctions and at some MPEC edges (Fig. 8.6)

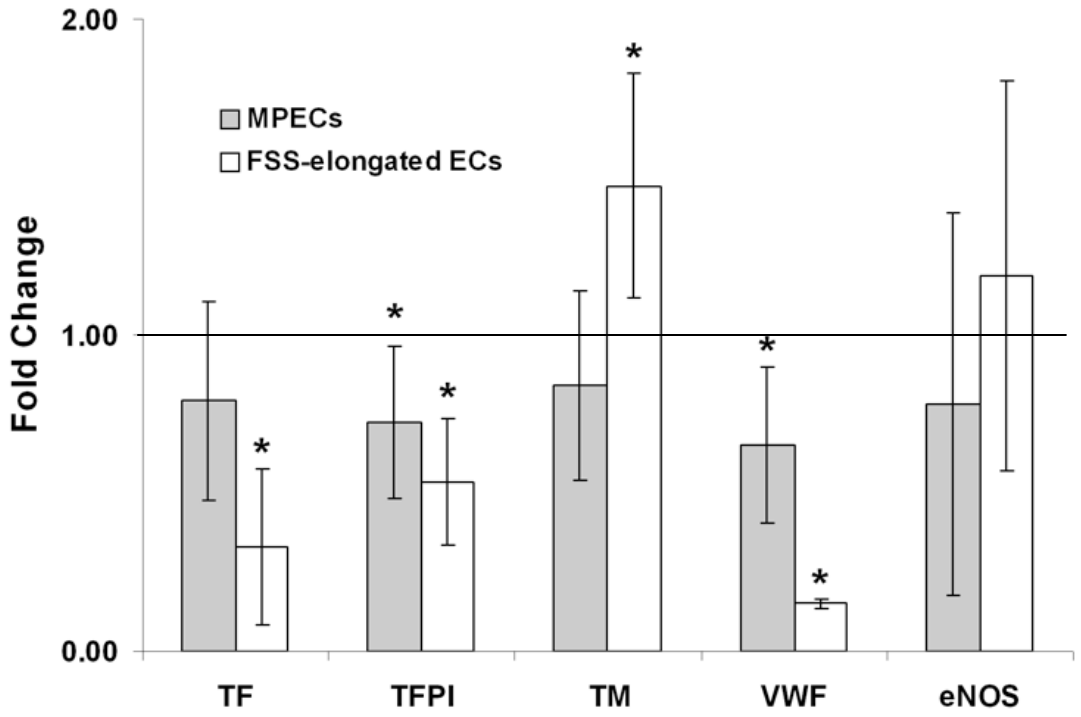

Figure 8.2. Cytoskeletal alignment regulation of EC thrombogenic gene expression. MPEC and FSS-elongated EC folg changes in gene expression were calculated with respect to non-patterned cobblestone ECs. Data represented as mean ± SD. The line at 1.0 represents non-patterned cobblestone EC gene expression levels. *p<0.05, paired Student's t-test.

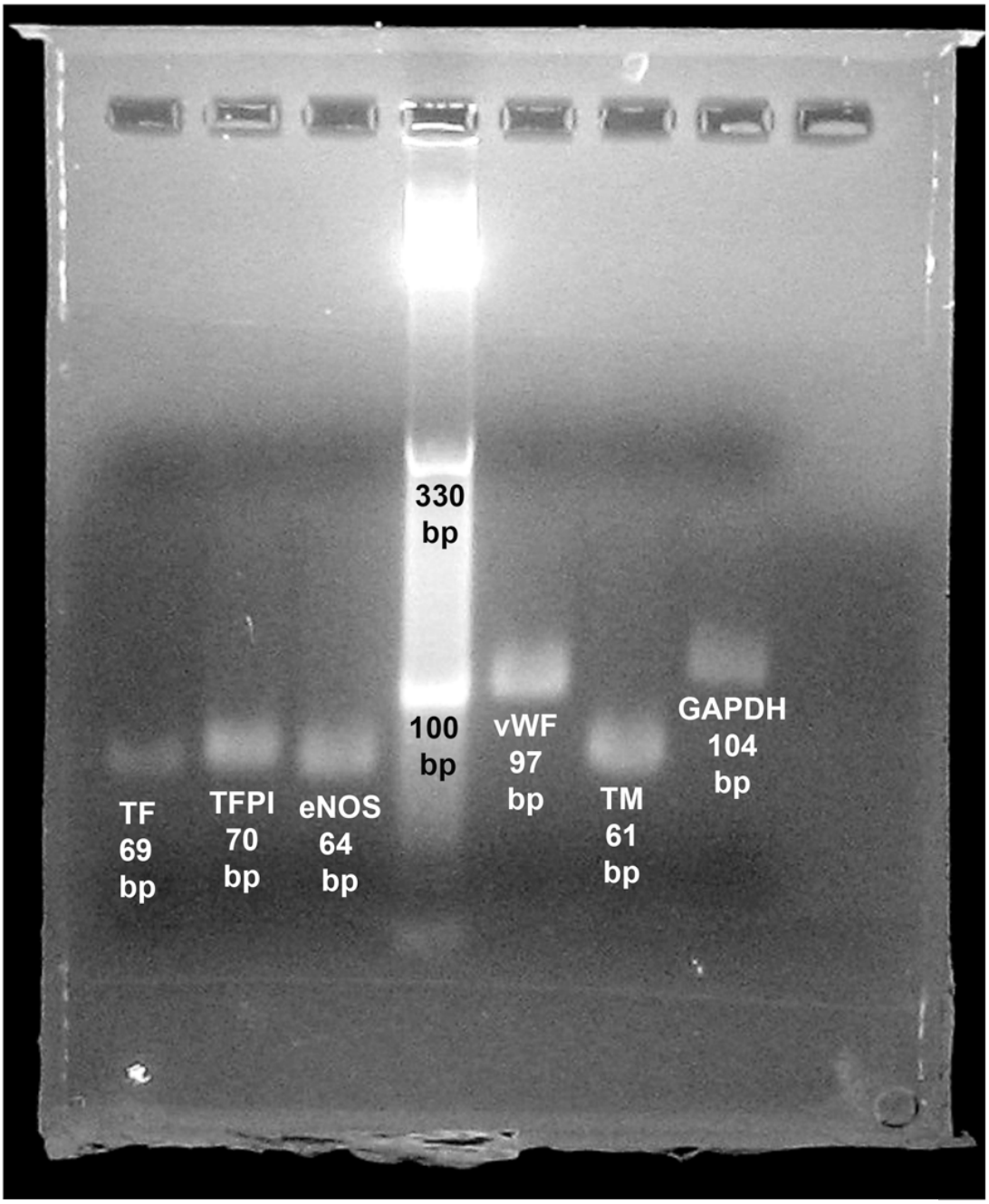

Figure 8.3 Electrophoresis Gel confirming transcript amplification in qt PCR. Results show that the appropriate size amplicon was produced in the qt PCR studies.

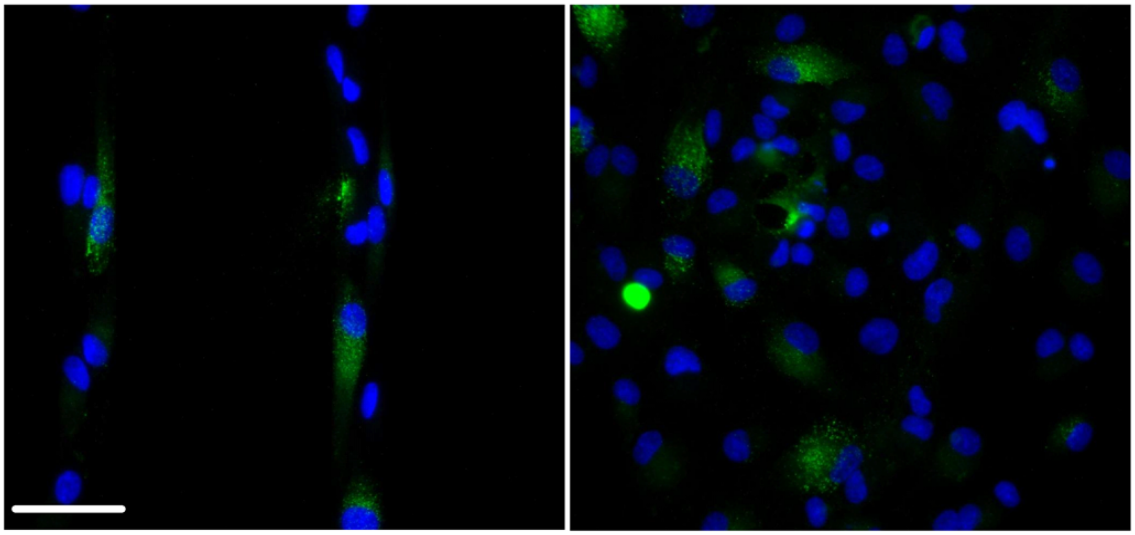

Figure 8.4. vWF staining of MPECs and non-patterned cobblestone ECs. Permeabilized MPECs (Left) and non-patterned cobblestone ECs (Right) both stain positively for vWF protein with characteristic punctuate staining pattern. Representative images are 40 X, Scale bar = 50 μm

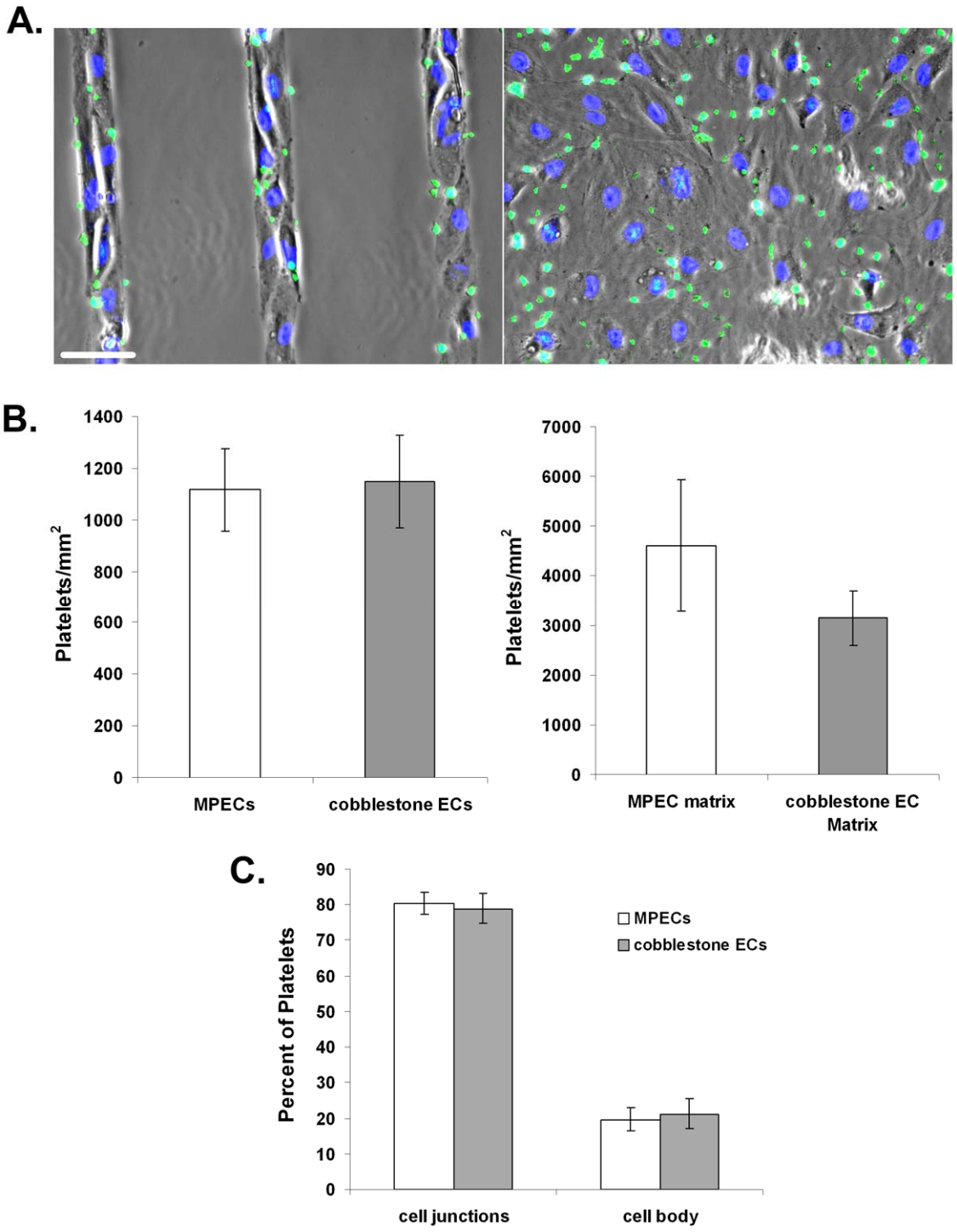

Figure 8.5. Functional evaluation of MPEC-mediated platelet adhesion. **A.** Representative overlaid phase, stained platelets (green), and stained nuclei (blue) images at 40 X. Scale bar = 50 μm. **B.** Total number of platelets adhered per mm^2 on MPECs, non-patterned cobblestone ECs (Left), and the exposed matrix (Right) of each sample. **C.** Spatial localization of adhered platelets, calculated as the percent of platelets adhered at either cell-cell junctions or on the cell body.

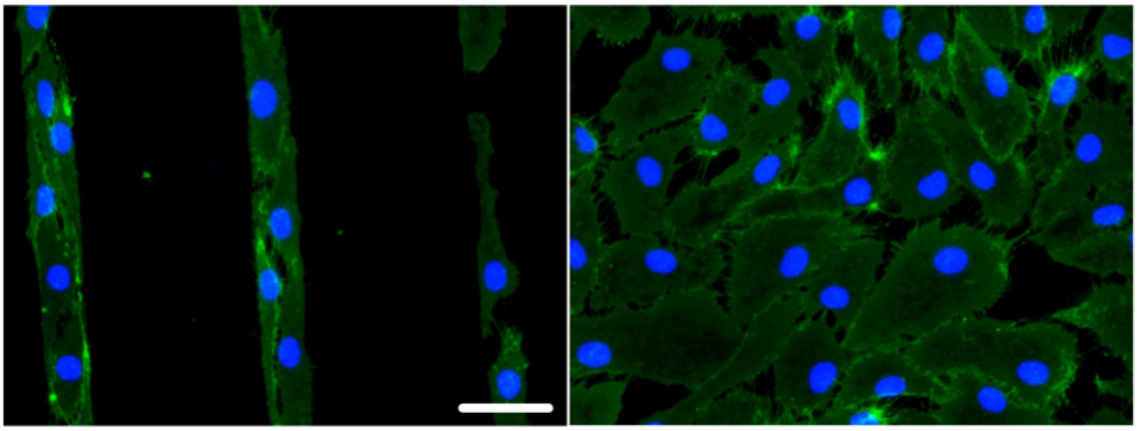

Figure 8.6. MPEC and non-patterned cobblestone EC staining of PECAM-1. Both MPECs (Left) and non-patterned cobblestone ECs (Right) stain positively for PECAM-1 at cell-cell junctions. Some MPECs also have positive PECAM-1 staining at the cell edges exposed to the BSA coated surface. Representative images taken at 40X. Scale bar = 50 μm.

8.6. Discussion

High, unidirectional FSS that induces EC elongation and cytoskeletal alignment also promotes an anti-thrombotic EC phenotype [19]. The EC elongation and cytoskeletal alignment of MPECs was equivalent to FSS induced elongation and alignment (Chapter V and VII). The gene expression results in this study for ECs exposed to 20 hours of FSS are consistent with previous work on FSS stimulated ECs [19, 88], where the pro-thrombotic genes were downregulated, such as TF, and the anti-thrombotic gene TM was upregulated. MPECs had regulatory effects on two genes – vWF and TFPI. Thus, EC shape and cytoskeletal alignment, independent of FSS, can be implicated in the regulation of select thrombogenic genes.

A balance between TF and TFPI regulates the initiation of the extrinsic coagulation cascade, where TF is the main trigger promoting coagulation and TFPI inhibits TF activity [181]. MPECs had no effect on expression of TF but significantly downregulated TFPI compared to cobblestone ECs. Therefore, EC shape and cytoskeletal alignment contribute to the regulation of TFPI, but not TF. Decreasing TPFI while maintaining the same levels of TF tips the scales towards pro-thrombotic gene expression in MPECs compared to cobblestone ECs. FSS-elongated ECs significantly downregulated both TF and TFPI expression compared to cobblestone ECs, thus maintaining a balance between TF and TFPI. FSS-elongated ECs downregulated TFPI to a greater degree than MPECs. As with VCAM-1 discussed in Chapter VII, this data supports cytoskeletal alignment, either induced by micropatterns or by FSS, as a mechanism regulating TFPI expression. The increased downregulation in TFPI by FSS-induced EC elongation compared to MPECs suggests a synergistic mechanism between cytoskeletal alignment and FSS. Furthermore, this data suggests that TF is regulated by FSS mechanisms that may not involve cytoskeletal alignment. Since TF and TFPI are normally colocalized in vivo [196], a cytoskeletal-dependent versus solely FSS-dependent mechanism may contribute to differential regulation that could alter the balance between expressions of these proteins, ultimately tipping the scale towards a pro- or anti- thrombotic EC state.

The thrombotic marker vWF regulates platelet adhesion and has demonstrated responsiveness to FSS at the transcription level [83]. MPECs significantly downregulated expression of vWF compared to cobblestone ECs, suggesting shape and

cytoskeletal alignment dependent regulation. FSS-elongated ECs also significantly downregulated vWF expression compared to cobblestone ECs, and this downregulation was to a greater extent than MPECs. Thus, vWF is another gene that is regulated synergistically by cytoskeletal alignment and FSS. Both vWF in MPECs and cobblestone ECs stained positive for vWF protein in the cell body. There were no obvious differences in staining patterns. However, vWF is also secreted into the subendothelial matrix, where it becomes functionally active and can bind platelets [190]. Therefore, the differences in vWF gene expression in elongated ECs, induced by micropatterned surfaces or FSS, compared to cobblestone ECs may represent differences in vWF secretion.

TM has anticoagulant function through activation of protein C [192]. The response of TM to FSS is controversial with reports of both up and downregulation by FSS-exposed ECs [85, 86]. In this study, the aligned cytoskeleton of MPECs had no significant effect on TM expression compared to cobblestone ECs. In contrast, FSS-elongated ECs significantly upregulated TM compared to cobblestone ECs. The lack of a change in TM expression due to EC elongation and cytoskeletal alignment alone suggests that TM is regulated by FSS through mechanisms unrelated to cytoskeletal structure.

NO promotes vasodilation of arteries and inhibition of platelet adhesion. The upregulation of eNOS, the NO catalyst, in response to FSS has been well documented [19, 87, 89, 193]. MPECs did not have a significant effect on eNOS expression. Previous research investigating the role of EC shape on eNOS expression showed that eNOS expression was significantly reduced by HUVEC elongation on spindle-shaped micropatterns compared to circular-shaped micropatterns between 24 and 48 hours [29]. Surprisingly, our data on FSS-elongated ECs showed no significant increase in eNOS expression at 24 hours. It should be noted the eNOS expression appeared to be dependent on EC confluence, where less confluent ECs exposed to FSS had decreased eNOS expression. However, this does not explain why eNOS was not significantly upregulated by FSS. Hydrocortisone is present in the media at 550 nM, which is known to significantly decrease eNOS expression [209]. The presence of hydrocortisone combined with the low media serum levels used in this study may be the cause of the decrease eNOS expression. ECs grown in 10% serum did stain positive for eNOS (Fig. 5.1).

Exposing the EC surface to blood components is a widely used in vitro method for assessing EC thrombogenicity [189]. Platelets are the most commonly used blood component for the investigation of EC thrombogenic potential through platelet adhesion and aggregation [189]. In this study, PRP was used to evaluate differences in the ability of MPECs and cobblestone ECs to facilitate platelet adhesion. It should be noted that FSS-elongated ECs were not evaluated for platelet adhesion. The FSS-elongated EC condition was used solely as a comparison for MPEC gene expression. FSS-elongated EC inhibition of platelet adhesion has already been documented using baboon-derived ECs [210]. On the exposed matrix of both MPECs and cobblestone ECs, adhesion of platelets/mm^2 was not significantly different. As expected, more platelets adhered to the matrix than the EC surface. The base matrix, collagen I, is known to activate and facilitate platelet adhesion [211, 212]. ECM molecules collagen IV and fibronectin predominantly shown to be produced by MPECs and cobblestone ECs under these culture conditions (Chapter IV), may also contribute to platelet adhesion [213]. However, it is unknown if these matrix areas are exposed due to: (1) detachment of ECs, thus exposing matrix produced by ECs, or (2) lack of EC adhesion, in which case collagen I would be the major ECM component exposed. Furthermore, secreted vWF should also attach to the ECM, but the presence of vWF in the matrix was not measured.

To quantify the attachment of platelets to the EC surface, platelets were counted according to their specific adhesion location. In MPECs, the majority of platelets adhered to the exposed edges, where a portion of the EC came in contact with BSA. Due to the nature of the MPECs, the overall surface area of ECs exposed to BSA was much greater than in confluent EC monolayers. Platelet attachment at these edges may be due to exposure of molecules normally seen at the cell-cell junctions such as PECAM-1. Although this preferential location for platelet attachment on MPECs is worth noting, since cobblestone EC do not have a comparable surface for platelet adhesion at cell edges, these platelets were not counted as part of the total platelets adhered to the EC surface.

MPECs and cobblestone ECs had comparable platelets/mm^2 adhered to their cell surfaces. The locations of platelet adhesion were also not significantly different when calculating the percent of platelets at either cell-cell junctions or on the cell body. This relationship was also valid when calculating the number of platelets at cell-cell junctions or on the cell body per mm^2 of EC area. The preferred adhesion of platelets to cell-cell junctions is most likely facilitated by PECAM-1, the presence of which was

confirmed in both MPECs and non-patterned cobblestone ECs. Platelet adhesion to the cell surface has been shown to be facilitated by ICAM-1 [214]. Gene expression data from Chapter VII indicates that MPEC and cobblestone ECs have comparable expression of ICAM-1. Thus, the comparable levels of platelet adhesion to MPEC and cobblestone EC cell bodies may be due to comparable ICAM-1 expression on the EC surface. Furthermore, gene expression in this section suggests that eNOS, which catalyzes the formation of NO that prevents platelet activation (Section 8.3.7), is also comparable in MPECs and cobblestone ECs. However, gene expression does not always accurately demonstrate protein expression, and therefore, levels of pro- or anti-platelets protein expressions are not known. Overall, the platelet data suggests that MPECs and cobblestone ECs express comparable levels of proteins that are functionally active towards platelet adhesion compared to cobblestone ECs.

8.6.1. Limitations

The low cell numbers available from MPEC samples do not provide enough protein for analysis; therefore, protein expression of the tested thrombogenic genes cannot be determined. TF and TM activity (measured by chromogenic detection of FXa and APC, respectively) were below the levels of detection in MPEC samples, again due to the low cell numbers. EC secretion of TFPI, vWF, and NO cannot be measured on MPECs also because of low cell numbers and because non-patterned cells are often present near the MPECs. The non-patterned ECs present near the MPECs are removed from the surface prior to RNA extraction.

8.6.1. Conclusion

Micropatterned lanes were used to induce elongated EC shape independent of FSS. MPEC thrombogenicity was evaluated in terms of gene expression and platelet adhesion. Results delineated the effects of cytoskeletal alignment-induced versus FSS-induced gene expression. EC elongation and cytoskeletal alignment regulated vWF and TFPI expression, of which FSS was additive in its effects on expression. TF and TM were regulated by FSS and not cytoskeletal alignment. Functional evaluation of platelet adhesion to the MPEC surface suggested equivalent thrombogenicity compared to cobblestone ECs. Taken together, FSS is required to fully promote an anti-thrombotic EC phenotype. However, cytoskeletal alignment alone contributes to this phenotype through regulation of vWF and TFPI expression.

CHAPTER IX

Preliminary Data: Kruppel-Like Factor 2 Expression is Induced by EC Cytoskeletal Alignment

9.1. Abstract

Kruppel-like factor 2 (KLF2) is a transcription factor that is specifically upregulated in ECs by high, unidirectional FSS. Upregulation of KLF2 promotes anti-inflammatory and anti-thrombotic EC phenotype, and correlates in vivo to atheroprotective regions of the vasculature where ECs have elongated and aligned cytoskeletal structure. However, whether EC elongation and cytoskeletal alignment affects KLF2 expression has not been previously investigated. In this section, micropatterned lanes (25 μm wide with 100 μm spacing) were used to create elongated EC shape with aligned cytoskeletal components, independent of FSS. Micropattern-elongated EC (MPEC) expression of KLF2 was determined during the elongation process at 1, 2, 4, 6, and 24 hours compared to ECs on non-patterned surfaces that had random cytoskeletal spreading. MPEC expression was also compared to ECs exposed to 24 hours high, unidirectional FSS. Preliminary results indicated that cytoskeletal alignment upregulated KLF2 expression compared to the randomly oriented cytoskeletal organization of static ECs. At 24 hours, both MPECs and ECs exposed to FSS had upregulated KLF2, but FSS upregulated KLF2 to a greater extent than MPECs. Therefore, cytoskeletal alignment can induce KLF2 expression independent of FSS and

may play a role in FSS-induced upregulation of KLF2. Furthermore, the influence of cytoskeletal structure on KLF2 expression may be the mechanism behind cytoskeletal-dependent gene expression.

9.2. Introduction

ECs exposed to high, unidirectional FSS have elongated shape with aligned cytoskeletal components. In vivo and in vitro, high unidirectional FSS upregulates the transcription factor KLF2, which is linked to the promotion of the EC athero-protective phenotype including anti-inflammatory and anti-thrombotic functions. Chapters VII and VIII demonstrated that some inflammatory and thrombotic genes can be regulated by EC elongation and cytoskeletal alignment, independent of FSS. Therefore, in this section, EC elongation and alignment of cytoskeletal component was investigated as a possible inducer of KLF2 expression.

9.3. Background

9.3.1. Kruppel-Like Factor 2

First identified in mammalian cells in 1993 [215, 216], KLF2 has recently come under intense investigation as a critical transcription factor involved in mediating EC regulation of vascular homeostasis. Roles for KLF2 have been described in the regulation of EC expression of inflammatory and thrombotic markers. Thus far, KLF2 has been identified as the sole transcription factor differentially regulated by FSS and cytokines, which usually have overlapping effects, and therefore may play a unique role in EC responsiveness to FSS.

Structure: The sixteen identified KLFs make up a subfamily within the zinc-finger class of DNA transcription factors. KLF2 structurally differs from common zinc-finger transcription factors in several ways. KLFs have three Cys2/His2 zinc fingers at the carboxyl-terminal, a conserved sequence in the interfinger space, and they have three residues in each zinc finger that mediate DNA-binding [217]. Specifically, KLFs target GC-rich or CACCC sequences of DNA gene promoter regions [215, 217].

Expression: KLF 2, 4, and 6 are all expressed in ECs. KLF2 is the most thoroughly researched and KLF2 has been identified as a critical regulator of vascular development and function. The importance of KLF2 in vascular development was

demonstrated by the embryonic lethality of KLF2 knockout mice due to structural abnormalities in vessel formation [215, 218, 219]. In vivo, KLF2 is constitutively expressed throughout the endothelium; however, KLF2 expression is decreased in vascular branch points, indicating FSS-dependent regulation [220, 221].

Dekker, et al., performed an in depth analysis of genes regulated by prolonged FSS, using a stringent selection regime focusing only on EC genes that were (1) upregulated by HUVECs after 7 days of FSS exposure (12 ± 7 dynes/cm^2), (2) not responsive to atherosclerotic cytokines, and (3) exclusively expressed in the vasculature [220]. Out of 18,000 genes tested, the KLF2 transcription factor was the sole gene that fit the above requirements [220]. KLF2's behavior is unique because normally genes induced by FSS are also induced by cytokine, such as TNF-α stimulation. Instead, KLF2 induced expression by FSS and TNF-α is inversely related, where high, unidirectional FSS upregulated KLF2 expression and stimulation with TNF-α reduced KLF2 expression [220]. IL-1β has also demonstrated reduced KLF2 expression at the gene level in ECs [222], while treatment with HMG-CoA reductase inhibitors (statins) increased KLF2 expression [223].

9.3.5. Role in EC Function

KLF2 expression affects EC expression and activity of inflammatory and thrombotic genes and proteins. The role of KLF2 in these functions was elucidated using HUVECs that overexpressed KLF2 (using KLF2 adenovirus) or KLF2 gene knockdown using either IL-1β or KLF2 siRNA [217, 222]. The results of these studies are discussed below.

Inflammation: HUVECs treated with IL-1β, a pro-inflammatory agent that decreases KLF2, had increased expression of E-selectin, VCAM-1, and ICAM-1 [222]. In contrast, overexpression of KLF2 in IL-1β treated HUVECs resulted in decreased E-selectin and VCAM-1 gene and protein expression, while ICAM-1 was not affected [222]. Functionally, KLF2 overexpression also inhibited T-cell attachment and rolling on HUVECs stimulated with IL-1β [222]. Thus, KLF2 overexpression inhibited IL-1β pro-inflammatory effects in HUVECs. These results suggest that IL-1β pro-inflammatory activity is mediated by the downregulation of KLF2, and pro-inflammatory function can be rescued by KLF2 overexpression. Furthermore, the E-selectin, VCAM-1, and ICAM-1 expression profile induced by KLF2 is comparable to EC expression of these proteins under high, unidirectional FSS. Since KLF2 is known to be upregulated by high,

unidirectional FSS, the results implicate KLF2 as a possible mechanism responsible for the FSS-induced inflammatory response.

Thrombosis: Overexpression of KLF2 in HUVECs induced significant increases in TM and eNOS, and decreases in vWF compared to control HUVECs [217]. The pro-coagulant of effects of TNF-α stimulation was attenuated by HUVEC overexpression of KLF2, which prevented the increase of TF expression and the decrease of TM expression [217]. KLF2 also increased TM-mediated activation of PC and decreased TF activation of FX [217]. In contrast, HUVECs transfected with KLF2 siRNA have significant decreases in TM and eNOS expression, decreased TM activity, and increased TF activity [217]. In a physiological assessment of coagulation, KLF2 overexpression increased clotting time for whole blood perfused over the HUVEC surface compared to controls, and siRNA KLF2 HUVECs had reduced clotting times [217]. Again, KLF2 induced an anti-thrombotic EC gene expression profile that is comparable to EC exposure to high, unidirectional FSS. Thus, KLF2 may also have a critical role in regulating the FSS-dependent thrombotic effects on ECs.

Mechanism: NFκB is a transcriptional activator associated with effects on ECs that are opposite of KLF2, including pro-inflammatory and pro-thrombotic EC functions in vivo and in vitro [224]. Interestingly, KLF2 expression does not decrease NFκB expression but it does inhibit NFκB activity [222]. SenBanerjee, et al., determined that the mechanism for KLF2 inhibition of NFκB involving the competitive binding of cyclic AMP response element-binding protein (CBP/p300) [222]. CBP/p300 is a NFκB cofactor required for optimal NFκB transcriptional activity [222, 225]. Furthermore, CBP/p300 has been associated with KLF2 transcriptional activity [222, 226]. When HUVECs were co-transfected with CBP/p300 and KLF2, NFκB activity increased, suggesting that CBP/p300 is the limiting factor causing the suppression of NFκB [222]. Thus, KLF2 recruits and interacts with CBP/p300, which limits CBP/p300 availability for binding to NFκB and therefore decreases NFκB transcriptional activity.

9.3.6. Summary

KLF2 is a transcription factor that promotes anti-inflammatory and anti-thrombotic EC phenotype. KLF2 promotes this phenotype through the up- or down- regulation of specific EC genes (e.g. decreased E-selectin and VCAM-1 and upregulated TM and eNOS) due to the inhibition of NFκB activity. KLF2 expression is specifically upregulated in ECs exposed to high, unidirectional FSS in vivo and in vitro. Since the previous

chapters demonstrated that cytoskeletal alignment alone has regulatory effects on anti-inflammatory and anti-thrombotic EC gene expression, KLF2 may offer a mechanistic link between cytoskeletal alignment-dependent regulations of cell functions.

9.4. Materials and Methods

9.4.1. Experimental Design

Experiments for this study were designed to determine whether EC elongation and cytoskeletal alignment alone increases expression of the KLF2 transcription factor. The following three conditions were used: (1) Micropatterned-elongated ECs (MPECs), (2) cobblestone ECs on patterned surfaces, and (3) ECs plated on non-patterned surfaces for 4 hours and elongated by 20 hours of 12.5 dynes/cm^2 FSS. Micropatterning, EC isolation, EC plating, and qtPCR were all carried out as described in Common Materials and Methods (Chapter IV). Methods specific to this experiment are detailed below.

9.4.2. EC Culture and Surface Preparation

Mature carotid ECs were used in these experiments until passage 5. The micropattern design containing 25 μm wide lanes with 100 μm spacing was used and implemented with the microfluidic patterning technique.

9.4.3. Flow Studies

ECs were plated on non-patterned surfaces and incubated for 4 hours. The ECs were placed in the GlycoTech flow chamber and exposed to 12.5 dynes/cm^2 FSS for 20 hours (with FSS ramping described in Common Materials and Methods Section 4.6).

9.4.5. qtPCR

RNA isolation and reverse transcription were performed on MPECs and cobblestone ECs at 1, 2, 4, 6, and 24 hours after adhesion. RNA was isolated and reverse transcribed from FSS-elongated ECs after exposure to 20 hours of FSS (total of 24 hours after EC plating). Primers for KLF-2 and GAPDH were used for qtPCR studies (Table 4.1).

9.4.6. Statistical Analysis

Due to the preliminary nature of this data, sample size was n=2 and therefore was not large enough to perform statistical analysis.

9.5. Results

9.5.1. Timecourse of MPECs Expression of KLF2

EC elongation and cytoskeletal alignment were investigated as a possible mechanism behind FSS-induced KLF2 expression. MPECs expression of KLF2 was determined and compared to cobblestone ECs at 1, 2, 4, 6, and 24 hours (Fig. 9.1A). Preliminary results showed that initial stages of micropatterned-induced EC elongation do not affect KLF2 expression. At 2 hours, there was a small dip in MPEC expression of KLF2. By 4 hours, MPEC expression dramatically shifted to a 1.71 fold increase, representing the peak in MPEC expression of KLF2 (Fig. 9.1A). At 6 hours, MPEC expression decreased again to slightly above initial levels and then slowly increased to a 1.55 fold increase at 24 hours (Fig. 9.1A). This experiment has been repeated showing a similar trend in MPEC expression of KLF2 compared to cobblestone ECs. These preliminary data indicate that an aligning cytoskeleton has differing KLF2 expression compared to a randomly orienting cytoskeleton.

9.5.2. MPECs versus FSS-elongated EC Expression of KLF2

Expression of KLF2 in micropattern-induced and FSS-induced elongated ECs was compared at 24 hours. Fold changes in MPEC and FSS-elongated EC expression of KLF2 was determined with respect to non-patterned cobblestone ECs (Fig. 9.1B). At 24 hours, fold changes in KLF2 expression for MPEC and FSS-elongated EC expression was 1.55 and 3.02, respectively (Fig. 9.1B). Therefore, MPECs and FSS-elongated ECs both induced KLF2 gene expression, but FSS-elongated ECs upregulated KLF2 by almost twice as much as MPECs.

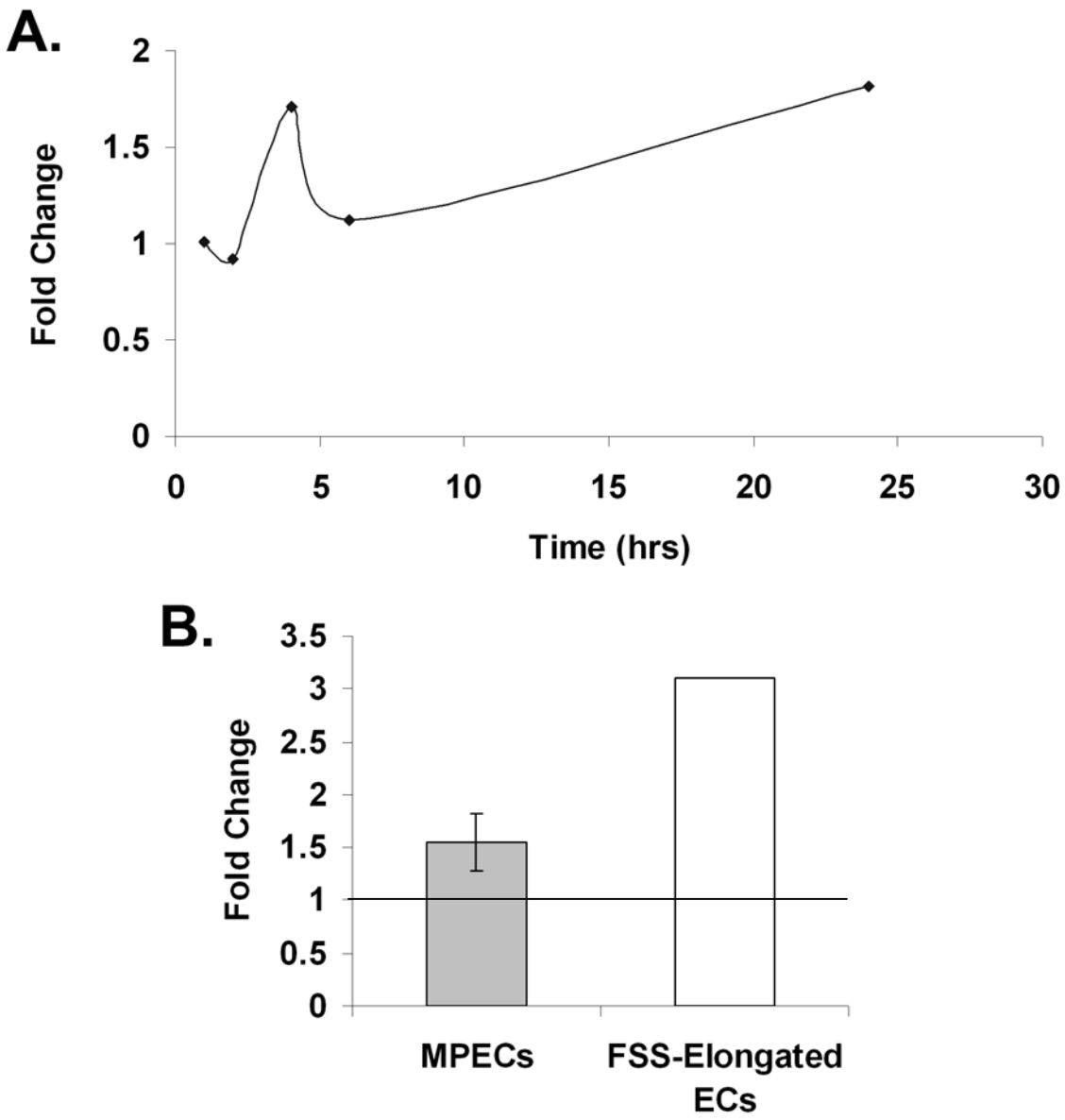

Figure 9.1. MPEC expression of KLF2 mRNA. **A.** Representative timecourse of MPEC expression of KLF2, fold change compared to non-patterned cobblestone ECs. **B.** MPEC and FSS-elongated EC mRNA expression of KLF2 at 24 hours, compared to cobblestone ECs. Line at 1.00 represents non-patterned cobblestone EC expression of KLF2. Error bars represent range of values for n=2.

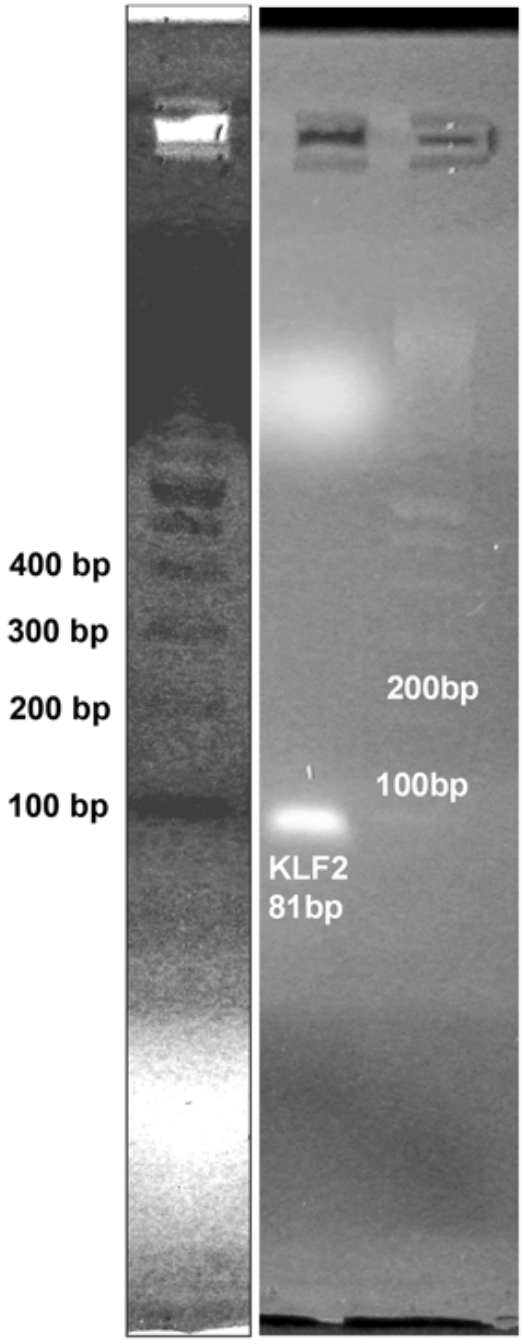

Figure 9.2. Electrophoresis gel of KLF2 transcript. Gel confirms appropriate amplicon size for the KLF2 primer set. Left: Cropped 100 bp ladder inverted and adjusted to increase band visibility.

9.6. Discussion

Gene expression data from Chapter VII and VIII suggest cytoskeletal alignment-dependent regulation of some of the genes involved in inflammation and thrombosis. KLF2 is an attractive mechanism for cytoskeletal-dependent regulation of gene expression because (1) KLF2 is a known regulator of EC immunogenic and thrombotic phenotype, and (2) KLF2 expression is induced by high, unidirectional FSS. Preliminary results from this line of investigation suggest that under static conditions, alignment of the cytoskeletal promotes KLF2 expression compared to a randomly oriented cytoskeletal spreading in ECs.

KLF2 gene expression was evaluated at 1, 2, 4, 6, and 24 hours for MPECs and cobblestone ECs. MPECs had cytoskeletal structures that were aligning over these 24 hours (Chapter V, Fig. 5.3) while the cobblestone EC cytoskeletal was undergoing random spreading. Comparison between the gene expressions at each time point indicated that cytoskeletal alignment upregulated KLF2 gene expression, most notably at 4-6 hours where expression levels peaked relative to cobblestone ECs. Interestingly, Dekker, et al., showed a peak in KLF2 expression per cell at 6 hours in HUVECs exposed to 25 dynes/cm^2 laminar FSS. This similar trend in ECs that are aligning, induced either by micropatterned surfaces or by FSS, suggests a possible cytoskeletal dependent regulation of KLF2. Furthermore, the MPECs early peak in KLF2 expression compared to non-patterned cobblestone EC occurs when the actin and microtubules are aligning. The guided alignment on micropatterned lanes versus the random spreading on non-patterned surfaces may increase cytoskeletal stability, which may also affect KLF2 expression (see Chapter X, Section 10.2.2). Since microtubules are the first cytoskeletal structures to align both in MPECs and FSS-elongated ECs (Chapter V) microtubules may play an important role in early KLF2 expression. Furthermore, under FSS, early events in EC elongation include a net depolymerization of actin, which correspond to a decrease in RhoA, a known regulator of actin dynamics. RhoA has also been linked to the downregulation of KLF2 expression [223]. Thus, the decrease in RhoA activity early in EC elongation induced by FSS may also contribute to KLF2 upregulation, and the return of RhoA when actin fibers reform and remodel may contribute to the subsequent decrease in KLF2 [227]. However, the timecourse of RhoA activity is unknown for MPECs. The relationship between the cytoskeleton and possible mechanisms that regulate KLF2 expression will be explored further in Chapter X.

To delineate the effects of cytoskeletal alignment and FSS, MPEC and FSS-elongated ECs expression of KLF2 was determined relative to cobblestone ECs. Both MPECs and FSS-elongated ECs upregulated KLF 2 gene expression. Similar to the cytoskeletal alignment-regulated genes reported in the previous chapters, where FSS-induced EC elongation had a greater effect on gene expression, FSS-induced elongation upregulated KLF2 to a greater extent than micropattern-induced EC elongation. Again, this validates that cytoskeletal alignment, whether it is induced by micropatterned surfaces or FSS, has a regulatory role in KFL2 expression, and that FSS effects are synergistic with cytoskeletal alignment.

9.6.1. Limitations

Validation of the inverse relationship between KLF2 upregulation and decrease in NFκB would further validate KLF2 activity in MPECs; however, low cell numbers do not provide adequate amounts of protein for analysis. Isolation of the individual roles of actin and microtubules would contribute to the understanding of KLF2 cytoskeletal-dependent regulation, but disruption in actin attenuates EC elongation (Chapter V) and disruption of microtubules abolishes EC elongation (Chapter V). The use of actin and microtubule stabilizes, phalloidin and taxol, may be sufficient for future use in elucidating the mechanism behind cytoskeletal-mediated KLF2 expression (Chapter XI).

9.6.2. Conclusion

Cytoskeletal alignment, independent of FSS, is capable of upregulating KLF2 expression. Upregulation of KLF2 promotes an anti-inflammatory and anti-thrombotic EC phenotype. Thus, regulation of KLF2 by cytoskeletal alignment may provide the mechanism behind cytoskeletal alignment-dependent regulation of EC gene expression. Furthermore, cytoskeletal alignment-dependent expression of KLF2 suggests that the elongated and aligned EC shape itself is athero-protective since KLF2 promotes athero-protective EC functions. The studies performed in this chapter need to be repeated to validate these preliminary findings.

CHAPTER X

Discussion

10.1 Summary of Key Findings

The overall goal of this reseach was to determine whether the architecture of the cytoskeleton influences EC functions related to atherosclerosis. Lanes of micropatterned substrate were used to model EC elongated shape associated with high, unidirectional FSS and atheroprotective EC function, independent of FSS. This model was validated in Chapter V, indicating that the micropatterned lanes induced alignment of actin and microtubules within the ECs that was equivalent to FSS-induced alignment. EC elongation and alignment on micropatterned lanes was dependent on microtubules, and independent of actin. The polarization of the MTOC was dependent on FSS, which induced EC localization of the MTOC upstream of the nucleus. Thus, micropattern-induced and FSS-induced EC shape and cytoskeletal alignment are comparable, with the exception of MTOC polarity. Chapter VI determined the influence of EC elongation and alignment on the composition of ECM for two EC sources, carotid and progenitor. EPCs were examined in this chapter due to their potential as an autologous EC source for endothelializing vascular grafts. EPCs elongated on the micropatterned lanes, but they did not remain confined to the micropatterned substrate for extended periods of time compared to the mature ECs. EPCs were able to deposit and remodel ECM to a greater extent than mature ECs on both micropatterned and non-patterned surfaces. Mature ECs that remained on the micropatterned lanes had shape-dependent deposition of ECM components. Micropatterned-elongated mature ECs deposited more collagen IV and less fibronectin than matched mature cobblestone ECs, suggesting cytoskeletal

dependent regulation of ECM composition. In Chapter VII, EC regulation of inflammation was measured in terms of cytoskeletal alignment. Results indicated that micropatterned-induced EC cytoskeletal alignment downregulated VCAM-1 mRNA expression and had no effect on ICAM-1 mRNA expression. FSS-induced EC alignment also downregulated VCAM-1, but upregulated ICAM-1. Downregulation of VCAM-1 is associated with reduced inflammation while increased expression of ICAM-1 is associated with pro-inflammatory states. Thus micropatterned-induced EC cytoskeletal alignment may produce an EC surface that is less immunogenic than ECs exposed to high, unidirectional FSS. Furthermore, monocytes formed weaker attachments to the micropattern-elongated EC surface compared to cobblestone ECs, indicating that VCAM-1 and ICAM-1 expression on the surface was decreased. Cytoskeletal alignment-dependent thrombogenicity was investigated in chapter VIII. Micropattern-induced cytoskeletal alignment regulated TFPI and vWF mRNA expression. Otherwise, cytoskeletal alignment did not affect some of the major regulators of the coagulation cascade such as TF, TM, and eNOS. Functional evaluation of platelet activation showed no difference in platelet adhesion on the surface of micropattern-elongated ECs and cobblestone ECs. Finally, Chapter IX began the investigation of the mechanism behind cytoskeletal structure-dependent regulation of EC function. Interestingly, preliminary data suggests that the FSS-regulated transcription factor KLF-2 was upregulated by cytoskeletal alignment compared to random cytoskeletal spreading. KLF-2 is a known regulator of EC inflammatory and thrombogenic functions and offers a promising link between cytoskeletal alignment and EC function. Overall, this data suggests that cytoskeletal structure is an independent regulator of EC function.

10.2. Mechanisms of Cytoskeletal-Dependent Regulation

A mechanosensory complex for EC detection and responsiveness to FSS remains elusive. The well documented responsiveness of the cytoskeleton to mechanical stimuli strongly suggests the EC response to FSS is cytoskeletal-mediated. Previous research demonstrated cytoskeletal-dependent regulation of cell protein expression, secretion, and gene transcription. While the exact mechanism linking the cytoskeleton to these known regulatory functions is not completely defined, several converging pathways have been suggested that correlates the cytoskeleton with regulation of cell functions.

10.2.1. Spatial Localization and Trafficking

The first pathway is an indirect mechanism of cytoskeletal regulation through spatial localization of protein and genes. The cytoskeleton is a negatively charged protein network with a massive surface area [106]. Each of the major cytoskeletal components (actin, microtubules, intermediate filaments) in an average 20 μm cell has a surface area of ~47,000 μm^2 [106]. Thus, each component has a surface area that is approximately 70 times larger than the plasma membrane (~700 μm^2) [106]. The cytoskeleton has demonstrated binding to a wide variety of proteins including glycolytic enzymes, protein kinases, lipid kinases, and GTPases [106]. Binding to the cytoskeleton either sequesters these proteins or, upon cytoskeletal disruption, releases them allowing them to interact with their target molecules [106]. Trafficking of proteins occurs along the cytoskeletal network either through binding to motor proteins [106, 228] or guided diffusion [229]. The cytoskeleton can also bind and traffic mRNA, allowing for targeted delivery of mRNA to promote protein translation in specific spatial cellular locations [230, 231]. Thus, the binding and movement of proteins and mRNA via the cytoskeleton indirectly facilitates localized interactions to promote protein clustering, activation, and mRNA translation.

10.2.2. Protein and Transcription Factor Activation

The second pathway directly involves the cytoskeleton in the initiation of protein activation and transcription. The cytoskeleton binds proteins and mRNA, which can increase mRNA stability while also contributing to spatial localization. Furthermore, cytoskeletal dynamics regulate transcription factors including NFκB, and activates proteins including MEK, ERK1/2 (MAPK kinases), TGF- β, and IL-1β [42, 43, 232-234] (Table 10.1). In particular, cytoskeletal dependent regulatory effects are initiated by either cytoskeletal disruption or stability. When the actin or microtubule cytoskeletal components become disrupted, MEK, ERK, IL-1β, NFκB, and TGF-β are upregulated. The converse is true under cytoskeletal stabilization, which also promotes increased inhibitory kappa B (IκB). Interestingly, regulation due to cytoskeletal disruption parallels oscillatory FSS-induced regulation of these transcription factors and proteins (Table 10.1) [235]. In particular, disturbed FSS demonstrated upregulation of NFκB [235]. Due to the prominent role of NFκB in the regulation of the molecules of interest in this study, e.g. ICAM-1 and VCAM-1 [236], cytoskeletal regulation of NFκB will be discussed in detail below.

NFκB is a heterodimeric protein made up of a p50 and p65 subunit. Upregulation of NFκB is associated with disturbed FSS, and promotes pro-inflammatory and pro-thrombotic EC protein and gene expression [224]. Interestingly, microtubules are a known regulator of NFκB activation and transcription [42]. In particular, treatment of HeLa S3 cells with nocodozale, which disrupts microtubules (Chapter V), increased NFκB protein and gene expression. IκB, which associates with NFκB to render it inactive, was decreased by the disruption of microtubules [42]. In contrast, stabilizing microtubules using taxol blocked NFκB induction and increased IκB. Disruption of actin had no effect on either NFκB or IκB. However, RhoA, a regulator of actin dynamics, can also induce NFκB transcriptional activity by promoting the degradation of IκB and the nuclear translocation of p50/p65 dimers [237]. The mechanism behind microtubule- and RhoA- dependent regulation of NFκB is likely through the phosphorylation IκB, which causes IκB to degrade and release the bound NFκB allowing for nuclear import. Thus, microtubule-dependent activation of kinases, such as MEK, may induce IκB degradation and subsequently increase NFκB. Of interest, the known potent stimulator of NFκB activity, TNF- α, has been shown to induce cytoskeletal reorganization [238, 239]. TNF-α is also commonly associated with atherosclerotic plaques [240] found in regions of disturbed flow. While this data strongly links cytoskeletal reorganization with regulation of cell functions, the exact mechanism linking the cytoskeleton to such functions as gene transcription is still unknown.

KLF2, discussed in detail in Chapter IX, is a novel transcription factor regulated by FSS. KLF2 promotes a similar gene expression profile as that of micropattern-induced EC cytoskeletal alignment, including decreased VCAM-1, vWF, and unchanged ICAM-1. Furthermore, expression of KLF2 is increased by high, unidirectional FSS and decreased by disrupted, low, oscillatory FSS. A balance between KLF2 and NFκB activity is mediated by competitive binding of the cofactor CP/P300. IL-1β also regulates KLF2 by decreasing expression of KLF2 mRNA. Taken together, high, undirectional FSS and the known cytoskeletal-dependent regulation of both NFκB and IL-1β, and their known roles in KLF2 regulation, suggests that cytoskeletal dynamics may also contribute to the regulation of KLF2. Preliminary results in Chapter IX indicated that KLF-2 regulation is cytoskeletal-dependent. Previous research has already implicated cytoskeletal regulation of KLF2 through RhoA [223]. Decrease in Rho A increased KLF2, suggesting that actin stability may contribute to KLF2 upregulation [223]. At this point, the individual roles of actin and microtubules in KLF2 regulation is unknown.

Proposed Model: Although the exact cytoskeletal dynamics of micropattern-elongated ECs was not determined in this research, some parallels can be drawn between micropattern-induced and FSS-induced elongation. Both are dependent on microtubules, which are the first cytoskeletal component to align. Both have a decrease in actin stress fibers early in alignment, although this decrease is greater in FSS-induced EC elongation. Under FSS, the early decrease in actin is also associated with a decrease in RhoA [227]. Under FSS, actin fiber reformation and remodeling is coupled with increased RhoA activity. By 24 hours of FSS, actin has elongated and aligned and continues polymerizing, but the decreased actin remodeling is associated with a decline in RhoA activity [227]. Data in Chapter V showed that micropattern-elongated EC (MPEC) actin and microtubules also completed aligning at 24 hours, and maintained this same alignment until 48 hours (the last measured timepoint). Differences in micropattern-induced and FSS-induced cytoskeletal alignment also exist and were highlighted in Chapter V. Briefly, MPECs alignment beings almost immediately upon adhesion while FSS-induced EC elongation occurs several hours after stimulation with FSS. Specific to MPECs, cytoskeletal alignment occurs while maintaining at least a partial dense peripheral actin band and actin fibers can be found in some MPECs early in the alignment process, although actin fibers are not necessary for alignment as shown by treatment with cytochalasin D.

Since the final elongated EC shape and cytoskeletal alignment are comparable between MPECs and FSS-elongated ECs, the following proposed model of cytoskeletal-dependent KLF2 regulation is suggested (Fig. 10.1). The stabilization and internal tension of aligned microtubules decreases NFκB and IL-Iβ, and increases IκB, which contributes to upregulation of KLF2 activity. NFκB has also been shown to bind and inhibit the KLF2 promoter region, therefore, the decrease in NFκB may also promote increased transcription of KLF2 [222]. The increased stability and internal tension of actin decreases the amount of RhoA. Downregulation of RhoA decreases NFκB and promotes the upregulation of KLF2 [237]. This theory needs to be validated be measuring the specific regulation of KLF2 by individual cytoskeletal components and RhoA activity in micropattern-elongated ECs (see Chapter XI: Future Work).

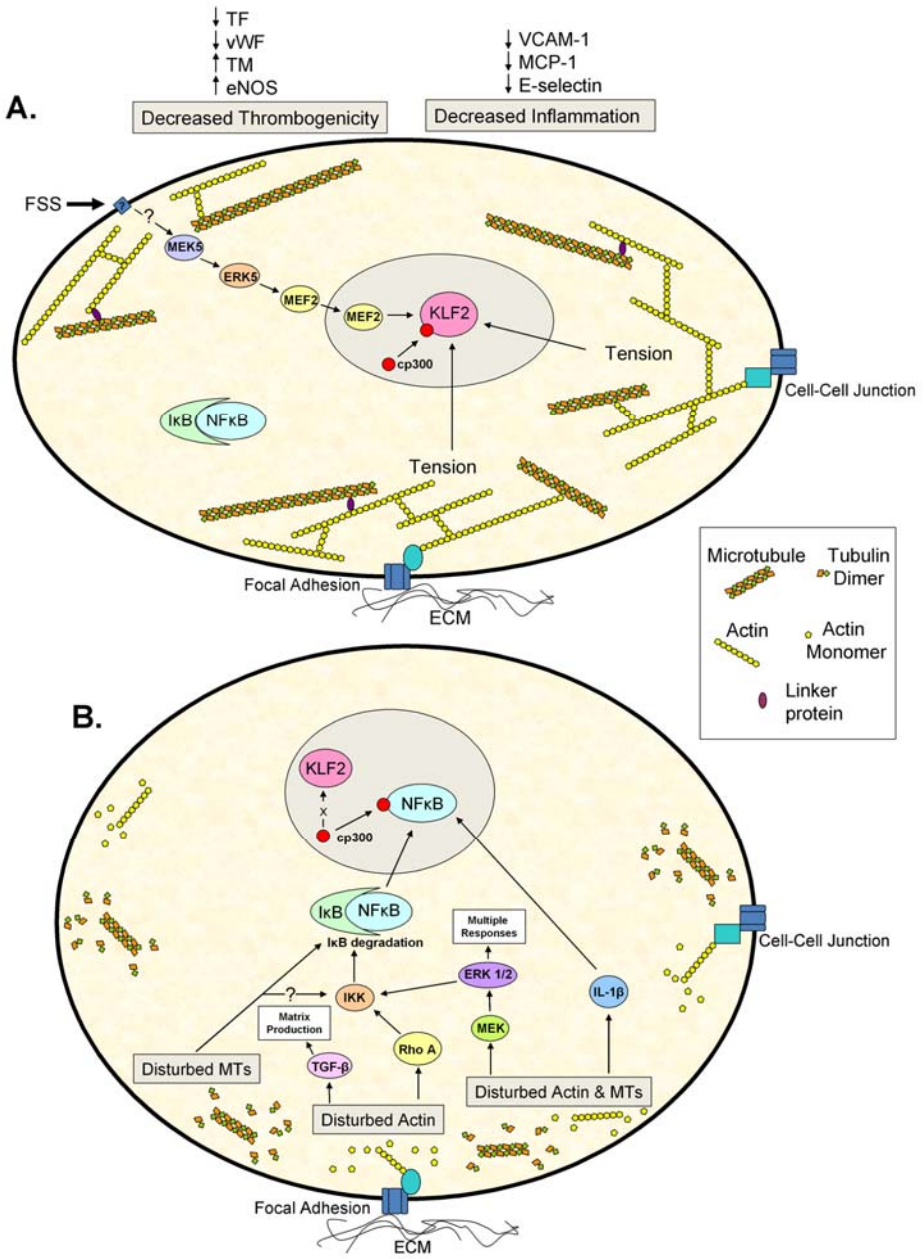

Figure 10.1. Proposed model of cytoskeletal-dependent regulation of EC functions related to atherosclerosis. **A.** Mechanical regulation of KLF2 by both FSS and internal tension, mediated by the cytoskeleton, results in an athero-protective EC phenotype. FSS-dependent upregulation of KLF2 through the MEK5/ERK5/MEF5 pathway is initiated either by a mechanosensor or through deformation and remodeling of the cytoskeleton. In this model, NFκB is held inactive in the cytoplasm by IκB. This research suggests that internal tension originating from cell anchor points also promotes upregulation of KLF2. **B.** Multiple pathways triggered by cytoskeletal disruption converge to promote upregulation of NFκB. Several factors lead to the phosphorylation of IκB, which causes both IκB degradation and NFκB translocation to the nucleus. In this model, the transcription cofactor cp300 binds NFκB, instead of KLF2, increasing transcriptional activity. NFκB promotes an athero-prone EC phenotype.

10.2.3. Extracellular Matrix Signaling

Finally, cytoskeletal-dependent signaling is most commonly associated with ECM signaling cues through attachment points known as focal adhesions (FAs). Interestingly, EC regulation of the composition of ECM has been linked to cytoskeletal structure. In particular, cytochalasin dependent disruption of actin led to increases in the ECM regulators TGF-β, TIMP-1, and collagenase, and decrease in MMP-9 [43, 232, 241]. Actin disruption also led to increased pro-collagen and fibronectin production [43]. Interestingly, micropattern-elongated ECs had decreased fibronectin and increased collagen IV deposition compared to cobblestone ECs (Chapter VI). Taken together, this shows that cytoskeletal structure affects the composition of ECM. However, the composition of ECM also affects cytoskeletal-mediated intracellular signaling. For example, fibronectin-rich ECM environment promotes increased EC vascular permeability through PAK- mediated decrease in β-catenin, a protein that associates with cadherins and is essential for the formation of cell-cell junctions [111]. While it is unknown which factor is dominant, ECM composition or cytoskeletal structure, it is likely that ECM composition and cytoskeletal structure are closely coordinated to promote the desired EC function.

Table 10.1. Disturbed cytoskeletal vs. FSS regulation

	DISTURBED		
	ACTIN	**MICROTUBULES**	**FSS ***
NFκB	**No effect [42]**	↑ **[42]**	↑ **[235]**
IκB	**No effect [42]**	↓ **[42]**	↓ **[235]**
AP-1	**unknown**	**No effect [42]**	↑ **[235]**
Fibronectin	↑ **[43]**		↑ **[111]**
MMP9	↓**[241]**		↑ **[242]**
Procollagen	↑ **[43]**		
Collagenase	↑ **[232]**		
TIMP-1	↑ **[232]**		**No effect [242]**
TGF- β	↑ **[232]**		↑**[243, 244]**
IL-1β	↑**[234]**	↑ **[234, 239]**	
MEK	↑ **[233]**	↑ **[233]**	
ERK1/2	↑ **[233]**	↑ **[233]**	↑**[245]**
SRF	↑ **[40, 233]**		
PAI-1	↑ **[233]**	↑ **[233]**	↑**[9]**
uPA	↑ **[233]**	↑ **[233]**	↑**[246]**

* Regulation often compared to static conditions. Many of these genes/proteins are also upregulated by steady laminar FSS compared to static conditions. Very few studies directly compare expression induced by disturbed versus laminar FSS.

10.3. Implications of FSS-Dependent Changes in Cytoskeletal Structure

In Chapter V the MTOC was identified as a FSS-regulated cytoskeletal structural component. In particular, the MTOC becomes polarized under steady FSS and localizes upstream of the nucleus. Whether this MTOC polarization has functional implications is unknown. The MTOC does play a role in mitosis and migration [104, 247]. In terms of mitosis, the conditions used in this study likely induced quiescence due to contact inhibition and low serum levels. Previous research has shown that ECs under steady FSS migrate in the direction of flow, while micropattern-elongated ECs exposed to steady FSS did not show a preferred direction of migration [38]. Thus, the upstream

localization of the MTOC induced by steady FSS may promote directed EC migration. Both micropattern-elongated ECs and non-patterned ECs need to be exposed to FSS for longer time periods to determine the following: (1) if upstream localization of the MTOC in micropattern-elongated ECs exposed to FSS (showed in Chapter V) eventually promotes a preferred migration direction, or (2) whether non-patterned ECs exposed to FSS still migrated parallel to FSS after they become elongated. The MTOC also contributes to microtubule stability and serves as a focal point of the microtubule network. Thus, the MTOC may contribute to EC function through stabilization of microtubules (which, for example, decreases NFκB) and through spatial trafficking and localization of protein and mRNA.

10.4. Mechanical Regulation of EC Function

The results from this research delineated cytoskeletal-structural and FSS effects on EC function. EC expression of E-selectin, ICAM-1, TF, TM, and eNOS were regulated by FSS and not cytoskeletal alignment. However, FSS is a mechanical stimuli, and mechanotransduction is mediated by the cytoskeleton [26, 248]. Thus, FSS mechanical stimulation, and not cytoskeletal alignment, may be required to trigger cytoskeletal-dependent signaling for some molecules, such as TM. This suggests that certain signaling cascades are only activated after surpassing a specific mechanical threshold. Furthermore, the additive effects on cytoskeletal alignment and FSS on expression of VCAM-1, vWF, and TFPI implies that aligned cytoskeletal conformation is required for optimal mechanical force-induced cytoskeletal signaling.

Anchor points, including focal adhesions (FAs) and cell-cell junctions, are the major sites for FSS-induced tension on the cytoskeleton [26, 27]. FAs are locations where a cell interacts with the ECM through integrin clusters. FAs are also linked to the cytoskeleton through linker proteins, such as vinculin. Under high, unidirectional FSS, ECs remodel and align their FAs in the direction of FSS, demonstrating that FAs are responsive to mechanical stimuli [249]. ECs elongated on micropatterned lanes have also demonstrated alignment of FAs [30]. The alignment of FAs and the cytoskeleton may promote mechanotransduction due to internal cellular tension imposed by the elongated EC, independent of FSS. Furthermore, the type of ECM associated with the FAs contributes to the type of signal cascade triggered by tension due to FSS [100]. Interestingly, the FAs comprised of integrin $\alpha_v\beta_3$, predominantly formed on fibronectin,

are responsible for tension-induced upregulation of IκB kinase, which phosphorylates and degrades IκB [100]. As previously noted (Chapter VI), MPECs deposited less fibronectin compared to cobblestone ECs, suggesting that MPECs may not form many FAs containing $\alpha_v\beta_3$ reducing tension-induced upregulation of NFκB. Thus, the aligned cytoskeletal structure influences on the composition of ECM and possibly on the formation of FAs may simultaneously promote specific FSS-induced mechanotransduction. This cooperative signaling possibly explains why FSS effects on EC expression appeared to act synergistically with the effects of cytoskeletal alignment.

Cell-cell junctions act as anchor points between neighboring cells through molecules such as cadherins and cell adhesion molecules. Cell-cell junctions also are connected to the cytoskeleton through linker molecules. High, unidirectional FSS modulates expression and phosphorylation of cell-cell junctions including VECAD, catenins, and tight junctions [101]. While the signaling cascades induced by tension on cell-cell junctions are largely unknown, MAP kinase pathways including MEK and ERK1/2 have been implicated [250]. Functionally, the upregulation of cell-cell junctions, e.g. VECAD, is often associated with decreased EC permeability [64]. Recent data also suggests that the formation of cell-cell junctions regulates EC proliferation through tension-induced signaling via the actin cytoskeleton [251]. ECs elongated on micropatterned lanes have limited surface area that can facilitate the formation of cell-cell contacts. This is due to the nature of micropatterned surface, such that an entire side of the cell is freely exposed to a passivated BSA-coated region. Cell-cell junctions can form end-to-end, with a maximum contact area of 25 μm (the width of the micropatterned lanes). Multiple cells can adhere and spread across the 25 μm wide lane, providing a neighboring cell for the formation of cell-cell contacts, but these cells usually lack cell junctional anchor points at the opposing cell surface. Thus, internal mechanical tension derived from cell-cell junctions of MPECs is likely to be minimal compared to confluent ECs. The large number of cell-cell contacts formed under high, unidirectional FSS may offer additional tension-induced signaling mechanism that act to either: (1) enhance cytoskeletal-alignment dependent signaling or (2) possibly generate additional cascades that stimulate gene expression solely dependent on FSS (e.g. TM).

10.5. The Practical Application of Micropattern Technology

As we learn more about the significance of external cues in promoting cell functions, we also learn how to improve the engineering of implantable devices and scaffolds. Further advances in micropatterning techniques, particularly in the field of nanotechnology, offer practical methods to construct surfaces that drive specific cell spatial localization, differentiation, and signaling. The mounting evidence demonstrating cell-shape control of cell fate suggests that micro- or nano-scale patterning is a promising approach to engineer cell function. Some of the methods currently available for printing of micropatterns, besides the soft lithography used in this study, include modified ink-jet and laser guided printing [252]. Nanotechnology approaches, such as nanofilms and nanostructuralize scaffolds, can aid in the assembly of a complex pattern of multiple extracellular cues, including: (1) ECM molecules to mimic the natural cell environment, (2) specific ligands to promote rapid cell adhesion and cell function, and (3) growth factors or drugs to enhance cell and device functionality [253]. Patterning on biomaterials, including medical grade poly methyl-methacrylate, has already shown successful cell adhesion and control of cell localization in vitro [92]. The complex integration of spatially controlled surface cues to promote cell adhesion and function in a single-step cell seeding process may be the future of “off the shelf” vascular graft technology.

10.6. Summary and Conclusions

All adherent cells have internal tension exerted by the continuous cytoskeletal network [26]. Alterations in cytoskeletal structure affect internal tension. Cytoskeletal changes induced by micropatterned-lanes or by FSS have both demonstrated effects on internal cell tension and stiffness [29, 254]. Tension-induced signaling mediated by the cytoskeleton can either act indirectly, by binding and releasing proteins and mRNA, or directly, by activating transcription factors. Previous research has shown that microtubule integrity regulates the key transcription factor NFκB [42]. This research proposes a model for cytoskeletal-dependent regulation of the novel transcription factor KLF2, which is inversely related to NFκB activity and has been linked to athero-related EC functions. Furthermore, results from this research indicated that cytoskeletal alignment influences the composition of ECM, which affects the types of FAs formed by

ECs and the specific signaling cascade induced upon activation. Gene expression results reveal that certain genes are regulated in some degree by cytoskeletal alignment while others required stimulation with high, unidirectional FSS. These regulations suggest the following: (1) the sensitivity of a tension-induced response varies such that internal tension due to cytoskeletal alignment alone is sufficient to initiate the expression of certain genes, e.g. VCAM-1, while others must overcome larger mechanical thresholds, possibly through the application of external forces, to induce expression, e.g. TM, (2) the signaling response to tension is dependent on the strength of the tensional force, where internal tension induced by cytoskeletal alignment induces less signaling activity than the larger force of FSS, and (3) both major source points of tension, FAs and cell-cell junctions, may be required to promote cytoskeletal-dependent signaling that is athero-protective. The ability to engineer cytoskeletal structure using surface micropatterning may offer a way to pre-condition cells to promote specific cell behaviors. Importantly, this process would involve the fabrication of the device/scaffold surface rather than the commonly used extensive ex vivo manipulation after cell seeding. Collectively, this study presents evidence that the cytoskeleton is not simply a passive internal cellular support, but rather, serves as an interactive organelle involved in the regulation of important EC functions that contribute to cardiovascular health.

Chapter XI

Future Work

The results of this study have begun to unravel the important role of the cytoskeleton in regulating EC function, and, as such, have revealed many more interesting lines of questioning. Further exploration into the mechanism behind cytoskeletal dependent regulation of EC function, in particular the regulation of KLF2, is needed to fully understand how cytoskeletal architecture can choreograph specific EC signaling. The investigation into cytoskeletal regulation of the EC functions examined in this study can also be continued and expanded. Some possible research studies are detailed in this chapter.

11.1. Mechanism of Cytoskeletal-Dependent Regulation of EC Functions

Chapter IX begins to explore the how cytoskeletal alignment regulates EC function through regulation of the relevant transcription factor KLF2. Preliminary results suggest that cytoskeletal alignment can induce KLF2 expression independent of FSS. In Chapter X, a model for cytoskeletal alignment dependent regulation of KLF2 was suggested, involving the dynamic nature of actin and microtubules. Validating the role of NFκB and IκB suggested in this model will be difficult due to the previously discussed limitations (Chapter IX, Section 9.6.1). However, the individual roles of actin and microtubules in the KLF2 regulation can be elucidated using the actin and microtubule stabilizers, phalloidin and taxol, respectively. Following treatment, the mRNA levels of KLF2 can be measured using qtPCR. Cytoskeletal stabilizers are suggested for this line

of research instead of destabilizers because disrupting the cytoskeleton affects EC cytoskeletal alignment on micropatterned lanes (Chapter V). Destabilizers of actin and microtubules, cytochalasin D and nocodazole, respectively, could be used on non-patterned ECs, although this would determine the role of the cytoskeleton independent of cytoskeletal alignment.

To validate that the upregulation in KLF2 is responsible for the resulting micropatterned-elongated EC gene expression, KLF2 expression should be knocked down or overexpressed in MPECs. IL-1β treatment knocks down KLF2 expression and statin treatment upregulates KLF2 expression [222, 223]. A more specific way to control KLF2 expression is by transfection with either KLF2 siRNA or the KLF2 gene to knockdown or overexpress KLF2, respectively. Results from this research will determine if KLF2 is involved in cytoskeletal alignment dependent gene expression, e.g. decrease in VCAM-1, or if other mechanisms regulate this function.

11.2. Further Investigation into Cytoskeletal Alignment Dependent EC Function

The results of this study implicate cytoskeletal alignment in the regulation of EC deposition of ECM, inflammatory function, and some factors that contribute to EC thrombogenicity. In all of these studies, it would be interesting to isolate the individual roles of actin and microtubules to determine how alignment regulates these EC functions. The use of the actin and microtubule stabilizers mentioned in the previous section (11.1) would serve to separate the roles of actin and microtubule alignment that contribute to specific EC functions.

11.2.1. Extracellular Matrix

Chapter VI describes the cytoskeletal alignment-dependent regulation of EC deposition of ECM. Interestingly, different ECM molecules were deposited based on EC cytoskeletal structure. Elongated and aligned ECs deposited more collagen IV and less fibronectin than non-patterned cobblestone ECs. As discussed in Chapter VI Section 6.6, the mechanism behind this cytoskeletal structure dependence is unknown and maybe due to either changes in deposition or degradation. Interestingly, previous

research has demonstrated that the integrity of the cytoskeleton regulates TGF-β, MMP-9, and TIMP-1 [43, 232, 241]. The roles of TGF- β, MMP-9, and TIMP-2 in the regulation of ECM are discussed in Chapter VI Section 6.6. MPEC expression at the mRNA levels of TGF- β, MMP-9, and TIMP-2 can be determined using qtPCR, but the limited cell numbers make it difficult to determine protein levels of these molecules. Furthermore, the functional activity of MMP-9 can be examined by treatment with TIMPs, followed by staining of ECM to determine the effects of MMP-9 inhibition on the composition of ECM. Finally, direct comparison between MPECs and FSS-elongated EC expression and deposition of ECM molecules is needed to fully understand the importance of cytoskeletal alignment-dependent deposition of ECM.

11.2.2. Vascular Inflammation

Chapter VII demonstrated the interestingly link between cytoskeletal alignment and decreased EC inflammatory function. Monocytic U937 cells were used to determine EC leukocyte adhesiveness, and the results indicated that leukocytes formed weaker interactions on MPECs compared to non-patterned cobblestone ECs. The significant decrease in VCAM-1 mRNA expression was suggested as an explanation for the decrease in leukocyte firm adhesion on MPEC surface. To validate this suggestion, pre-treatment of MPECs with antibodies to the proteins involved in leukocyte rolling and adhesion (E-selectin, VCAM-1, ICAM-1) can be used to elucidate the roles of each protein in facilitating leukocytes adhesiveness on the MPEC surface.

11.2.3. Thrombogenicity

Chapter VIII described the limited role of cytoskeletal alignment in the regulation of EC thrombogenicity. However, this coagulation cascade is very complex and only select molecules were tested in this study. Cytoskeletal structure may contribute to the expression of proteins involved in other aspects of the coagulation. For instance, plasminogen-activator inhibitor-1 (PAI-1), which is a regulator of plasminogen system involved in fibrinolysis, regulation by cytoskeletal stability has been well-documented (Chapter X, Table 10.1). Thus, PAI-1 and other molecules involved in the plasminogen system, such as tissue plasminogen activator, may be regulated by cytoskeletal alignment. The investigation into expression of molecules involved in the plasminogen system and their function would be valuable to the understanding cytoskeletal alignment contributions to EC thrombogenic functions.

In situ MPEC thrombogenicity can be evaluated using the well-established ex vivo baboon shunt model [255]. In this model, an external shunt attaches the femoral artery to the femoral vein. The parallel plate flow chamber can be attached to the external flow loop, exposing the cells to whole blood. The accumulation of Indium-111 labeled platelets can be measured using a scintillation camera to quantify thrombi formation.

11.3. Additive Effects of FSS on MPECs

Many of the gene expression results suggested that steady FSS may act synergistically with cytoskeletal alignment to promote athero-protective EC functions. This is not surprising since steady FSS and cytoskeletal alignment are linked. To test the effect of FSS on gene expression levels of MPECs three conditions should be used: (1) high, unidirectional FSS applied to the MPECs, (2) static MPECs, and (3) FSS-elongated ECs. Furthermore, the timecourse of gene expression should be evaluated under these conditions to determine whether a pre-aligned cytoskeleton functionally respond to steady FSS faster than ECs that need to spend 24 hours remodeling their cytoskeleton. These studies could also be repeated with the application of low, oscillatory FSS to determine the effects on cytoskeletal structure and EC function.

Attempts to apply FSS to MPECs in this study for gene and functional analysis had limited success. In many cases, the application of FSS resulted in the death of MPECs. This is likely due to the high sensitivity of MPECs due to few cell-cell contacts with neighboring cells combined with the stressed circumstances induced by the low serum levels in the media. Thus, it would be important to create micropatterns that can withstand 10% serum levels in media. The use of pluronics may sufficiently passivate the inter-lane regions of the micropatterns for FSS studies.

References

1. **Kusumoto, F., M.D., *Cardiovascular Pathophysiology*. 1999, Madison: Fence Creek Publishing.**
2. **Barakat, A.I., T. Karino, and C.K. Colton, *Microcinematographic studies of flow patterns in the excised rabbit aorta and its major branches.* Biorheology, 1997. 34(3): p. 195-221.**
3. **DeBakey, M.E., G.M. Lawrie, and D.H. Glaeser, *Patterns of atherosclerosis and their surgical significance.* Ann Surg, 1985. 201(2): p. 115-31.**
4. **Burdick, M.M., et al., *Cell-cell interactions in inflammation and cancer metastasis.* IEEE Eng Med Biol Mag, 2001. 20(3): p. 86-91.**
5. **Davies, P.F., et al., *Hemodynamics and the focal origin of atherosclerosis: a spatial approach to endothelial structure, gene expression, and function.* Ann N Y Acad Sci, 2001. 947: p. 7-16; discussion 16-7.**
6. **McCue, S., et al., *Shear stress regulates forward and reverse planar cell polarity of vascular endothelium in vivo and in vitro.* Circ Res, 2006. 98(7): p. 939-46.**
7. **Kim, D.W., A.I. Gotlieb, and B.L. Langille, *In vivo modulation of endothelial F-actin microfilaments by experimental alterations in shear stress.* Arteriosclerosis, 1989. 9(4): p. 439-45.**
8. **Marieb, E.N., *Human Anatomy & Physiology*. 6th ed. 2004, San Francisco: Pearson Benjamin Cummings. 1242.**
9. **Berk, B.C., et al., *Atheroprotective Mechanisms Activated by Fluid Shear Stress in Endothelial Cells.* Drug News Perspect, 2002. 15(3): p. 133-139.**
10. **Toborek, M. and S. Kaiser, *Endothelial cell functions. Relationship to atherogenesis.* Basic Res Cardiol, 1999. 94(5): p. 295-314.**
11. **Lerman, A. and A.M. Zeiher, *Endothelial function: cardiac events.* Circulation, 2005. 111(3): p. 363-8.**
12. **Thom, T., et al., *Heart disease and stroke statistics--2006 update: a report from the American Heart Association Statistics Committee and Stroke Statistics Subcommittee.* Circulation, 2006. 113(6): p. e85-151.**
13. **Schwartz, C.J., et al., *The pathogenesis of atherosclerosis: an overview.* Clin Cardiol, 1991. 14(2 Suppl 1): p. I1-16.**
14. **Stone, P.H., et al., *Prediction of sites of coronary atherosclerosis progression: In vivo profiling of endothelial shear stress, lumen, and outer vessel wall characteristics to predict vascular behavior.* Curr Opin Cardiol, 2003. 18(6): p. 458-70.**
15. **Wakhloo, A.K., et al., *Hemodynamics of carotid artery atherosclerotic occlusive disease.* J Vasc Interv Radiol, 2004. 15(1 Pt 2): p. S111-21.**
16. **Nerem, R.M., M.J. Levesque, and J.F. Cornhill, *Vascular endothelial morphology as an indicator of the pattern of blood flow.* J Biomech Eng, 1981. 103(3): p. 172-6.**
17. **Nerem, R.M., et al., *The study of the influence of flow on vascular endothelial biology.* Am J Med Sci, 1998. 316(3): p. 169-75.**
18. **Shibeshi, S.S. and W.E. Collins, *The Rheology of Blood Flow in a Branched Arterial System.* Appl Rheol, 2005. 15(6): p. 398-405.**

19. **Traub, O. and B.C. Berk, *Laminar shear stress: mechanisms by which endothelial cells transduce an atheroprotective force.* Arterioscler Thromb Vasc Biol, 1998. 18(5): p. 677-85.**
20. **Glagov, S., et al., *Hemodynamics and atherosclerosis. Insights and perspectives gained from studies of human arteries.* Arch Pathol Lab Med, 1988. 112(10): p. 1018-31.**
21. **Levesque, M.J., et al., *Correlation of endothelial cell shape and wall shear stress in a stenosed dog aorta.* Arteriosclerosis, 1986. 6(2): p. 220-9.**
22. **Davies, P.F., et al., *Spatial relationships in early signaling events of flow-mediated endothelial mechanotransduction.* Annu Rev Physiol, 1997. 59: p. 527-49.**
23. **Garcia-Cardena, G., et al., *Biomechanical activation of vascular endothelium as a determinant of its functional phenotype.* Proc Natl Acad Sci U S A, 2001. 98(8): p. 4478-85.**
24. **Malek, A.M., S.L. Alper, and S. Izumo, *Hemodynamic shear stress and its role in atherosclerosis.* Jama, 1999. 282(21): p. 2035-42.**
25. **Barakat, A.I., *Responsiveness of vascular endothelium to shear stress: potential role of ion channels and cellular cytoskeleton (review).* Int J Mol Med, 1999. 4(4): p. 323-32.**
26. **Ingber, D.E., *Tensegrity: the architectural basis of cellular mechanotransduction.* Annu Rev Physiol, 1997. 59: p. 575-99.**
27. **Helmke, B.P., *Molecular control of cytoskeletal mechanics by hemodynamic forces.* Physiology (Bethesda), 2005. 20: p. 43-53.**
28. **Dike, L.E., et al., *Geometric control of switching between growth, apoptosis, and differentiation during angiogenesis using micropatterned substrates.* In Vitro Cell Dev Biol Anim, 1999. 35(8): p. 441-8.**
29. **Kidoaki, S. and T. Matsuda, *Shape-engineered vascular endothelial cells: nitric oxide production, cell elasticity, and actin cytoskeletal features.* J Biomed Mater Res A, 2007. 81(3): p. 728-35.**
30. **Uttayarat, P., et al., *Topographic guidance of endothelial cells on silicone surfaces with micro- to nanogrooves: orientation of actin filaments and focal adhesions.* J Biomed Mater Res A, 2005. 75(3): p. 668-80.**
31. **Wu, C.C., et al., *Directional shear flow and Rho activation prevent the endothelial cell apoptosis induced by micropatterned anisotropic geometry.* Proc Natl Acad Sci U S A, 2007. 104(4): p. 1254-9.**
32. **DeMeester, S.L., et al., *Stress-induced fractal rearrangement of the endothelial cell cytoskeleton causes apoptosis.* Surgery, 1998. 124(2): p. 362-71.**
33. **Chen, C.S., et al., *Geometric control of cell life and death.* Science, 1997. 276(5317): p. 1425-8.**
34. **Chen, C.S., et al., *Micropatterned surfaces for control of cell shape, position, and function.* Biotechnol Prog, 1998. 14(3): p. 356-63.**
35. **Chen, C.S., et al., *Cell shape provides global control of focal adhesion assembly.* Biochem Biophys Res Commun, 2003. 307(2): p. 355-61.**
36. **Li, S., et al., *Effects of morphological patterning on endothelial cell migration.* Biorheology, 2001. 38(2-3): p. 101-8.**

37. **Hsu, S., et al.,** ***Effects of shear stress on endothelial cell haptotaxis on micropatterned surfaces.*** **Biochem Biophys Res Commun, 2005. 337(1): p. 401-9.**
38. **Lin, X. and B.P. Helmke,** ***Micropatterned structural control suppresses mechanotaxis of endothelial cells.*** **Biophys J, 2008. 95(6): p. 3066-78.**
39. **Kato, S., J. Ando, and T. Matsuda,** ***MRNA expression on shape-engineered endothelial cells: adhesion molecules ICAM-1 and VCAM-1.*** **J Biomed Mater Res, 2001. 54(3): p. 366-72.**
40. **Vartiainen, M.K., et al.,** ***Nuclear actin regulates dynamic subcellular localization and activity of the SRF cofactor MAL.*** **Science, 2007. 316(5832): p. 1749-52.**
41. **Wu, J.I. and G.R. Crabtee,** ***Cell signaling. Nuclear actin as choreographer of cell morphology and transcription.*** **Science, 2007. 316(5832): p. 1710-1.**
42. **Rosette, C. and M. Karin,** ***Cytoskeletal control of gene expression: depolymerization of microtubules activates NF-kappa B.*** **J Cell Biol, 1995. 128(6): p. 1111-9.**
43. **Varedi, M., et al.,** ***Cytoskeleton regulates expression of genes for transforming growth factor-beta 1 and extracellular matrix proteins in dermal fibroblasts.*** **J Cell Physiol, 1997. 172(2): p. 192-9.**
44. **Bordenave, L., et al.,** ***In vitro endothelialized ePTFE prostheses: clinical update 20 years after the first realization.*** **Clin Hemorheol Microcirc, 2005. 33(3): p. 227-34.**
45. **Alobaid, N., et al.,** ***Single stage cell seeding of small diameter prosthetic cardiovascular grafts.*** **Clin Hemorheol Microcirc, 2005. 33(3): p. 209-26.**
46. **Veith, F.J., et al.,** ***Six-year prospective multicenter randomized comparison of autologous saphenous vein and expanded polytetrafluoroethylene grafts in infrainguinal arterial reconstructions.*** **J Vasc Surg, 1986. 3(1): p. 104-14.**
47. **Herring, M., A. Gardner, and J. Glover,** ***Seeding endothelium onto canine arterial prostheses. The effects of graft design.*** **Arch Surg, 1979. 114(6): p. 679-82.**
48. **Zilla, P., et al.,** ***Endothelial cell seeding of polytetrafluoroethylene vascular grafts in humans: a preliminary report.*** **J Vasc Surg, 1987. 6(6): p. 535-41.**
49. **Zilla, P., et al.,** ***Clinical in vitro endothelialization of femoropopliteal bypass grafts: an actuarial follow-up over three years.*** **J Vasc Surg, 1994. 19(3): p. 540-8.**
50. **Fischlein, T., et al.,** ***Clinical lining of prosthetic femoropopliteal bypass grafts with cultured autologous endothelial cells.*** **Transplant Proc, 1992. 24(6): p. 3043.**
51. **Deutsch, M., et al.,** ***Clinical autologous in vitro endothelialization of infrainguinal ePTFE grafts in 100 patients: a 9-year experience.*** **Surgery, 1999. 126(5): p. 847-55.**
52. **Meinhart, J., M. Deutsch, and P. Zilla,** ***Eight years of clinical endothelial cell transplantation. Closing the gap between prosthetic grafts and vein grafts.*** **Asaio J, 1997. 43(5): p. M515-21.**
53. **Meinhart, J.G., et al.,** ***Clinical autologous in vitro endothelialization of 153 infrainguinal ePTFE grafts.*** **Ann Thorac Surg, 2001. 71(5 Suppl): p. S327-31.**

54. **Fernandez, P., et al.,** ***Gene response in endothelial cells cultured on engineered surfaces is regulated by shear stress.*** **Tissue Eng, 2007. 13(7): p. 1607-14.**

55. **Ott, M.J. and B.J. Ballermann,** ***Shear stress-conditioned, endothelial cell-seeded vascular grafts: improved cell adherence in response to in vitro shear stress.*** **Surgery, 1995. 117(3): p. 334-9.**

56. **Dardik, A., A. Liu, and B.J. Ballermann,** ***Chronic in vitro shear stress stimulates endothelial cell retention on prosthetic vascular grafts and reduces subsequent in vivo neointimal thickness.*** **J Vasc Surg, 1999. 29(1): p. 157-67.**

57. **Pasic, M., et al.,** ***Seeding with omental cells prevents late neointimal hyperplasia in small-diameter Dacron grafts.*** **Circulation, 1995. 92(9): p. 2605-16.**

58. **Daxini, S.C., et al.,** ***Micropatterned polymer surfaces improve retention of endothelial cells exposed to flow-induced shear stress.*** **Biorheology, 2006. 43(1): p. 45-55.**

59. **Levesque, M.J. and R.M. Nerem,** ***The elongation and orientation of cultured endothelial cells in response to shear stress.*** **J Biomech Eng, 1985. 107(4): p. 341-7.**

60. **Galbraith, C.G., R. Skalak, and S. Chien,** ***Shear stress induces spatial reorganization of the endothelial cell cytoskeleton.*** **Cell Motil Cytoskeleton, 1998. 40(4): p. 317-30.**

61. **Malek, A.M. and S. Izumo,** ***Mechanism of endothelial cell shape change and cytoskeletal remodeling in response to fluid shear stress.*** **J Cell Sci, 1996. 109 (Pt 4): p. 713-26.**

62. **Brooks, A.R., P.I. Lelkes, and G.M. Rubanyi,** ***Gene expression profiling of human aortic endothelial cells exposed to disturbed flow and steady laminar flow.*** **Physiol Genomics, 2002. 9(1): p. 27-41.**

63. **Wasserman, S.M. and J.N. Topper,** ***Adaptation of the endothelium to fluid flow: in vitro analyses of gene expression and in vivo implications.*** **Vasc Med, 2004. 9(1): p. 35-45.**

64. **Miao, H., et al.,** ***Effects of flow patterns on the localization and expression of VE-cadherin at vascular endothelial cell junctions: in vivo and in vitro investigations.*** **J Vasc Res, 2005. 42(1): p. 77-89.**

65. **Conklin, B.S., R.P. Vito, and C. Chen,** ***Effect of low shear stress on permeability and occludin expression in porcine artery endothelial cells.*** **World J Surg, 2007. 31(4): p. 733-43.**

66. **Thoumine, O., R.M. Nerem, and P.R. Girard,** ***Changes in organization and composition of the extracellular matrix underlying cultured endothelial cells exposed to laminar steady shear stress.*** **Lab Invest, 1995. 73(4): p. 565-76.**

67. **Thoumine, O., R.M. Nerem, and P.R. Girard,** ***Oscillatory shear stress and hydrostatic pressure modulate cell-matrix attachment proteins in cultured endothelial cells.*** **In Vitro Cell Dev Biol Anim, 1995. 31(1): p. 45-54.**

68. **Chiu, J.J., et al.,** ***Shear stress increases ICAM-1 and decreases VCAM-1 and E-selectin expressions induced by tumor necrosis factor-[alpha] in endothelial cells.*** **Arterioscler Thromb Vasc Biol, 2004. 24(1): p. 73-9.**

69. **Chiu, J.J., et al.,** ***Analysis of the effect of disturbed flow on monocytic adhesion to endothelial cells.*** **J Biomech, 2003. 36(12): p. 1883-95.**

70. **Ando, J., et al., *Down-regulation of vascular adhesion molecule-1 by fluid shear stress in cultured mouse endothelial cells.* Ann N Y Acad Sci, 1995. 748: p. 148-56; discussion 156-7.**
71. **Tsuboi, H., et al., *Flow stimulates ICAM-1 expression time and shear stress dependently in cultured human endothelial cells.* Biochem Biophys Res Commun, 1995. 206(3): p. 988-96.**
72. **Walpola, P.L., et al., *Expression of ICAM-1 and VCAM-1 and monocyte adherence in arteries exposed to altered shear stress.* Arterioscler Thromb Vasc Biol, 1995. 15(1): p. 2-10.**
73. **Chappell, D.C., et al., *Oscillatory shear stress stimulates adhesion molecule expression in cultured human endothelium.* Circ Res, 1998. 82(5): p. 532-9.**
74. **Nagel, T., et al., *Shear stress selectively upregulates intercellular adhesion molecule-1 expression in cultured human vascular endothelial cells.* J Clin Invest, 1994. 94(2): p. 885-91.**
75. **Morigi, M., et al., *Fluid shear stress modulates surface expression of adhesion molecules by endothelial cells.* Blood, 1995. 85(7): p. 1696-703.**
76. **Chiu, J.J., S. Usami, and S. Chien, *Vascular endothelial responses to altered shear stress: pathologic implications for atherosclerosis.* Ann Med, 2009. 41(1): p. 19-28.**
77. **Shyy, Y.J., et al., *Fluid shear stress induces a biphasic response of human monocyte chemotactic protein 1 gene expression in vascular endothelium.* Proc Natl Acad Sci U S A, 1994. 91(11): p. 4678-82.**
78. **Fisher, A.B., et al., *Endothelial cellular response to altered shear stress.* Am J Physiol Lung Cell Mol Physiol, 2001. 281(3): p. L529-33.**
79. **Lin, M.C., et al., *Shear stress induction of the tissue factor gene.* J Clin Invest, 1997. 99(4): p. 737-44.**
80. **Mazzolai, L., et al., *Tissue factor activity is upregulated in human endothelial cells exposed to oscillatory shear stress.* Thromb Haemost, 2002. 87(6): p. 1062-8.**
81. **Grabowski, E.F., et al., *Shear stress decreases endothelial cell tissue factor activity by augmenting secretion of tissue factor pathway inhibitor.* Arterioscler Thromb Vasc Biol, 2001. 21(1): p. 157-62.**
82. **Westmuckett, A.D., et al., *Fluid flow induces upregulation of synthesis and release of tissue factor pathway inhibitor in vitro.* Arterioscler Thromb Vasc Biol, 2000. 20(11): p. 2474-82.**
83. **Hough, C., et al., *Influence of a GT repeat element on shear stress responsiveness of the VWF gene promoter.* J Thromb Haemost, 2008. 6(7): p. 1183-90.**
84. **Galbusera, M., et al., *Fluid shear stress modulates von Willebrand factor release from human vascular endothelium.* Blood, 1997. 90(4): p. 1558-64.**
85. **Malek, A.M., et al., *Endothelial expression of thrombomodulin is reversibly regulated by fluid shear stress.* Circ Res, 1994. 74(5): p. 852-60.**
86. **Takada, Y., et al., *Fluid shear stress increases the expression of thrombomodulin by cultured human endothelial cells.* Biochem Biophys Res Commun, 1994. 205(2): p. 1345-52.**

87. **Topper, J.N., et al.,** ***Identification of vascular endothelial genes differentially responsive to fluid mechanical stimuli: cyclooxygenase-2, manganese superoxide dismutase, and endothelial cell nitric oxide synthase are selectively up-regulated by steady laminar shear stress.*** **Proc Natl Acad Sci U S A, 1996. 93(19): p. 10417-22.**
88. **Cunningham, K.S. and A.I. Gotlieb,** ***The role of shear stress in the pathogenesis of atherosclerosis.*** **Lab Invest, 2005. 85(1): p. 9-23.**
89. **Uematsu, M., et al.,** ***Regulation of endothelial cell nitric oxide synthase mRNA expression by shear stress.*** **Am J Physiol, 1995. 269(6 Pt 1): p. C1371-8.**
90. **Silacci, P., et al.,** ***Unidirectional and oscillatory shear stress differentially modulate NOS III gene expression.*** **Nitric Oxide, 2000. 4(1): p. 47-56.**
91. **Ensley, A.,** ***Functional evaluation of circulating endothelial progenitor cells for vascular tissue engineering.*** **2006.**
92. **Folch, A. and M. Toner,** ***Cellular micropatterns on biocompatible materials.*** **Biotechnol Prog, 1998. 14(3): p. 388-92.**
93. **Jahne, B.,** ***Practical Handbook on Image Processing for Scientific Application.*** **1997: CRC press. 589.**
94. **Russ, J.C.,** ***The Image Processing Handbook Second Edition.*** **2nd ed. 1995: CRC Press Inc. 674.**
95. **Pagano, M.G., K,** ***Principles of Biostatistics.*** **Second ed. 2000, Pacific Grove: Brooks/Cole. 525.**
96. **Shannon, C.E.,** ***A mathematical theory of communication.*** **Bell Syst. Tech. J., 1948. 27: p. 379-423.**
97. **Lee, T.Y. and A.I. Gotlieb,** ***Microfilaments and microtubules maintain endothelial integrity.*** **Microsc Res Tech, 2003. 60(1): p. 115-27.**
98. **Osborn, E.A., et al.,** ***Endothelial actin cytoskeleton remodeling during mechanostimulation with fluid shear stress.*** **Am J Physiol Cell Physiol, 2006. 290(2): p. C444-52.**
99. **Davies, P.F.,** ***Mechanisms involved in endothelial responses to hemodynamic forces.*** **Atherosclerosis, 1997. 131 Suppl: p. S15-7.**
100. **Lehoux, S., Y. Castier, and A. Tedgui,** ***Molecular mechanisms of the vascular responses to haemodynamic forces.*** **J Intern Med, 2006. 259(4): p. 381-92.**
101. **Helmke, B.P. and P.F. Davies,** ***The cytoskeleton under external fluid mechanical forces: hemodynamic forces acting on the endothelium.*** **Ann Biomed Eng, 2002. 30(3): p. 284-96.**
102. **Noria, S., et al.,** ***Assembly and reorientation of stress fibers drives morphological changes to endothelial cells exposed to shear stress.*** **Am J Pathol, 2004. 164(4): p. 1211-23.**
103. **McCue, S., S. Noria, and B.L. Langille,** ***Shear-induced reorganization of endothelial cell cytoskeleton and adhesion complexes.*** **Trends Cardiovasc Med, 2004. 14(4): p. 143-51.**
104. **Alberts, B.J., A; Lewis, J; Raff, M; Roberts, K;and Walter, P,** ***Molecular Biology of the Cell.*** **4th ed. 2002, New York: Garland Science. 1463.**
105. **Borisy, G.G. and T.M. Svitkina,** ***Actin machinery: pushing the envelope.*** **Curr Opin Cell Biol, 2000. 12(1): p. 104-12.**

106. Janmey, P.A., *The cytoskeleton and cell signaling: component localization and mechanical coupling.* Physiol Rev, 1998. 78(3): p. 763-81.
107. Bursch, W., et al., *Autophagic and apoptotic types of programmed cell death exhibit different fates of cytoskeletal filaments.* J Cell Sci, 2000. 113 (Pt 7): p. 1189-98.
108. Rogers, K.A. and V.I. Kalnins, *Comparison of the cytoskeleton in aortic endothelial cells in situ and in vitro.* Lab Invest, 1983. 49(6): p. 650-4.
109. Girard, P.R. and R.M. Nerem, *Endothelial cell signaling and cytoskeletal changes in response to shear stress.* Front Med Biol Eng, 1993. 5(1): p. 31-6.
110. Chen, T.G., J.Z. Chen, and X.X. Wang, *Effects of rapamycin on number activity and eNOS of endothelial progenitor cells from peripheral blood.* Cell Prolif, 2006. 39(2): p. 117-25.
111. Orr, A.W., et al., *Matrix-specific p21-activated kinase activation regulates vascular permeability in atherogenesis.* J Cell Biol, 2007. 176(5): p. 719-27.
112. Methe, H., S. Hess, and E.R. Edelman, *Endothelial immunogenicity--a matter of matrix microarchitecture.* Thromb Haemost, 2007. 98(2): p. 278-82.
113. Methe, H., et al., *Matrix adherence of endothelial cells attenuates immune reactivity: induction of hyporesponsiveness in allo- and xenogeneic models.* Faseb J, 2007. 21(7): p. 1515-26.
114. Ruoslahti, E., E.G. Hayman, and M.D. Pierschbacher, *Extracellular matrices and cell adhesion.* Arteriosclerosis, 1985. 5(6): p. 581-94.
115. Davis, G.E. and D.R. Senger, *Endothelial extracellular matrix: biosynthesis, remodeling, and functions during vascular morphogenesis and neovessel stabilization.* Circ Res, 2005. 97(11): p. 1093-107.
116. Lehnert, D., et al., *Cell behaviour on micropatterned substrata: limits of extracellular matrix geometry for spreading and adhesion.* J Cell Sci, 2004. 117(Pt 1): p. 41-52.
117. Khoshnoodi, J., V. Pedchenko, and B.G. Hudson, *Mammalian collagen IV.* Microsc Res Tech, 2008. 71(5): p. 357-70.
118. Yurchenco, P.D. and J.C. Schittny, *Molecular architecture of basement membranes.* Faseb J, 1990. 4(6): p. 1577-90.
119. Poschl, E., et al., *Collagen IV is essential for basement membrane stability but dispensable for initiation of its assembly during early development.* Development, 2004. 131(7): p. 1619-28.
120. Sasaki, T., R. Fassler, and E. Hohenester, *Laminin: the crux of basement membrane assembly.* J Cell Biol, 2004. 164(7): p. 959-63.
121. Colognato, H. and P.D. Yurchenco, *Form and function: the laminin family of heterotrimers.* Dev Dyn, 2000. 218(2): p. 213-34.
122. Smyth, N., et al., *Absence of basement membranes after targeting the LAMC1 gene results in embryonic lethality due to failure of endoderm differentiation.* J Cell Biol, 1999. 144(1): p. 151-60.
123. Mosher, D.F. and L.T. Furcht, *Fibronectin: review of its structure and possible functions.* J Invest Dermatol, 1981. 77(2): p. 175-80.
124. Hayden, M.R., J.R. Sowers, and S.C. Tyagi, *The central role of vascular extracellular matrix and basement membrane remodeling in metabolic*

syndrome and type 2 diabetes: the matrix preloaded. **Cardiovasc Diabetol, 2005. 4(1): p. 9.**

125. Kunz, J., *Can atherosclerosis regress? The role of the vascular extracellular matrix and the age-related changes of arteries.* Gerontology, 2002. 48(5): p. 267-78.

126. Sima, A.V., C.S. Stancu, and M. Simionescu, *Vascular endothelium in atherosclerosis.* Cell Tissue Res, 2009. 335(1): p. 191-203.

127. L'Heureux, N., et al., *A completely biological tissue-engineered human blood vessel.* Faseb J, 1998. 12(1): p. 47-56.

128. Ogle, B.M. and D.L. Mooradian, *Manipulation of remodeling pathways to enhance the mechanical properties of a tissue engineered blood vessel.* J Biomech Eng, 2002. 124(6): p. 724-33.

129. Hinds, M.T., et al., *Development of a reinforced porcine elastin composite vascular scaffold.* J Biomed Mater Res A, 2006. 77(3): p. 458-69.

130. Salacinski, H.J., et al., *Cellular engineering of vascular bypass grafts: role of chemical coatings for enhancing endothelial cell attachment.* Med Biol Eng Comput, 2001. 39(6): p. 609-18.

131. Seeger, J.M. and N. Klingman, *Improved in vivo endothelialization of prosthetic grafts by surface modification with fibronectin.* J Vasc Surg, 1988. 8(4): p. 476-82.

132. Seeger, J.M. and N. Klingman, *Improved endothelial cell seeding with cultured cells and fibronectin-coated grafts.* J Surg Res, 1985. 38(6): p. 641-7.

133. Lin, Y., et al., *Origins of circulating endothelial cells and endothelial outgrowth from blood.* J Clin Invest, 2000. 105(1): p. 71-7.

134. Sata, M., *Role of circulating vascular progenitors in angiogenesis, vascular healing, and pulmonary hypertension: lessons from animal models.* Arterioscler Thromb Vasc Biol, 2006. 26(5): p. 1008-14.

135. Popa, E.R., et al., *Circulating CD34(+) progenitor cells modulate host angiogenesis and inflammation in vivo.* J Mol Cell Cardiol, 2006.

136. Liew, A., F. Barry, and T. O'Brien, *Endothelial progenitor cells: diagnostic and therapeutic considerations.* Bioessays, 2006. 28(3): p. 261-70.

137. Collins, R.G., et al., *P-Selectin or intercellular adhesion molecule (ICAM)-1 deficiency substantially protects against atherosclerosis in apolipoprotein E-deficient mice.* J Exp Med, 2000. 191(1): p. 189-94.

138. Beranek, J.T., *Vascular endothelial cell is a stem cell for neointimal formation after injury.* J Thorac Cardiovasc Surg, 2001. 121(4): p. 820-1.

139. Assmus, B., et al., *Transplantation of Progenitor Cells and Regeneration Enhancement in Acute Myocardial Infarction (TOPCARE-AMI).* Circulation, 2002. 106(24): p. 3009-17.

140. Badorff, C., et al., *Transdifferentiation of blood-derived human adult endothelial progenitor cells into functionally active cardiomyocytes.* Circulation, 2003. 107(7): p. 1024-32.

141. Rafii, S. and D. Lyden, *Therapeutic stem and progenitor cell transplantation for organ vascularization and regeneration.* Nat Med, 2003. 9(6): p. 702-12.

142. Croizat, H., et al., ***Primitive haematopoietic progenitors in the blood of patients with sickle cell disease appear to be endogenously mobilized.*** **Br J Haematol, 2000. 111(2): p. 491-7.**

143. Shi, Q., et al., ***Evidence for circulating bone marrow-derived endothelial cells.*** **Blood, 1998. 92(2): p. 362-7.**

144. Walter, D.H., et al., ***Statin therapy accelerates reendothelialization: a novel effect involving mobilization and incorporation of bone marrow-derived endothelial progenitor cells.*** **Circulation, 2002. 105(25): p. 3017-24.**

145. Werner, N., et al., ***Intravenous transfusion of endothelial progenitor cells reduces neointima formation after vascular injury.*** **Circ Res, 2003. 93(2): p. e17-24.**

146. Kaushal, S., et al., ***Functional small-diameter neovessels created using endothelial progenitor cells expanded ex vivo.*** **Nat Med, 2001. 7(9): p. 1035-40.**

147. Griese, D.P., et al., ***Isolation and transplantation of autologous circulating endothelial cells into denuded vessels and prosthetic grafts: implications for cell-based vascular therapy.*** **Circulation, 2003. 108(21): p. 2710-5.**

148. Isenberg, B.C., C. Williams, and R.T. Tranquillo, ***Small-diameter artificial arteries engineered in vitro.*** **Circ Res, 2006. 98(1): p. 25-35.**

149. Vartanian, K.B., Kirkpatrick, S.J., Hanson, S.R., Hinds, M.T., ***Endothelial Cell Cytoskeletal Alignment Independent of Fluid Shear Stress on Micropatterned Surfaces.*** **Biochemical and Biophysical Research Communications, 2008. in press.**

150. Yoder, M.C., et al., ***Redefining endothelial progenitor cells via clonal analysis and hematopoietic stem/progenitor cell principals.*** **Blood, 2007. 109(5): p. 1801-9.**

151. Hinds, M., et al., ***Potential of Baboon Endothelial Progenitor Cells for Tissue Engineered Vascular Grafts.*** **Journal of Biomedical Materials Research, Part A, in press, 2007.**

152. Tan, J.L., et al., ***Simple approach to micropattern cells on common culture substrates by tuning substrate wettability.*** **Tissue Eng, 2004. 10(5-6): p. 865-72.**

153. Ignotz, R.A. and J. Massague, ***Transforming growth factor-beta stimulates the expression of fibronectin and collagen and their incorporation into the extracellular matrix.*** **J Biol Chem, 1986. 261(9): p. 4337-45.**

154. Grotendorst, G.R., ***Connective tissue growth factor: a mediator of TGF-beta action on fibroblasts.*** **Cytokine Growth Factor Rev, 1997. 8(3): p. 171-9.**

155. Sales, V.L., et al., ***Transforming growth factor-beta1 modulates extracellular matrix production, proliferation, and apoptosis of endothelial progenitor cells in tissue-engineering scaffolds.*** **Circulation, 2006. 114(1 Suppl): p. I193-9.**

156. Newby, A.C., ***Dual role of matrix metalloproteinases (matrixins) in intimal thickening and atherosclerotic plaque rupture.*** **Physiol Rev, 2005. 85(1): p. 1-31.**

157. Iglesias-De La Cruz, M.C., et al., ***Phenotypic modifications of human mesangial cells by extracellular matrix: the importance of matrix in the contractile response to reactive oxygen species.*** **Exp Nephrol, 2000. 8(2): p. 97-103.**

158. Alon, R. and K. Ley, *Cells on the run: shear-regulated integrin activation in leukocyte rolling and arrest on endothelial cells.* Curr Opin Cell Biol, 2008. 20(5): p. 525-32.
159. Ito, T. and U. Ikeda, *Inflammatory cytokines and cardiovascular disease.* Curr Drug Targets Inflamm Allergy, 2003. 2(3): p. 257-65.
160. Huo, Y. and K. Ley, *Adhesion molecules and atherogenesis.* Acta Physiol Scand, 2001. 173(1): p. 35-43.
161. Rao, R.M., et al., *Endothelial-dependent mechanisms of leukocyte recruitment to the vascular wall.* Circ Res, 2007. 101(3): p. 234-47.
162. Butcher, E.C., *Leukocyte-endothelial cell recognition: three (or more) steps to specificity and diversity.* Cell, 1991. 67(6): p. 1033-6.
163. Carlos, T.M. and J.M. Harlan, *Leukocyte-endothelial adhesion molecules.* Blood, 1994. 84(7): p. 2068-101.
164. Tedder, T.F., et al., *The selectins: vascular adhesion molecules.* Faseb J, 1995. 9(10): p. 866-73.
165. Rosen, S.D. and C.R. Bertozzi, *The selectins and their ligands.* Curr Opin Cell Biol, 1994. 6(5): p. 663-73.
166. Krieglstein, C.F. and D.N. Granger, *Adhesion molecules and their role in vascular disease.* Am J Hypertens, 2001. 14(6 Pt 2): p. 44S-54S.
167. Carpen, O., et al., *Association of intercellular adhesion molecule-1 (ICAM-1) with actin-containing cytoskeleton and alpha-actinin.* J Cell Biol, 1992. 118(5): p. 1223-34.
168. Petri, B. and M.G. Bixel, *Molecular events during leukocyte diapedesis.* Febs J, 2006. 273(19): p. 4399-407.
169. Carman, C.V. and T.A. Springer, *A transmigratory cup in leukocyte diapedesis both through individual vascular endothelial cells and between them.* J Cell Biol, 2004. 167(2): p. 377-88.
170. Kraiss, L.W., et al., *Fluid flow regulates E-selectin protein levels in human endothelial cells by inhibiting translation.* J Vasc Surg, 2003. 37(1): p. 161-8.
171. Davies, M.J., et al., *The expression of the adhesion molecules ICAM-1, VCAM-1, PECAM, and E-selectin in human atherosclerosis.* J Pathol, 1993. 171(3): p. 223-9.
172. Reckless, J., et al., *Monocyte chemoattractant protein-1 but not tumor necrosis factor-alpha is correlated with monocyte infiltration in mouse lipid lesions.* Circulation, 1999. 99(17): p. 2310-6.
173. Chen, Y.L., Y.J. Chang, and M.J. Jiang, *Monocyte chemotactic protein-1 gene and protein expression in atherogenesis of hypercholesterolemic rabbits.* Atherosclerosis, 1999. 143(1): p. 115-23.
174. Gu, L., et al., *Absence of monocyte chemoattractant protein-1 reduces atherosclerosis in low density lipoprotein receptor-deficient mice.* Mol Cell, 1998. 2(2): p. 275-81.
175. Gosling, J., et al., *MCP-1 deficiency reduces susceptibility to atherosclerosis in mice that overexpress human apolipoprotein B.* J Clin Invest, 1999. 103(6): p. 773-8.
176. Ikeda, U., et al., *Monocyte chemoattractant protein-1 and coronary artery disease.* Clin Cardiol, 2002. 25(4): p. 143-7.

177. Cybulsky, M.I., et al., ***A major role for VCAM-1, but not ICAM-1, in early atherosclerosis.*** **J Clin Invest, 2001. 107(10): p. 1255-62.**

178. Mitchell, R.N., ***Graft Vascular Disease: Immune Response Meets the Vessel Wall.*** **Annu Rev Pathol, 2008.**

179. Brooks, A.R., P.I. Lelkes, and G.M. Rubanyi, ***Gene expression profiling of vascular endothelial cells exposed to fluid mechanical forces: relevance for focal susceptibility to atherosclerosis.*** **Endothelium, 2004. 11(1): p. 45-57.**

180. Yoshida, M., et al., ***Hmg-CoA reductase inhibitor modulates monocyte-endothelial cell interaction under physiological flow conditions in vitro: involvement of Rho GTPase-dependent mechanism.*** **Arterioscler Thromb Vasc Biol, 2001. 21(7): p. 1165-71.**

181. Price, G.C., S.A. Thompson, and P.C. Kam, ***Tissue factor and tissue factor pathway inhibitor.*** **Anaesthesia, 2004. 59(5): p. 483-92.**

182. Broze, G.J., Jr., ***Tissue factor pathway inhibitor and the revised theory of coagulation.*** **Annu Rev Med, 1995. 46: p. 103-12.**

183. Mackman, N., R.E. Tilley, and N.S. Key, ***Role of the extrinsic pathway of blood coagulation in hemostasis and thrombosis.*** **Arterioscler Thromb Vasc Biol, 2007. 27(8): p. 1687-93.**

184. Steffel, J., T.F. Luscher, and F.C. Tanner, ***Tissue factor in cardiovascular diseases: molecular mechanisms and clinical implications.*** **Circulation, 2006. 113(5): p. 722-31.**

185. Daubie, V., et al., ***Tissue factor: a mini-review.*** **J Tissue Eng Regen Med, 2007. 1(3): p. 161-9.**

186. Parry, G.C. and N. Mackman, ***Transcriptional regulation of tissue factor expression in human endothelial cells.*** **Arterioscler Thromb Vasc Biol, 1995. 15(5): p. 612-21.**

187. Scarpati, E.M. and J.E. Sadler, ***Regulation of endothelial cell coagulant properties. Modulation of tissue factor, plasminogen activator inhibitors, and thrombomodulin by phorbol 12-myristate 13-acetate and tumor necrosis factor.*** **J Biol Chem, 1989. 264(34): p. 20705-13.**

188. Huang, Z.F., T.C. Wun, and G.J. Broze, Jr., ***Kinetics of factor Xa inhibition by tissue factor pathway inhibitor.*** **J Biol Chem, 1993. 268(36): p. 26950-5.**

189. McGuigan, A.P. and M.V. Sefton, ***The influence of biomaterials on endothelial cell thrombogenicity.*** **Biomaterials, 2007. 28(16): p. 2547-71.**

190. Sadler, J.E., ***Biochemistry and genetics of von Willebrand factor.*** **Annu Rev Biochem, 1998. 67: p. 395-424.**

191. Wu, K.K. and P. Thiagarajan, ***Role of endothelium in thrombosis and hemostasis.*** **Annu Rev Med, 1996. 47: p. 315-31.**

192. Van de Wouwer, M., D. Collen, and E.M. Conway, ***Thrombomodulin-protein C-EPCR system: integrated to regulate coagulation and inflammation.*** **Arterioscler Thromb Vasc Biol, 2004. 24(8): p. 1374-83.**

193. Fish, J.E. and P.A. Marsden, ***Endothelial nitric oxide synthase: insight into cell-specific gene regulation in the vascular endothelium.*** **Cell Mol Life Sci, 2006. 63(2): p. 144-62.**

194. Davis, M.E., et al., *Shear stress regulates endothelial nitric oxide synthase expression through c-Src by divergent signaling pathways.* Circ Res, 2001. 89(11): p. 1073-80.

195. Thiruvikraman, S.V., et al., *In situ localization of tissue factor in human atherosclerotic plaques by binding of digoxigenin-labeled factors VIIa and X.* Lab Invest, 1996. 75(4): p. 451-61.

196. Kaikita, K., et al., *Co-localization of tissue factor and tissue factor pathway inhibitor in coronary atherosclerosis.* J Pathol, 1999. 188(2): p. 180-8.

197. Crawley, J., et al., *Expression, localization, and activity of tissue factor pathway inhibitor in normal and atherosclerotic human vessels.* Arterioscler Thromb Vasc Biol, 2000. 20(5): p. 1362-73.

198. Nichols, T.C., et al., *von Willebrand factor and occlusive arterial thrombosis. A study in normal and von Willebrand's disease pigs with diet-induced hypercholesterolemia and atherosclerosis.* Arteriosclerosis, 1990. 10(3): p. 449-61.

199. Merlini, P.A., et al., *Expression of endothelial protein C receptor and thrombomodulin in human coronary atherosclerotic plaques.* Ital Heart J, 2004. 5(1): p. 42-7.

200. Ishii, H., et al., *Oxidized low density lipoprotein reduces thrombomodulin transcription in cultured human endothelial cells through degradation of the lipoprotein in lysosomes.* J Biol Chem, 1996. 271(14): p. 8458-65.

201. Wilcox, J.N., et al., *Expression of multiple isoforms of nitric oxide synthase in normal and atherosclerotic vessels.* Arterioscler Thromb Vasc Biol, 1997. 17(11): p. 2479-88.

202. Sarkar, S., et al., *Addressing thrombogenicity in vascular graft construction.* J Biomed Mater Res B Appl Biomater, 2007. 82(1): p. 100-8.

203. Sarkar, S., et al., *Achieving the ideal properties for vascular bypass grafts using a tissue engineered approach: a review.* Med Biol Eng Comput, 2007. 45(4): p. 327-36.

204. Lin, P.H., et al., *Heparin-coated balloon-expandable stent reduces intimal hyperplasia in the iliac artery in baboons.* J Vasc Interv Radiol, 2003. 14(5): p. 603-11.

205. Bergqvist, D., N. Jensen, and N.H. Persson, *Heparinization of polytetrafluoroethylene (ePTFE) grafts. The effect on pseudointimal hyperplasia.* Int Angiol, 1988. 7(1): p. 65-70.

206. Lee, K.H., et al., *Heparin-coated angiographic catheters: an in vivo comparison of three coating methods with different heparin release profiles.* Cardiovasc Intervent Radiol, 2004. 27(5): p. 507-11.

207. Aldenhoff, Y.B., et al., *Coils and tubes releasing heparin. Studies on a new vascular graft prototype.* Biomaterials, 2004. 25(16): p. 3125-33.

208. Iakovou, I., et al., *Incidence, predictors, and outcome of thrombosis after successful implantation of drug-eluting stents.* Jama, 2005. 293(17): p. 2126-30.

209. Aida, K., et al., *The effects of betamethasone (BM) on endothelial nitric oxide synthase (eNOS) expression in adult baboon femoral arterial endothelial cells.* J Steroid Biochem Mol Biol, 2004. 91(4-5): p. 219-24.

210. Ensley, A., ***Functional Evaluation of Circulating Endothelial Progenitor Cells for Vascular Tissue Engineering*****, in** ***Bioengineering*****. 2006, Georgia Institute of Technology: Atlanta. p. 247.**

211. Saelman, E.U., et al., ***Platelet adhesion to collagen and endothelial cell matrix under flow conditions is not dependent on platelet glycoprotein IV.*** **Blood, 1994. 83(11): p. 3240-4.**

212. Saelman, E.U., et al., ***Platelet adhesion to collagen types I through VIII under conditions of stasis and flow is mediated by GPIa/IIa (alpha 2 beta 1-integrin).*** **Blood, 1994. 83(5): p. 1244-50.**

213. Vlodavsky, I., et al., ***Platelet interaction with the extracellular matrix produced by cultured endothelial cells: a model to study the thrombogenicity of isolated subendothelial basal lamina.*** **Thromb Res, 1982. 28(2): p. 179-91.**

214. Bombeli, T., B.R. Schwartz, and J.M. Harlan, ***Adhesion of activated platelets to endothelial cells: evidence for a GPIIbIIIa-dependent bridging mechanism and novel roles for endothelial intercellular adhesion molecule 1 (ICAM-1), alphavbeta3 integrin, and GPIbalpha.*** **J Exp Med, 1998. 187(3): p. 329-39.**

215. Feinberg MW, L.Z., Fisch S, and Jain MK, ***An Emerging Role for Kruppel-Like Factors in Vascular Biology.*** **Trends in Cardiovascular Medicine, 2004. 14(6): p. 241-246.**

216. Miller, I.J. and J.J. Bieker, ***A novel, erythroid cell-specific murine transcription factor that binds to the CACCC element and is related to the Kruppel family of nuclear proteins.*** **Mol Cell Biol, 1993. 13(5): p. 2776-86.**

217. Lin, Z., et al., ***Kruppel-like factor 2 (KLF2) regulates endothelial thrombotic function.*** **Circ Res, 2005. 96(5): p. e48-57.**

218. Wani, M.A., R.T. Means, Jr., and J.B. Lingrel, ***Loss of LKLF function results in embryonic lethality in mice.*** **Transgenic Res, 1998. 7(4): p. 229-38.**

219. Kuo, C.T., et al., ***The LKLF transcription factor is required for normal tunica media formation and blood vessel stabilization during murine embryogenesis.*** **Genes Dev, 1997. 11(22): p. 2996-3006.**

220. Dekker, R.J., et al., ***Prolonged fluid shear stress induces a distinct set of endothelial cell genes, most specifically lung Kruppel-like factor (KLF2).*** **Blood, 2002. 100(5): p. 1689-98.**

221. Wang, N., et al., ***Shear stress regulation of Kruppel-like factor 2 expression is flow pattern-specific.*** **Biochem Biophys Res Commun, 2006. 341(4): p. 1244-51.**

222. SenBanerjee, S., et al., ***KLF2 Is a novel transcriptional regulator of endothelial proinflammatory activation.*** **J Exp Med, 2004. 199(10): p. 1305-15.**

223. Sen-Banerjee, S., et al., ***Kruppel-like factor 2 as a novel mediator of statin effects in endothelial cells.*** **Circulation, 2005. 112(5): p. 720-6.**

224. Read, M.A., et al., ***NF-kappa B and I kappa B alpha: an inducible regulatory system in endothelial activation.*** **J Exp Med, 1994. 179(2): p. 503-12.**

225. Sheppard, K.A., et al., ***Transcriptional activation by NF-kappaB requires multiple coactivators.*** **Mol Cell Biol, 1999. 19(9): p. 6367-78.**

226. Song, C.Z., et al., ***Functional interaction between coactivators CBP/p300, PCAF, and transcription factor FKLF2.*** **J Biol Chem, 2002. 277(9): p. 7029-36.**

227. Tzima, E., *Role of small GTPases in endothelial cytoskeletal dynamics and the shear stress response.* Circ Res, 2006. 98(2): p. 176-85.

228. Slepchenko, B.M., et al., *Switching of membrane organelles between cytoskeletal transport systems is determined by regulation of the microtubule-based transport.* J Cell Biol, 2007. 179(4): p. 635-41.

229. Shafrir, Y., D. ben-Avraham, and G. Forgacs, *Trafficking and signaling through the cytoskeleton: a specific mechanism.* J Cell Sci, 2000. 113 (Pt 15): p. 2747-57.

230. Singer, R.H., *The cytoskeleton and mRNA localization.* Curr Opin Cell Biol, 1992. 4(1): p. 15-9.

231. Biegel, D. and J.S. Pachter, *mRNA association with the cytoskeletal framework likely represents a physiological binding event.* J Cell Biochem, 1992. 48(1): p. 98-106.

232. Varedi, M., et al., *Alteration in cell morphology triggers transforming growth factor-beta 1, collagenase, and tissue inhibitor of metalloproteinases-I expression in normal and hypertrophic scar fibroblasts.* J Invest Dermatol, 1995. 104(1): p. 118-23.

233. Samarakoon, R. and P.J. Higgins, *MEK/ERK pathway mediates cell-shape-dependent plasminogen activator inhibitor type 1 gene expression upon drug-induced disruption of the microfilament and microtubule networks.* J Cell Sci, 2002. 115(Pt 15): p. 3093-103.

234. Ritzenthaler, J.D. and J. Roman, *Interleukin-1beta gene transcription in U937 cells is modulated by type I collagen and cytoskeletal integrity via distinct signaling pathways.* J Interferon Cytokine Res, 2001. 21(2): p. 105-16.

235. Nagel, T., et al., *Vascular endothelial cells respond to spatial gradients in fluid shear stress by enhanced activation of transcription factors.* Arterioscler Thromb Vasc Biol, 1999. 19(8): p. 1825-34.

236. Tzima, E., et al., *A mechanosensory complex that mediates the endothelial cell response to fluid shear stress.* Nature, 2005. 437(7057): p. 426-31.

237. Perona, R., et al., *Activation of the nuclear factor-kappaB by Rho, CDC42, and Rac-1 proteins.* Genes Dev, 1997. 11(4): p. 463-75.

238. Molony, L. and L. Armstrong, *Cytoskeletal reorganizations in human umbilical vein endothelial cells as a result of cytokine exposure.* Exp Cell Res, 1991. 196(1): p. 40-8.

239. Allen, J.N., D.J. Herzyk, and M.D. Wewers, *Colchicine has opposite effects on interleukin-1 beta and tumor necrosis factor-alpha production.* Am J Physiol, 1991. 261(4 Pt 1): p. L315-21.

240. Ohta, H., et al., *Disruption of tumor necrosis factor-alpha gene diminishes the development of atherosclerosis in ApoE-deficient mice.* Atherosclerosis, 2005. 180(1): p. 11-7.

241. Chintala, S.K., et al., *Induction of matrix metalloproteinase-9 requires a polymerized actin cytoskeleton in human malignant glioma cells.* J Biol Chem, 1998. 273(22): p. 13545-51.

242. Magid, R., T.J. Murphy, and Z.S. Galis, *Expression of matrix metalloproteinase-9 in endothelial cells is differentially regulated by shear stress. Role of c-Myc.* J Biol Chem, 2003. 278(35): p. 32994-9.

243. Volger, O.L., et al., ***Distinctive expression of chemokines and transforming growth factor-beta signaling in human arterial endothelium during atherosclerosis.*** **Am J Pathol, 2007. 171(1): p. 326-37.**

244. Lum, R.M., L.M. Wiley, and A.I. Barakat, ***Influence of different forms of fluid shear stress on vascular endothelial TGF-beta1 mRNA expression.*** **Int J Mol Med, 2000. 5(6): p. 635-41.**

245. Kadohama, T., et al., ***Effects of different types of fluid shear stress on endothelial cell proliferation and survival.*** **J Cell Physiol, 2007. 212(1): p. 244-51.**

246. Sokabe, T., et al., ***Differential regulation of urokinase-type plasminogen activator expression by fluid shear stress in human coronary artery endothelial cells.*** **Am J Physiol Heart Circ Physiol, 2004. 287(5): p. H2027-34.**

247. Kupfer, A., D. Louvard, and S.J. Singer, ***Polarization of the Golgi apparatus and the microtubule-organizing center in cultured fibroblasts at the edge of an experimental wound.*** **Proc Natl Acad Sci U S A, 1982. 79(8): p. 2603-7.**

248. Alenghat, F.J. and D.E. Ingber, ***Mechanotransduction: all signals point to cytoskeleton, matrix, and integrins.*** **Sci STKE, 2002. 2002(119): p. PE6.**

249. Davies, P.F., A. Robotewskyj, and M.L. Griem, ***Quantitative studies of endothelial cell adhesion. Directional remodeling of focal adhesion sites in response to flow forces.*** **J Clin Invest, 1994. 93(5): p. 2031-8.**

250. Langille, B.L., ***Morphologic responses of endothelium to shear stress: reorganization of the adherens junction.*** **Microcirculation, 2001. 8(3): p. 195-206.**

251. Gray, D.S., et al., ***Engineering amount of cell-cell contact demonstrates biphasic proliferative regulation through RhoA and the actin cytoskeleton.*** **Exp Cell Res, 2008. 314(15): p. 2846-54.**

252. Falconnet, D., et al., ***Surface engineering approaches to micropattern surfaces for cell-based assays.*** **Biomaterials, 2006. 27(16): p. 3044-63.**

253. Mironov, V., V. Kasyanov, and R.R. Markwald, ***Nanotechnology in vascular tissue engineering: from nanoscaffolding towards rapid vessel biofabrication.*** **Trends Biotechnol, 2008. 26(6): p. 338-44.**

254. Iwai, S., et al., ***Biodegradable polymer with collagen microsponge serves as a new bioengineered cardiovascular prosthesis.*** **J Thorac Cardiovasc Surg, 2004. 128(3): p. 472-9.**

255. Harker, L.A. and S.R. Hanson, ***Experimental arterial thromboembolism in baboons. Mechanism, quantitation, and pharmacologic prevention.*** **J Clin Invest, 1979. 64(2): p. 559-60.**

Appendix A

MATLAB code for image analysis program used to quantify alignment.

```
% Locate fiber orientation in images
% Image must be square
% Algorithm:  Begin with edge detection based on approximation to
% the derivative.  Perform Radon transform on the segmented image.
% Calculate maximum projection angles.  Relate to image orientation.
% Calculate probability density function of fiber orientation.
%
%10/30/02 S J Kirkpatrick
%
close all
clear all
I=imread
('\\Emc.bme.ohsu.edu\projects\hinds_lab\KeriVartan\micropatterning\ThrombogenicECProject\Flo
w\Cytoskeleton\KV090325\MP10003.jpg');
%I=im2bw(I);
I=rgb2gray(I);
%I=imrotate(I,60);
%Var=.75;%add noise to image
%I=imnoise(I,'gaussian',0,Var);
figure(1);imshow(I);colorbar

I=imcrop;
%kernal =[1;0;-1]/2;%first order discrete difference
kernal=[-1;8;0;-8;1]/12;%second order first derivative operator.  Detects curvature in the gradient
%kernal=[1;-9;45;0;-45;9;-1]/60;%third order first derivative operator
%kernal2=[-3 32 -168 672 0 -672 168 -32 3]%fourth order first derivative operator
%Antisymmetric derivative filters with recursive U correction filter
%kernal=[-0.575841;0.416642;0.0478413;-0.00435846];%third order
%Another class of antisymmetric derivative filters -weighted least square optimized
%kernal=[0.74038;-0.12019];%
%kernal=[-1;27;-27;1]/24%second order with even number of coefficients%(first derivative)
%BW=filter2(kernal,I,'valid');%
%%%%%%%%%%%%%%%%%%
%Second derivative operators
%kernal=[-2.20914;1.10457];%r=1
%kernal=[-2.71081;1.48229;-0.126882];%r=2
%kernal=[-2.92373;1.65895;-0.224751;0.0276655];%r=3
%kernal=[-3.03578;1.75838;-0.291985;0.0597665;-0.00827];%r=4
%kernal=[-3.10308;1.81996;-0.338852;0.088077;-0.0206659;0.00301915];%r=5
%
I=double(I);
BW=filter(kernal,1,I,[],2);%filter in x-direction
BW2=filter(kernal,1,I);%filter in y-direction
BW3=BW+BW2;% If using a second derivative, this is the Laplacian
%BW3=filter2(kernal,I);
```

```
mag=sqrt((BW.^2)+(BW2.^2));
unit=BW3./mag;
%BW=edge(I,'canny');

figure(2);imagesc(I);colormap(gray);axis square
figure(3);imshow(BW);%colormap(gray)% Horizontal derivative  image
figure(4);imshow(BW2);%colormap(gray)% Vertical derivative image
figure(5);image(mag);colormap(gray(20))% Magnitude of the gradient image
figure(6);imshow(BW3);%colormap(gray)%colorbar% Gradient image
BW3=imcrop;

%%
%At this point, the gradient image (BW3) can be divided by the magnitude of
%the gradient image(mag) to create a unit vector image.  Then perform a
%Radon transform on the unit vector image.  Seems to be not as good,
%though.
%mag=sqrt(BW3.^2);
%unit=BW3./mag;
theta=0:179;
[R,xp]=radon(BW3,theta);
figure(7);imagesc(theta, xp,R);colorbar;xlabel('\theta (degrees)');ylabel ('xp');colormap(hot)
set(gca,'XTick',0:20:360);
Beta=max(abs(R));
figure(8);plot(theta,Beta,'linewidth',2);title('Maximum Projection Angle');xlabel('\theta
(degrees)');ylabel('Maximum Value of R')
figure(9);plot((theta-90),Beta,'linewidth',2);title('Fiber Angle Spectrum Relative to
Horizontal');xlabel('\theta (degrees)');
%ylabel('Maximum Value of R')
figure(10);plot((90-(theta-90)),Beta,'linewidth',2);title('Fiber Angle Spectrum Relative to
Vertical');xlabel('\theta (degrees)');
%ylabel('Maximum Value of R');
%
%Probability Distribution Function
Area=trapz((theta-90),Beta);
Prob=(Beta./Area);
Prob1=Prob/max(Prob);
figure(11);plot((theta-90),Prob1,'r','linewidth',2);title('Normalized Probability Distribution of Fiber
Orientation Relative to Horizontal'); xlabel('\theta (degrees)');ylabel('P(\theta)');
%Normalize KV
Prob2=Prob./sum(Prob);
figure(12);plot((theta-90),Prob2,'r','linewidth',2);title('Normalized Probability 2'); xlabel('\theta
(degrees)');ylabel('P(\theta)');
Area2=trapz((theta-90), Prob1)
Area3=trapz((theta-90), Prob2)%area should equal 1
x=theta-90;

%moment about the peak
max1=max(Prob2(:));
thetamax=find((Prob2)==max1);
Peak=thetamax-90
val=(theta-90)-Peak;
val=val.^2;
val=Prob2.*val;
mom1=sum(val)
%mom2=mom1/180 %would divide by N if finite population
```

```
root=sqrt(mom1)%variance of an abstract population
%mom2=sum(root)

%Calculate Entropy
ent=log2(Prob2);
ent2=Prob2.*ent;
H=-sum(ent2)

%Ave=mean(Prob)
%Variance=var(Prob)
%
%peak=find((Prob)==1)
%p1=peak-90
%V1=(Prob-90-p1);
%V2=(V1.*V1)/(theta-90)

% spect=fftshift(fft2(BW3));
% spect=spect.*conj(spect);
% figure(12);imagesc(log(abs(spect)))
% %SNR = 10*log10((mean(I(:))/sqrt(Var)))
% %end
```

Appendix B

Comparison of MPEC vs. FSS-elongated EC gene expression.

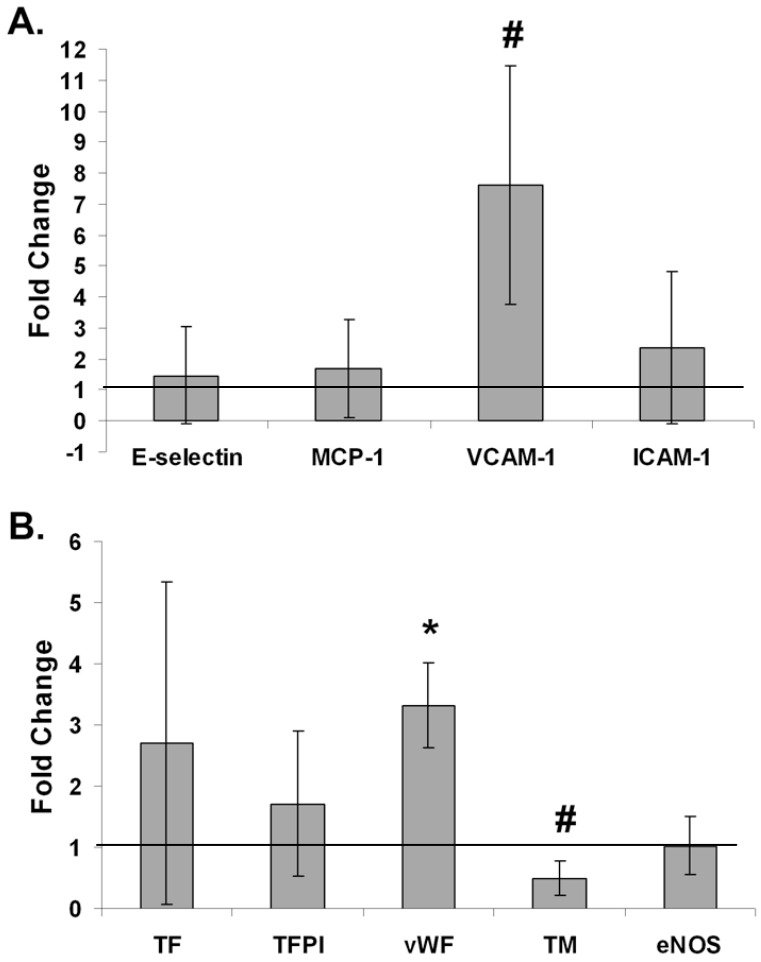

Figure Appendix B.1. MPEC vs FSS-elongated EC gene expression. **A.** Inflammatory markers. **B.** Thrombosis markers. Line at 1.00 represents FSS-elongated EC gene expression level. Paired Student's t-test on dCt data. *p<0.05, #p=0.05. Results indicated that many of the genes are expressed at comparable levels between micropattern-elongated and FSS-elongated ECs. MPECs express more VCAM-1 and vWF and less TM, which is consistent with data discsussed in Chapter VII and VIII.

Keri Beth Vartanian was born in Boston, Massachusettes on August 23, 1981. She moved to Portland, Oregon with her family in 1984. After high school, she attended the University of Arizona where she graduated Magna Cum Laude from the Honors College with a Bachelors of Science degree in Biochemistry in 2003. Her work on her undergraduate honors thesis entitled "Thrombin TP-508 acts as a Potent Stimulator of Angiogenesis via Non-Proteolytically Activated Receptors," spurred her interest in pursuing scientific research as a career. After college, Keri accepted a post-baccalaureate fellowship at the National Heart Lung Blood Institute at the National Institutes of Health in Bethesda, Maryland. Keri worked at the NIH for a year on research involving the regeneration of the mammalian central nervous system.

Keri began graduate school at Oregon Health & Science University in August of 2004. Her graduate work is focused on understanding endothelial cell dysfunction related to cardiovascular disease. She was awarded an Achievement Rewards for College Scientists and an American Heart Pre-doctoral Fellowship. Her involvement in her graduate research, as well as her previous research, has resulted in several publications and presentations at national and international conferences. Her publications include the following:

PAPERS

Vartanian, KB, Kirkpatrick, SJ, McCarty, OJT, Vu, TQ, Hanson, SR, Hinds, MT. "Distinct extracellular matrix microenvironments of progenitor and carotid endothelial cells." Journal of Biomedical Materials Research: Part A, Nov. 2008 (Epub)

Vartanian, KB, Kirkpatrick, SJ, Hanson, SR, Hinds, MT. "Endothelial cell cytoskeletal alignment independent of fluid shear stress on micropatterned surfaces." Biochemical and Biophysical Research Communications. July 2008

Hinds MT, Ma M, Tran N, Ensley E, Kladakis SM, **Vartanian KB**, Markway BD, Nerem RM, and Hanson SR. "Potential of Baboon Endothelial Progenitor Cells for Tissue Engineered Vascular Grafts." Journal of Biomedical Materials Research: Part A, Sept. 2008.

Levitz D, **Vartanian K**, Jacques SL. "Monitoring cellular remodeling of collageneous matrix using optical coherence tomography." Proceedings of SPIE, 2006. Volume 6163.

Levitz D, Hinds, MT, Tran N, **Vartanian K**, Hanson SR, and Jacques SL. "Measuring optical properties of a blood vessel model using optical coherence tomography." Proceedings of SPIE, 2006. Volume 6078

Vartanian KB, Chen Y.S., Kennedy J, Ryaby J, Wang H, Hoying JB. "The non-Proteolytically Active Thrombin Peptide TP508 Stimulates Angiogenic Sprouting." The Journal of Cellular Physiology. Jan. 2006

P. Krsko, **K. Vartanian**, H. Geller, M. Libera. "Controlled Macrophage Adhesion on Micropatterned Hydrogel Surfaces." Material Research Society Symposium Proceedings, 2005, V845, pp. aa'8.7.1-6

ABSTRACTS

Vartanian KB, Bradley BJ, McCarty OJT, Hanson SR, Hinds MT. "Endothelial Cell Elongation Impacts Thrombogenicity Independent of Fluid Shear Stress." American Society of Hematology. December 2008.

Vartanian KB, Kirkpatrick SJ, Hanson SR, Hinds MT. "Elongated Endothelial Cells on Micropatterned Lanes Have Cytoskeletal Alignment and Distinct Extracellular Matrix Deposition." International Vascular Biology Meeting, June 2008.

Vartanian KB, Vu TQ, Hanson SR, McCarty OJT, Hinds MT. "Effects of Spatial Localization on Vascular Cell Biology: Use of Micropatterned Substrata." Micro Nano Breakthrough, Sept. 2007

Vartanian KB, Hanson SR, Hinds MT. "Endothelial Progenitor Cells Have Increased Deposition of Vascular Extracellular Matrix Proteins Compared to Mature Endothelial Cells" North American Vascular Biology Organization. March 2007

Markway, BD, Tran, NT, Marzec, UM, **Vartanian, KB,** Hanson, SR, Hinds, MT. "Collagen Increases Surface Tissue Factor Activity in Baboon Endothelial Progenitor Cells." Biomaterials, April 2006

Vartanian KB, Marzec U, Hanson SR and Hinds MT. "Coagulation potential of circulating endothelial cells." Biomedical Engineering Society Annual Meeting. Sept. 2005

Vartanian KB, Katagiri Y, Peter P, Tan F, Wang H, Geller HM. "Quantitative Analysis of Microtubule Polymerization in Extracellular Matrix-Mediated Axon Guidance." The American Society for Cell Biology. Dec. 2004

Krsko P, Hong Y, **Vartanian KB**, Geller HM, Libera M. "Surface-Patterned PEO Nanohydrogels to Control Cell-Substrate Interactions." Materials Research Society. Nov. 2004

Vartanian KB, Chen H, Kidd K, Hoying JB. "Acceleration of Angiogenesis in Microvessels Treated with Thrombin TP-508." Federation of American Societies for Experimental Biology. April 2003